The
PHILOSOPHICAL MAGAZINE

FIRST PUBLISHED IN 1798

. 45 SEVENTH SERIES No. 362 March 1954

UNIVERSITY OF HAWAII
LIBRARY
APR 13 '54

A Journal of Theoretical Experimental and Applied Physics

EDITOR
PROFESSOR N. F. MOTT, M.A., D.Sc., F.R.S.

EDITORIAL BOARD
SIR LAWRENCE BRAGG, O.B.E., M.C., M.A., D.Sc., F.R.S.
SIR GEORGE THOMSON, M.A., D.Sc., F.R.S.
PROFESSOR A. M. TYNDALL, C.B.E., D.Sc., F.R.S.

PRICE 15s. 0d.
Annual Subscription £8 0s. 0d. payable in advance

AND PUBLISHED BY TAYLOR & FRANCIS LTD., RED LION COURT, FLEET ST., LONDON, E.C.4.

ALERE FLAMMAM

THE MATHEMATICAL WORKS OF JOHN WALLIS, D.D., F.R.S.

by

J. F. SCOTT, Ph.D., B.A.

"His work will be indispensable to those interested in the early history of The Royal Society. I commend to all students of the Seventeenth Century, whether scientific or humane, this learned and lucid book."—Extract from foreword by Prof. E. N. da C. Andrade, D.Sc., Ph.D., F.R.S.

Recommended for publication by University of London

12/6 net

Printed and Published by

TAYLOR & FRANCIS, LTD.
RED LION COURT, FLEET STREET, LONDON, E.C.4.

DECADE 1941–50

We are requested by many of our clients overseas, to purchase on their behalf

PHILOSOPHICAL MAGAZINE

and all other important Scientific Journals for the years 1941–50 during which time, owing to war restrictions their supply was stopped.

YOUR OFFERS WILL BE APPRECIATED

Complete sets and longer runs also required by

THE SCIENTIFIC BOOK SUPPLY SERVICE
(T. FREDERICK DE LOCHE)
5 FETTER LANE, FLEET ST., LONDON, E.C.4.

UNIVERSITY OF THE WITWATERSRAND

Johannesburg, South Africa

Applications are invited for a LECTURESHIP IN PHILOSOPHY.

The salary scale is £800 by £50 to £1,050 per annum. In addition, a married man will receive £234 per annum cost-of-living allowance.

An allowance is made towards travelling expenses.

Further particulars and information as to the method of application should be obtained from the Secretary, Association of Universities of the British Commonwealth, 5 Gordon Square, London, W.C.1.

The closing date for the receipt of applications, in London and South Africa, is 31*st March*, 1954.

XXVII. *On Simplifying the Reduction by Least Squares of Angular Distribution Experiments in Nuclear Physics*

By P. C. Price
Cavendish Laboratory, Cambridge*

[Received November 26, 1953]

Abstract

The reduction of angular distribution experiments by the method of least squares is often very laborious. An experimental procedure is described which simplifies the computations by using a particular set of experimental angles and of relative weights of the observations at each angle. The method of calculation is an application of Gauss' Formula of Numerical Integration ; a proof that this method is a 'least squares' reduction is given in an Appendix. Four-figure tables are included to facilitate the use of the method.

§ 1. Introduction

The essential part of the reduction of an angular distribution or correlation experiment is the calculation by the method of least squares of the coefficients in one of the formulae

$$y(x)=a_0+a_1x+\dots+a_kx^k+\dots+a_nx^n, \qquad (1.1)$$

$$y(x)=p_0P_0(x)+p_1P_1(x)+\dots+p_kP_k(x)+\dots+p_nP_n(x), \qquad (1.2)$$

where $x=\cos\theta$, θ is the angle between the directions of the incident and emergent particles in 'centre-of-mass space', and y is the counting rate in particles/steradian at the angle θ (which may be calculated from the counting rate observed in 'laboratory space'). $P_k(x)$ is the kth Legendre polynomial in x, normalized to $P_k(1)=1$.

The reduction to (1.1) or (1.2) has two stages : a solution for the coefficients by least squares and an enquiry into the significance of the higher terms. The latter may be carried out, for a particular term, by solving (1.1) in a form containing that term and also in a form omitting it, and comparing the 'goodness of fit' in the two cases by a variance ratio test. This has been done, for example, by Cohen (1953). It is clear that a thorough reduction may require two or three laborious least square calculations.

The problem of simplifying the fitting of polynomials by least squares has been considered by Birge (1947), who gives a full account of the use of orthogonal polynomials in the case of equidistant observations of equal weight. His work is not so useful in reducing angular distribution experiments as in some other problems ; considerations are given below which suggest that a different approach, also using orthogonal polynomials, may be more profitable.

---

* Communicated by E. S. Shire.

(i) It is artificial, in this kind of experiment, to choose observational points which are equidistant in x, and to arrange that the observations have equal weight. These points will not correspond to evenly spaced angles in laboratory space, and to achieve equal weights the time spent at each angle must be as carefully planned as if the weights were required in any other ratio. The only advantage obtained through any procedure of this kind is the possibility of using a simplified least squares reduction.

(ii) It is advantageous to obtain the angular distribution in the form (1.2). Blatt and Biedenharn (1953) have given formulae for the coefficients B_n in the expression for the differential cross section

$$d\sigma = \sum_{n=0}^{\infty} B_n P_n(\cos\theta)\,.\,d\Omega, \quad . \quad . \quad . \quad . \quad . \quad . \quad . \quad (1.3)$$

in terms of the channel spins and orbital angular momenta concerned and the scattering matrix. The quantities B_n, required for comparison with their theory, are much more easily obtained from the p_n of (1.2) than from the a_n of (1.1).

(iii) If the observations are reduced to the form (1.2) by using the Legendre polynomials as orthogonal polynomials the least square values of the other coefficients p_k are not affected by any assumption made about the value of a particular coefficient p_j. In particular, if a term in (1.2) which is found to be not significantly non-zero is postulated to vanish, then the values already calculated for the other coefficients will remain valid.

(iv) It is evident that this greatly simplifies the problem of the significance of small terms in (1.2). The significance of the term $p_jP_j(x)$ can be immediately estimated from the size of the probable error of p_j.

(v) The calculation of the probable errors of the coefficients p_k is vastly simplified if the Legendre polynomials are also orthogonal polynomials. In this case the formulae for the p_k become, as we shall see, linear functions of the observational results, whose standard deviations are known ; hence the standard errors of the p_k can be derived by using the formula for the standard deviation σ_f of a function $f(x_1, \ldots x_k, \ldots x_n)$ of n random variables with standard deviations $\sigma_1, \ldots \sigma_k, \ldots \sigma_n$ respectively :

$$\sigma_f^2 = \sum_{k=1}^{n} \left(\frac{\partial f}{\partial x_k}\right)^2 \sigma_k^2. \quad . \quad . \quad . \quad . \quad . \quad . \quad . \quad . \quad . \quad (1.4)$$

The considerations (i)–(v) above suggest that if the experimental angles and relative weights are so chosen that for those points and weights the orthogonal polynomials up to the nth order are the corresponding Legendre polynomials, a great deal of labour in the reduction of the experiment can be saved. We indicate in § 2 a convenient solution of the problem of finding such angles and relative weights, and deduce explicit formulae for the coefficients p_k and their standard errors as functions of the experimental results and the constants given in the tables.

The proof that this solution is a least-square reduction of the observations is relegated to the Appendix. The application of the formulae of § 2 to the practical study of nuclear reactions is discussed in § 3. In § 4 we describe the tables, which are found in § 5, and give an account of the methods of calculation employed.

§ 2. THE EXPERIMENTAL ANGLES AND WEIGHTS AND THE FORMULAE OF REDUCTION

Before we continue the discussion of the method of least squares, we shall introduce the subject of Gaussian integration and prove a mathematical equation which is equivalent to (1.2).

The orthogonality relations of Legendre polynomials

$$\left.\begin{aligned}(k+\tfrac{1}{2})\int_{-1}^{1} P_j(x)P_k(x)\,dx=\delta_{jk}&=1 \qquad j=k\\ &=0 \qquad j\neq k\end{aligned}\right\} \quad . \; . \; . \; . \; . \quad (2.1)$$

imply that in (1.2)

$$p_k=(k+\tfrac{1}{2})\int_{-1}^{1} P_k(x)y(x)\,dx \qquad k=0, 1, \ldots . n. \quad (2.2)$$

There are several methods of estimating the integral of a function from its values at a set of arguments ; Simpson's rule is one of the best known. We shall use another formula due to Gauss (1814), which states that if $f(x)$ is a polynomial of order less than $2n+1$, and the points x_i are defined as the roots of

$$P_{n+1}(x)=0 \quad . \; . \; . \; . \; . \; . \; . \; . \; . \quad (2.3)$$

then

$$\int_{-1}^{1} f(x)\,dx=\sum_i a_i f(x_i) \quad . \; . \; . \; . \; . \; . \; . \; . \quad (2.4)$$

where the a_i are given by

$$a_i=\frac{1}{P'_{n+1}(x_i)}\int_{-1}^{1}\frac{P_{n+1}(x)}{x-x_i}\,dx. \quad . \; . \; . \; . \; . \; . \quad (2.5)$$

A proof of Gauss' Formula of Numerical Integration is given in Whittaker and Robinson (1944).

We observe that the integrand of (2.2), $P_k(x)y(x)$, is a polynomial of order less than $2n+1$; hence we can use Gauss' formula to calculate this integral exactly. We obtain

$$p_k=\sum_i c_{ik}y(x_i) \qquad k=0, 1, \ldots . n \quad (2.6)$$

where

$$c_{ik}=(k+\tfrac{1}{2})a_iP_k(x_i) \qquad k=0, 1, \ldots . n. \quad (2.7)$$

We return now to the method of least squares. Let us postulate that observations $y'(x_i)$ of $y(x)$ are made at the angles corresponding to the points x_i, with standard deviations $\sigma(x_i)$. Then it can be shown that if these standard deviations are in the right ratios the formula (2.6) can be used as a 'least squares' reduction of the observations to the form (1.2), in which the Legendre polynomials are the appropriate orthogonal polynomials. We can express this idea in a theorem :

Theorem.—The reduction of the observations $y'(x_i)$ by the method of least squares to the form (1.2), or to any formula differing from (1.2) only by the omission of some terms from the right-hand side of the latter, is effected by the formulae

$$p_k' = \sum_i c_{ik} y'(x_i) \quad . \quad . \quad . \quad . \quad . \quad . \quad . \quad . \quad (2.8)$$

provided that

$$\sigma^{-2}(x_i) = \text{const.} \times a_i. \quad . \quad . \quad . \quad . \quad . \quad . \quad . \quad (2.9)$$

The proof of this theorem is relegated to the Appendix.

One more formula is required, namely the expression for the standard errors q_k of the estimated coefficients p_k'. Before we prove this formula we shall establish our notation. We shall for simplicity restrict ourselves to the case of even $n=2r$, and we shall number off the x_i as follows :

$$\left.\begin{array}{ll} 0=x_0<x_1< \ldots . <x_r<1 & \\ x_{-i}=-x_i & i=0, 1, \ldots . r. \end{array}\right\} \quad . \quad . \quad (2.10)$$

We shall put $\sigma(x_0)=\sigma_0$, as a measure of the absolute accuracy of the experiment, the other standard deviations being given by

$$\sigma^2(x_i) = a_0\sigma_0^2/a_i. \quad . \quad . \quad . \quad . \quad . \quad . \quad . \quad . \quad . \quad (2.11)$$

Then from (2.8) and (1.4)

$$q_k^2 = \sum_i c_{ik}^2 \sigma^2(x_i) \quad . \quad . \quad . \quad . \quad . \quad . \quad . \quad . \quad (2.12)$$

which reduces, on applying (2.6), (2.7) and (2.11), to

$$q_k = \sigma_0[(2k+1)c_{00}]^{1/2}. \quad . \quad . \quad . \quad . \quad . \quad . \quad . \quad (2.13)$$

§ 3. APPLICATIONS TO NUCLEAR PHYSICS

The application of the method to angular distribution and correlation experiments is obvious ; we give below a discussion which may clarify some of the details.

(i) *The Basic Formulae Collected*

These are (2.8), (2.13), and the condition on the relative weights (2.11). We modify the form of the last equation by introducing the quantities $w_i=a_i/a_0$, which are given in the tables.

$$p_k' = \sum_{i=-r}^{+r} c_{ik} y'(x_i), \quad . \quad . \quad . \quad . \quad . \quad . \quad . \quad . \quad (2.8)$$

$$q_k = \sigma_0[(2k+1)c_{00}]^{1/2}, \quad . \quad . \quad . \quad . \quad . \quad . \quad . \quad (2.13)$$

$$\sigma^{-2}(x_i) = w_i\sigma_0^{-2}. \quad . \quad . \quad . \quad . \quad . \quad . \quad . \quad . \quad . \quad . \quad (3.1)$$

(ii) *The Relative Weights of the Observations*

The eqns. (2.8) and (2.13) do not give a least square solution unless (3.1) is satisfied. This is achieved by adjusting the time spent in observing at each angle.

In most angular distribution experiments the counting rates $y'(x_i)$ are obtained by measuring the ratio between the counts produced in a movable counter and in a fixed ‘ monitor ’ counter. In such a case the standard error in the counting rate is due to three factors: the statistical fluctuations in the movable counter, the statistical fluctuations in the monitor counter, and the errors due to bad experimental design. We shall ignore the last, as in most experiments of this kind the statistical errors are so large that any competently designed experiment will make other errors negligible by comparison. Let us suppose that the time of observation at x_i is t_i, and the counting rates of the movable and monitor counters are n_i and n' respectively. Then

$$y'(x_i)=A\mu_i(n_i/n') \quad . \quad . \quad . \quad . \quad . \quad . \quad . \quad . \quad (3.2)$$

where A is independent of i, and μ_i is the factor required by the reduction to centre-of-mass space. By applying (1.4) to (3.2) we can obtain the expressions

$$t_i/t_0=w_i\left(\frac{\mu_i}{\mu_0}\right)^2\cdot\left(\frac{n_i}{n_0}\right)\cdot\frac{1+(n_i/n')}{1+(n_0/n')}, \quad . \quad . \quad . \quad . \quad . \quad (3.3)$$

$$\sigma_0^2=y'^2(x_0)\frac{n_0+n'}{n_0n't_0} \quad . \quad . \quad . \quad . \quad . \quad . \quad . \quad . \quad . \quad . \quad (3.4)$$

for the relative times of observation required to satisfy (3.1), and for the parameter σ_0 in (2.13).

(iii) *Difficulties in the Practical Application*

Two points arise in the practical use of this method that should be noted. The first is that if this method is used to fit (1.2) up to the term $p_nP_n(x)$ there is no method of detecting errors due to the presence of unsuspected higher terms. Therefore the experimenter should choose a value of n higher than the highest term he expects to find non-zero, and should verify that the highest term in the expansion does in fact vanish. If it is found that this term does not vanish, and there are no certain theoretical grounds for excluding the possibility of still higher terms being present, there is no alternative to repeating the experiment for a higher value of n.

The second is a caution to those experimenters working on reactions producing charged particles. Before deciding to use this method, they should verify that all the recommended angles are accessible; the geometry of targets and counters, the difficulty of placing a target very obliquely to the beam, and the interference due to other groups of particles from the target, often conspire to prevent observation with a particular technique being made at certain angles.

(iv) *The Study of Overlapping Levels*

The excitation curves of nuclear reactions frequently display the phenomenon of overlapping resonances. The method of analysis of angular distributions outlined in this paper suggests a logical approach to the analysis of complicated excitation curves of this type. If yield curves are taken at a set of recommended angles in centre-of-mass space, these can be combined by (2.8) to give curves of the variation with bombarding energy of the parameters $p_0, \dots . p_n$. The coefficient p_0 is of course proportional to the total yield. Explicit formulae for the total yield and for the other coefficients in terms of the constants of the energy levels concerned are given in Blatt and Biedenharn (1953). We suggest that a method of this kind would give a clearer indication than is usually obtained of the nature of the resonances in the energy range studied.

§ 4. THE TABLES AND THEIR CALCULATION

The tables are primarily intended for use by nuclear physicists. They are therefore given only to four figures, as the observational time required to obtain more than four-figure accuracy in an angular distribution experiment is prohibitive. The tables have been given for even values of n up to and including $n=10$. They are accurate to 0·6 of a unit in the fourth decimal place.

The first column gives the number i as defined in (2.10). The second, third, and fourth columns give θ_i, $\sin\theta_i$ and $x_i=\cos\theta_i$, the last two to facilitate the reduction to laboratory space. The fifth column gives w_i (see (3.1) and (3.3)), and the last $n+1$ columns give the coefficients c_{ik} defined by (2.7).

The tables were calculated from (2.7) using the values of x_i, a_i given by Lowan, Davids and Levenson (1942), and the tables of Legendre polynomials by Tallqvist (1937). They were checked by forming the sums

$$\sum_{i=-r}^{+r} c_{ik} \qquad k \text{ even}$$

and

$$\sum_{i=-r}^{+r} c_{ik}x_i \qquad k \text{ odd}$$

which should vanish for $k\geqslant 2$ and equal unity for $k<2$. When discrepancies were found the values were recomputed either from the same sources or by the use of the recurrence relation

$$c_{i,k+1}=[2+1/(k+1)]c_{ik}x_i-[1+(2k+1)/(k+1)(2k-1)]c_{i,k-1} \quad . \quad (4.1)$$

which follows from (2.7) and the well-known recurrence relation for Legendre polynomials.

1	39 14	0·6325	+0·7746	0·6250	+0·2778	+0·6455	+0·5556
0	90 00	1·0000	0·0000	1·0000	+0·4444	0·0000	−1·1111
−1	140 46	0·6325	−0·7746	0·6250	+0·2778	−0·6455	+0·5556

$n=4$

i	θ_i	$\sin\theta_i$	$x_i=\cos\theta_i$	w_i	c_{i0}	c_{i1}	c_{i2}	c_{i3}	c_{i4}
2	25 01	0·4229	+0·9062	0·4165	+0·1185	+0·3220	+0·4334	+0·4155	+0·2620
1	57 25	0·8426	+0·5385	0·8413	+0·2393	+0·3866	−0·0779	−0·6992	−0·7420
0	90 00	1·0000	0·0000	1·0000	+0·2844	0·0000	−0·7111	0·0000	+0·9600
−1	122 35	0·8426	−0·5385	0·8413	+0·2393	−0·3866	−0·0779	+0·6992	−0·7420
−2	154 59	0·4229	−0·9062	0·4165	+0·1185	−0·3220	+0·4334	−0·4155	+0·2620

$n=6$

i	θ_i	$\sin\theta_i$	$x_i=\cos\theta_i$	w_i	c_{i0}	c_{i1}	c_{i2}	c_{i3}	c_{i4}	c_{i5}	c_{i6}
3	18 21	0·3150	+0·9491	0·3098	+0·0647	+0·1843	+0·2755	+0·3235	+0·3188	+0·2590	+0·1488
2	42 08	0·6709	+0·7415	0·6692	+0·1399	+0·3111	+0·2271	−0·0910	−0·4584	−0·6335	−0·4660
1	66 03	0·9139	+0·4058	0·9136	+0·1909	+0·2324	−0·2414	−0·5902	−0·2130	+0·5518	+0·7416
0	90 00	1·0000	0·0000	1·0000	+0·2090	0·0000	−0·5224	0·0000	+0·7053	0·0000	−0·8490
−1	113 57	0·9139	−0·4058	0·9136	+0·1909	−0·2324	−0·2414	+0·5902	−0·2130	−0·5518	+0·7416
−2	137 52	0·6709	−0·7415	0·6692	+0·1399	−0·3111	+0·2271	+0·0910	−0·4584	+0·6335	−0·4660
−3	161 39	0·3150	−0·9491	0·3098	+0·0647	−0·1843	+0·2755	−0·3235	+0·3188	−0·2590	+0·1488

$n=8$

i	θ_i	$\sin\theta_i$	$x_i=\cos\theta_i$	w_i	c_{i0}	c_{i1}	c_{i2}	c_{i3}	c_{i4}	c_{i5}	c_{i6}	c_{i7}	c_{i8}
4	14 30	0·2503	+0·9682	0·2461	+0·0406	+0·1180	+0·1841	+0·2323	+0·2574	+0·2563	+0·2278	+0·1730	+0·0953
3	33 17	0·5487	+0·8360	0·5470	+0·0903	+0·2265	+0·2477	+0·1308	−0·0884	−0·3270	−0·4859	−0·4883	−0·3115
2	52 10	0·7898	+0·6134	0·7892	+0·1303	+0·2398	+0·0419	−0·3130	−0·4885	−0·2658	+0·2349	+0·6193	+0·5385
1	71 05	0·9460	+0·3243	0·9458	+0·1562	+0·1519	−0·2673	−0·4385	+0·0409	+0·5805	+0·3586	−0·4293	−0·7061
0	90 00	1·0000	0·0000	1·0000	+0·1651	0·0000	−0·4128	0·0000	+0·5573	0·0000	−0·6708	0·0000	+0·7675
−1	108 55	0·9460	−0·3243	0·9458	+0·1562	−0·1519	−0·2673	+0·4385	+0·0409	−0·5805	+0·3586	+0·4293	−0·7061
−2	127 50	0·7898	−0·6134	0·7892	+0·1303	−0·2398	+0·0419	+0·3130	−0·4885	+0·2658	+0·2349	−0·6193	+0·5385
−3	146 43	0·5487	−0·8360	0·5470	+0·0903	−0·2265	+0·2477	−0·1308	−0·0884	+0·3270	−0·4859	+0·4883	−0·3115
−4	165 30	0·2503	−0·9682	0·2461	+0·0406	−0·1180	+0·1841	−0·2323	+0·2574	−0·2563	+0·2278	−0·1730	+0·0953

$n=10$

i	θ_i	$\sin\theta_i$	$x_i=\cos\theta_i$	w_i	c_{i0}	c_{i1}	c_{i2}	c_{i3}	c_{i4}	c_{i5}	c_{i6}	c_{i7}	c_{i8}	c_{i9}	c_{i10}
5	11 59	0·2075	+0·9782	0·2040	+0·0278	+0·0817	+0·1302	+0·1701	+0·1986	+0·2136	+0·2137	+0·1982	+0·1676	+0·1229	+0·0661
4	27 30	0·4616	+0·8871	0·4601	+0·0628	+0·1671	+0·2136	+0·1822	+0·0752	−0·0822	−0·2485	−0·3763	−0·4250	−0·3722	−0·2208
3	43 06	0·6833	+0·7302	0·6826	+0·0931	+0·2040	+0·1396	−0·0796	−0·3192	−0·4127	−0·2686	+0·0621	+0·4036	+0·5523	+0·3981
2	58 44	0·8547	+0·5191	0·8544	+0·1166	+0·1816	−0·0559	−0·3501	−0·3335	+0·0593	+0·4681	+0·4514	−0·0377	−0·5495	−0·5572
1	74 22	0·9630	+0·2695	0·9629	+0·1314	+0·1063	−0·2569	−0·3269	+0·1486	+0·4990	+0·1126	−0·5183	−0·4257	+0·3413	+0·6664
0	90 00	1·0000	0·0000	1·0000	+0·1365	0·0000	−0·3412	0·0000	+0·4606	0·0000	−0·5544	0·0000	+0·6343	0·0000	−0·7052
−1	105 38	0·9630	−0·2695	0·9629	+0·1314	−0·1063	−0·2569	+0·3269	+0·1486	−0·4990	+0·1126	+0·5183	−0·4257	−0·3413	+0·6664
−2	121 16	0·8547	−0·5191	0·8544	+0·1166	−0·1816	−0·0559	+0·3501	−0·3335	−0·0593	+0·4681	−0·4514	−0·0377	+0·5495	−0·5572
−3	136 54	0·6833	−0·7302	0·6826	+0·0931	−0·2040	+0·1396	+0·0796	−0·3192	+0·4127	−0·2686	−0·0621	+0·4036	−0·5523	+0·3981
−4	152 30	0·4616	−0·8871	0·4601	+0·0628	−0·1671	+0·2136	−0·1822	+0·0752	+0·0822	−0·2485	+0·3763	−0·4250	+0·3722	−0·2208
−5	168 01	0·2075	−0·9782	0·2040	+0·0278	−0·0817	+0·1302	−0·1701	+0·1986	−0·2136	+0·2137	−0·1982	+0·1676	−0·1229	+0·0661

ACKNOWLEDGMENTS

The writer is obliged to Mr. E. S. Shire for his encouragement and to Dr. J. C. P. Miller of the Mathematical Laboratory for advice on Gaussian integration and on the method of computing the tables. He is also grateful to Dr. D. H. Wilkinson, Dr. A. P. French, Mr. E. Breitenberger, Mr. J. Wishart, and Mr. H. E. Daniels for reading the first draft of this paper and making a number of helpful comments. He wishes to express his thanks to Trinity College, Cambridge, for a Senior Scholarship and to the Department of Scientific and Industrial Research for a maintenance grant.

REFERENCES

BIRGE, R. V., 1947, *Rev. Mod. Phys.*, **19**, 298.
BLATT, J. M., and BIEDENHARN, L. C., 1952, *Rev. Mod. Phys.*, **24**, 258.
COHEN, A. V., 1953, *Phil. Mag.*, **44**, 583.
GAUSS, C. F., 1814, *Gött. Comm.*, III.
LOWAN, A. N., DAVIDS, N., and LEVENSON, A., 1942, *Bull. Amer. Math. Soc.*, **48**, 739.
TALLQVIST, H., 1937, *Acta Soc. Sci. Fenn.*, **4** (2).
WHITTAKER, E. T., and ROBINSON, G., 1944, *The Calculus of Observations* (London : Blackie and Son, Ltd.), Sec. 80.

APPENDIX

The theorem of § 2 stated :

Theorem.—The reduction of the observations $y'(x_i)$ by the method of least squares to the form (1.2), or to any formula differing from (1.2) only by the omission of some terms from the right-hand side of the latter, is effected by the formulae

$$p_k' = \sum_i c_{ik} y'(x_i) \quad . \quad . \quad . \quad . \quad . \quad . \quad . \quad . \quad . \quad . \quad (2.8)$$

provided that

$$\sigma^{-2}(x_i) = \text{const.} \times a_i. \quad . \quad . \quad . \quad . \quad . \quad . \quad . \quad . \quad . \quad (2.9)$$

The quantities $\sigma^{-2}(x_i)$ are of course proportional to the relative weights of the observations $y'(x_i)$; we shall put them equal to w_i'.

If we reduce the set of observations given to the form (1.2) we solve the normal equations

$$\sum_i w_i' P_k(x_i) y'(x_i) = \sum_{j=0}^{n} p_j \left(\sum_i w_i' P_j(x_i) P_k(x_i)\right) \quad . \quad . \quad (\text{A } 1)$$

where k runs from 0 to n, giving $n+1$ equations in $n+1$ unknowns. If we reduce the same set of observations to a formula which is (1.2) with some terms omitted, we have to solve a set of equations of the same form as (A 1), but with j, k running only over the values between 0 and n that correspond to the terms left in the modified formula. We shall call these equations (A 2).

The eqns. (A 1) take a particularly simple form if the $(n+1)\times(n+1)$ matrix g_{jk} defined by

$$g_{jk}=\sum_i w_i'P_j(x_i)P_k(x_i) \qquad j,k=0,1,\ldots n \qquad \text{(A 3)}$$

is in diagonal form, and has no zero diagonal terms. Putting (A 3) into (A 1) we have

$$p_k'=\Sigma c_{ik}'y'(x_i) \qquad k=0,1,\ldots n \qquad \text{(A 4)}$$

where

$$c_{ik}'=\frac{1}{g_{kk}}w_i'P_k(x_i) \qquad k=0,1,\ldots n. \qquad \text{(A 5)}$$

Now if g_{jk} is diagonal, with no zero diagonal terms, any minor of g_{jk} obtained by deleting a set of rows and the corresponding set of columns will also possess this property. Therefore in the reduction of the observations to a modified formula, the eqns. (A 2) will also be reducible to (A 4) and (A 5), with k running only over the appropriate values.

To prove the theorem we have to show that the two statements

(i) g_{jk} is diagonal, with no zero diagonal terms,

(ii) $c_{ik}=c'_{ik}$

follow from the condition

$$w_i'=\text{const.}\times a_i=A\,a_i,\ \text{say.} \qquad \text{(A 6)}$$

Proof of (i).—If we put

$$y(x)=P_j(x) \qquad \text{(A 7)}$$

we obtain from (1.2)

$$p_k=\delta_{jk} \qquad \text{(A 8)}$$

and from (2.6) and (2.7)

$$p_k=\sum_i(k+\tfrac{1}{2})a_iP_k(x_i)P_j(x_i). \qquad \text{(A 9)}$$

Therefore by comparison with (A 6) and (A 3)

$$(k+\tfrac{1}{2})g_{jk}=A\delta_{jk}. \qquad \text{(A 10)}$$

Proof of (ii).—From (A 10) we deduce

$$(k+\tfrac{1}{2})g_{kk}=A \qquad \text{(A 11)}$$

and inserting this value for g_{kk}, and (A 6), into (A 5)

$$\left.\begin{aligned} c'_{ik}&=(k+\tfrac{1}{2})a_iP_k(x_i)\\ &=c_{ik}\end{aligned}\right\} \qquad \text{(A 12)}$$

from (2.7).

It should be observed that this fitting of (1.2) to the observations is not a 'least squares' fit in the usual sense, but an exact fit; the peculiarity of this method consists in the fact that the values of the coefficients obtained from this exact fit are the 'least squares' values for the coefficients obtained by fitting the same observations to any modified form of (1.2). This property, which is not in general true of exact solutions, arises from the fact that the Legendre polynomials up to $P_n(x)$ are the orthogonal polynomials over the points and relative weights chosen.

XXVIII. *The Yield Strength of Partly Ordered* Cu_3Au *Wires*

By W. D. Biggs and T. Broom
Department of Metallurgy, University of Birmingham*

[Received December 17, 1953]

Abstract

The dependence of yield stress on the size of ordered domains has been investigated by tensile deformation of polycrystalline wires of Cu_3Au. In agreement with a prediction by Cottrell it was found that the yield stress was greatest when the estimated domain size was about 50 Å.

§ 1. Introduction

The passage of dislocations through an ordered alloy has been examined theoretically by Cottrell (1954). The main ideas proposed are as follows. To avoid disordering a slip plane by the passage of a single dislocation, which would require a large force, dislocations move in pairs, each pair constituting a dissociated unit dislocation of the superlattice. The members of a pair are joined by a strip of anti-phase domain boundary. When such dislocations glide across a crystal disordering is produced at the places where they cut through anti-phase boundaries that intersect the slip plane. The pieces of boundary on either side of the slip plane are displaced in the slip direction relative to one another and a further piece of boundary is formed in the region of the slip plane connecting these displaced pieces. As slip continues, the area of anti-phase boundary in the slip plane grows, until the slip displacement is about one-half the average domain size, and thereafter remains fairly constant. The energy needed to disorder the material in the slip plane has to be provided from the source of the applied stress and the material will be hard while disordering takes place.

Cottrell shows that the hardening should be a maximum for a certain domain size in the following way. The energy of order per unit area in the slip plane will be about $(\alpha a/l)(\gamma/2)$ before slip and $\gamma/2$ after disordering by extensive slip. Here γ is the energy per unit area of an anti-phase boundary, a is the interatomic spacing, l is the average width of a domain, and α is a number ($\simeq 6$) whose value depends upon the precise shape of the domains. A slip displacement of about $l/2$ is needed to disorder the plane. By equating the change in the energy of order of the plane to the work, $\sigma l/2$, done by the applied stress during slip, the stress for disordering is found approximately to be

$$\sigma = \gamma l^{-1}(1 - \alpha a l^{-1})$$

---

* Communicated by A. H. Cottrell.

giving a maximum, $\sigma_m=\gamma/4\alpha a$, at a domain width $l=2\alpha a$. With $\alpha=6$ this is about 40 Å.

The alloy Cu_3Au is particularly suitable to test this prediction because data about the formation and size of domains are available. Jones and Sykes (1938) used x-ray diffraction methods to measure the domain size of Cu_3Au after isothermal annealing treatments below the critical temperature, and showed that the electrical resistivity of their specimens was very sensitive to domain size and could be correlated with it.

§ 2. EXPERIMENTAL WORK

Copper–gold wire 0·25 mm in diameter containing 25·8 atomic % Au was kindly provided by Mr. R. A. Dugdale (A.E.R.E., Harwell). The wire was homogenized by an initial annealing in argon at 880°c for 14 hours, and cut into test lengths of about 8 cm. Two such specimens were cooled very slowly from just above the critical temperature (390°c) to 200°c to produce large domains and a high degree of order. Other specimens were disordered by heating *in vacuo* at 580°c for one hour followed by quenching in water; some of them were then partially re-ordered by various isothermal anneals at 346°c. Tensile testing grips of 16 s.w.g. copper wire together with conventional current and potential leads for resistance measurements were soft soldered on the ends of the specimens, taking care to keep the latter cool during this operation. Tensile tests were made in a Polanyi bent-beam type of machine using a 'hard' beam permitting rapid load relaxation on yielding.

§ 3. RESULTS

Annealing and resistivity data are given in the following table, together with domain sizes deduced from the data of Jones and Sykes (1938) for isothermal annealing at 346°c. The well-ordered specimen produced by very slow cooling from 390° to 200°c had a resistivity of 4·23 $\mu\Omega$ cm, and presumably its domains were limited only by the size of the crystal grains, about 4×10^5 Å. This value of the resistivity and that of the disordered specimen (11·47 $\mu\Omega$ cm) are in good agreement with the values reported by Jones and Sykes.

Annealing time at 346°c (min)	0	1	3	10	80	1000
Resistivity ($\mu\Omega$ cm at 20°c)	11·47	10·55	10·42	9·78	8·70	6·88
Deduced domain size (Å)	3	43	48	63	112	250

The stress–strain curves for these specimens are given in fig. 1; duplicate experiments were made on the disordered and well-ordered specimens, but the data obtained were so reproducible that only one curve for each is given. Some jerky flow was observed during the extension of several specimens, but the fluctuations did not amount to more than 5 % of the applied load.

Fig. 1

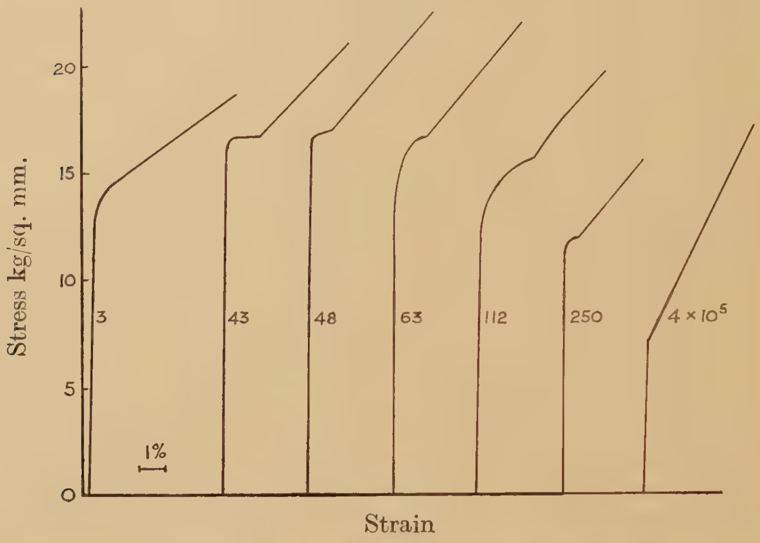

Stress–strain curves for Cu_3Au specimens; the numbers beside each curve indicate the deduced domain size in Ångstroms.

§ 4. Discussion

The results confirm that a maximum yield stress is associated with a critical domain size, which appears to be about 50 Å. The form of some of the stress–strain curves is noteworthy in that the initial deformation occurs at an almost constant stress before a steep work hardening region is reached. This is particularly noticeable when the domain size is about 50 Å, suggesting that the existence of order across slip planes presents an initial obstacle to slip, and that a reduction in the degree of ordering (by slip) diminishes this obstacle. This would be expected to be most prominent in the experiments on specimens with a critical domain size.

Acknowledgments

This experiment was suggested by Professor A. H. Cottrell. We are pleased to acknowldege his helpful advice and also the co-operation of colleagues in the Department.

References

Cottrell, A. H., 1954, Chapter in *The Relation of Properties to Structure* (Amer. Soc. Metals Seminar Series), to be published.
Jones, F. W., and Sykes, C., 1938, *Proc. Roy. Soc.* A, **166,** 376.

XXIX. *On the Nature of the Discrete Radio Sources*

By R. Q. Twiss
Services Electronics Research Laboratory, Baldock, Herts.*

[Received December 9, 1953]

Abstract

The theory that the galactic radio noise emitted by the discrete sources is due to the interaction of a local magnetic field and cosmic ray electrons is tested quantitatively for the source in Cassiopeia. It is shown that the average magnetic field must be of the order of 0·01 gauss, which is approaching the upper limit imposed by energy considerations. At frequencies below 15 Mc/sec resonant reabsorption of the r.f. energy becomes important and if the theory is valid the r.f. power received at the earth should vary at least as rapidly as $\nu^{5/2}$ below a critical frequency in the range 10–20 Mc/sec.

§ 1. Introduction

Several writers (Alfvén and Herlofson 1950, Ginsburg 1951, Hutchinson 1952) have suggested that the galactic radio noise from the discrete sources could be due to the interaction of cosmic ray electrons and a local magnetic trapping field. It has also been emphasized that such regions might be the source of cosmic ray protons (Unsöld 1949, Hutchinson 1952). We shall apply this hypothesis to the particular case of the radio source in Cassiopeia, which has been tentatively identified with a faint nebulosity within our galaxy (Baade and Minkowski).

On almost any theory of the original of the flux of cosmic ray electrons it would seem essential that the total energy of these electrons must be appreciably smaller than the total energy stored in the magnetic trapping field, which in turn must be smaller than the total kinetic energy of the ionized gas in the radio source. On this basis one can set both lower and upper limits to the average magnetic flux density, which come out at around 4×10^{-3} gauss and 2×10^{-2} gauss respectively. The energies of the relativistic electrons above ∼10 mev are distributed according to a suitable power law, which is completely determined by the r.f. spectrum given certain plausible assumptions about the nature of the magnetic field distribution.

§ 2. A Model for the Radio Source in Cassiopeia

According to preliminary data from interferometer measurements (Hanbury-Brown *et al.* 1952) the radio source in Cassiopeia can be represented as a uniformly radiating disc with an angular diameter of approximately 5′. Alternatively the source can be represented as a sphere with an angular diameter of $\sim 6'$ filled with a uniform distribution of radiators. This latter model is a more realistic one on the present theory and will be used in this paper.

---

* Communicated by the Author.

The distance of the radio source in Cassiopeia is not yet known, though if the identification with the faint visual nebulosity is correct this distance is almost certainly less than 1 kilo-parsec. In this model we have tentatively assumed that the source is at a distance of 300 parsecs away when the diameter of the equivalent spherical source is 1·7 light years. The total mass of ionized gas in the source is then about equal to the mass of the sun assuming an average density of 10^9 protons/m^3 as in the denser gas clouds. As we show below the model is not very sensitive to the diameter of the source which could vary by a factor of three without any profound effect.

At a frequency of 80 Mc/sec the flux density of unpolarized radiation at the earth from the Cassiopeia source is $2{\cdot}2\times10^{-22}$ watts/m^2/cycle, corresponding to an effective blackbody temperature of $\sim 7\times10^7$ °K, while between 80 and 160 Mc/sec the received power density varies as ν^{-1}. The frequency spectrum at frequencies below 80 Mc/sec is not accurately known, but Hanbury-Brown and Hazard (1953) have recently given a radio model for the galaxy in which the power spectrum of the discrete sources varies as $\nu^{-0{\cdot}8}$ over the frequency range 18·5–1200 Mc/sec. In this model the source in Cassiopeia is regarded as typical, though the position is likely to be complicated in practice by a dispersion both in absolute intensity and in spectrum. In this paper we shall assume that the r.f. power generated in unit volume of the source varies as $\nu^{-0{\cdot}9}$ for all $\nu > \nu_c$ where, tentatively, we have taken $\nu_c = 10$ Mc/sec. This assumption is certainly compatible with the present data, and, as we shall show, the frequency spectrum of the r.f. power *received* at the earth cannot vary as $\nu^{-0{\cdot}9}$ below 10 Mc/sec if the theory discussed in this paper is correct. The exact value of the frequency ν_c at which the power *generated* is a maximum, is quite uncritical on the present theory.

We shall assume that the volume of the radio source is filled with a magnetic flux density of magnitude B_0 webers/m^2, randomly oriented with respect to an observer on the earth,* together with a distribution of high energy electrons such that the density of particles with total energy E moving at an angle θ to the direction of the magnetic field obeys the power law distribution

$$N(E)\frac{dE}{E_0} = \gamma n_0 \left(\frac{E}{E_c}\right)^{-\gamma-1} \frac{dE}{E_0}\frac{\theta}{2\pi} \quad \text{for } E > E_c, \quad . \quad . \quad . \quad (1)$$

---

* If we select a point at random in the radio source this means that the direction of the magnetic field is randomly distributed around the line joining the source to the earth. This hypothesis which considerably simplifies the mathematics, seems justified by the fact that the radiation from the Cassiopeia source is unpolarized.

where $E_0=m_0c^2$ is the rest energy of the electron and E_c is a cut-off energy such that electrons with energy less than E_c do not radiate appreciably at frequencies greater than ν_c.

Below $E=E_c$ the energy spectrum of the electrons is undefined ; we shall assume only that their kinetic energy density is of the same order of magnitude as

$$U_c=\frac{\gamma}{\gamma-1}n_0\left(\frac{E_c}{E_0}\right)^{-\gamma+1}E_0, \quad . \quad . \quad . \quad . \quad . \quad . \quad . \quad (2)$$

the total energy density of electrons for which $E>E_c$.

From spectroscopic evidence it is known that individual filaments in the nebulosity have internal velocities in excess of 10^6 m/sec along the line of sight. The maximum available kinetic energy in unit volume is therefore of the order of

$$\tfrac{3}{2}\times 1{\cdot}6\times 10^{-27}\times 10^{9}\times 10^{12}\approx 2\times 10^{-6}\text{ joules}, \quad . \quad . \quad . \quad (3)$$

so that an *upper limit* to the *average* value of the magnetic energy density is imposed by the inequality

$$\frac{1}{2\mu_0}\overline{B_0{}^2}<2\times 10^{-6}$$

or

$$\overline{B_0}<2\times 10^{-6}\text{ webers/m}^2. \quad . \quad . \quad . \quad . \quad . \quad . \quad (4)$$

A *lower limit* to the magnetic flux density is imposed by the condition that the magnetic energy density be very much greater than the energy density of the relativistic electrons. From eqn. (2) this requires

$$\frac{1}{2\mu_0}B_0{}^2\gg\frac{\gamma}{\gamma-1}n_0\left(\frac{E_c}{E_0}\right)^{-\gamma+1}E_0. \quad . \quad . \quad . \quad . \quad (5)$$

§ 3. THE ENERGY SPECTRUM IN THE MODEL

In general the frequency spectrum of the r.f. radiation produced at a fixed point by a flux of electrons with energies distributed according to the power law of eqn. (1) will depend not only upon γ but also upon the distribution of the magnetic field. However in the case when there are no preferred orientations of *any* given strength of magnetic field in the radio source the frequency spectrum is proportional only to $\nu^{-\gamma/2}$.

To prove this let us consider these regions of the source in which the magnitude of the magnetic flux density lies between B_0 and (B_0+dB_0) webers/m². Then the power radiated by an electron moving at an angle θ to such a field is given by

$$W(E,\theta)=\frac{e^2}{6\pi\epsilon}\left(\frac{eB_0\sin\theta}{m_0}\right)^2\frac{\beta^2}{c}\left(\frac{E}{E_0}\right)^2\text{ watts}, \quad . \quad . \quad . \quad (6)$$

where $c\beta$ is the velocity of the electron energy E. In the present case the matter density is so low that ϵ can be put equal to the dielectric constant of free space ϵ_0.

It has been shown by Schwinger (1949) that the power spectrum of the energy radiated by a relativistic electron, for which $\beta \approx 1$ is proportional to

$$\nu (E/E_0)^{-2} \int_{\nu/\nu_1}^{\infty} K_{5/3}(\eta)\, d\eta, \quad . \quad . \quad . \quad . \quad . \quad . \quad . \quad . \quad (7)$$

where $$\nu_1 = 1\cdot5 \nu_H \sin\theta (E/E_0)^2, \quad . \quad . \quad . \quad . \quad . \quad . \quad . \quad (8)$$

and $$\nu_H = eB_0/2\pi m_0, \quad . \quad . \quad . \quad . \quad . \quad . \quad . \quad . \quad (9)$$

is the cyclotron frequency of an electron at rest, allowing for changes in units and notation.

For sufficiently small ν the power radiated in unit frequency interval is given by

$$P(\nu, \theta, E) = \frac{3^{1/6}\Gamma(2/3)}{\epsilon_0 c} e^2 \nu_H |\sin\theta| \left(\frac{\nu}{\nu_H |\sin\theta|}\right)^{1/3} \left(\frac{E}{E_0}\right)^{-2/3} \text{ watts}, \quad . \quad (10)$$

while for $\nu > \nu_1$

$$P(\nu, \theta, E) \sim \exp(-\nu/\nu_1),$$

and falls rapidly to zero with increasing ν.

To simplify the algebra we shall assume that $P(\nu, \theta, E)$ is given by eqn. (10) for all $0 < \nu < \nu_L$ and is zero for $\nu > \nu_L$ where

$$\nu_L \approx \nu_1$$

is chosen so that the total power radiated is given by eqn. (6). On this assumption, $P(\nu, \theta, E) = 0$ for given ν, θ if

$$E < E_1 = 0\cdot815 E_0 \left(\frac{\nu}{\nu_H |\sin\theta|}\right)^{1/2}. \quad . \quad . \quad . \quad . \quad . \quad . \quad (11)$$

The error in this procedure is appreciable when considering the radiation from a given electron, but is much less serious when one considers the power spectrum of the radiation emitted from the source as a whole. To find the latter we first integrate over that volume of the source in which the magnitude of the magnetic flux density lies between B_0 and $B_0 + dB_0$ to get the total power radiated into unit frequency by electrons energy E moving at an angle to the magnetic* field. We next integrate over the angle θ. It can thus be shown that the frequency spectrum of the r.f. power generated in this fraction of the volume of the source varies with ν as $\nu^{-\gamma/2}$ a result that is unchanged by the final integration over the distribution of B_0. To agree with experiment we put $\gamma = 1\cdot8$ when

$$P_T(\nu) = \frac{3\cdot0 \bar{\nu}_H^{1\cdot9}}{\nu^{0\cdot9}} n_0 D^3 \times 10^{-36} \text{ watts}, \quad . \quad . \quad . \quad . \quad (12)$$

where $P_T(\nu)$ is the total r.f. power generated in the radio source diameter D, and $\bar{\nu}_H$ is very close to the r.m.s. average of the cyclotron frequency of an electron at rest.

---

* The use of eqns. (7), (10), which give the power spectrum averaged over every possible observer orientation, is only justified in the special assumptions that we have made as to the randomness of the magnetic field distribution.

§ 4. THE MAGNETIC AND RELATIVISTIC ELECTRON FLUX DENSITY

The power density $p_R(\nu)$ of the r.f. radiation received at the earth is given by

$$p_R(\nu)=\frac{P_T(\nu)}{4\pi L^2}\doteq 2\cdot 38\left(\frac{D}{L}\right)^2\frac{n_0 D\bar{\nu}_H^{\,1\cdot 9}}{\nu^{0\cdot 9}}\times 10^{-37}\ \text{watts/m}^2\text{/cycle} \quad . \quad (13)$$

where L is the distance of the radio source from the earth, if for the moment we ignore the resonant reabsorption of energy inside the source.

Substituting for n_0, in the inequality 5 and putting $\gamma=1\cdot 8$ we get that

$$\bar{B}_0^{\,7/2}\geqslant 4\cdot 86\left(\frac{L}{D}\right)^2\frac{1}{D}\frac{\nu^{0\cdot 9}}{\nu_c^{\,0\cdot 9}}p_R(\nu)\times 10^2 \quad . \quad . \quad . \quad . \quad . \quad (14)$$

for the special case where the magnitude of the magnetic flux density is constant throughout the source.

From the numerical values

$$p_R(8\times 10^7)=2\cdot 2\times 10^{-22},\ \ \nu=8\times 10^7,\ \ \nu_c=10^7,\ \ D=1\cdot 6\times 10^{16},\ \frac{L}{D}=572 \quad . \quad . \quad . \quad (15)$$

it follows that the average value of the magnetic field must be greater than $4\cdot 2\times 10^{-3}$ gauss if the total energy stored in the relativistic electron cloud is to be less than 10^{-3} of the total energy in the uniformly distributed magnetic field. Fields of this order of magnitude are only possible if the energy stored in the magnetic trapping field is about 4% of the upper limit to the available kinetic energy, as may be seen from eqn. (4).

The position is somewhat eased if we assume that the mass of the nebulosity is concentrated into a set of smaller regions with a volume l^{-3} that of the whole source. The total kinetic energy is then left unchanged but the total magnetic energy is reduced by a factor

$$l^{-3+12/7}=l^{-9/7}. \quad . \quad . \quad . \quad . \quad . \quad . \quad . \quad . \quad (16)$$

For $l=10$ the local density of ions and magnetic flux would rise to $10^{12}/\text{m}^3$ and $\sim 10^{-6}$ webers/m^2 respectively, while the total magnetic energy would be reduced by a factor $\sim 1/20$.

From the inequality (14) we see that a change of 3 : 1 in the distance of the source D or a change at 10 : 1 in ν_c, the frequency of maximum energy generation, will change the minimum value of the magnetic field strength by factors of 1·37 and 1·7 respectively, so that the theory does not depend critically upon the exact values of these parameters.

§ 5. THE ESCAPE OF THE RADIO FREQUENCY ENERGY

Up to now we have assumed that all the r.f. energy generated by the interaction of relativistic electrons with the magnetic field would escape with negligible reabsorption. To find the conditions under which this is valid, we make use of a thermodynamic argument as follows.

Let $A(E, \theta, \nu)$ be the probability that an electron energy E moving at an angle θ to the magnetic field should spontaneously emit a photon with energy in the range $h\nu \rightarrow h(\nu+d\nu)$ so that

$$h\nu\, A(E, \theta, \nu)=P(E, \theta, \nu) \quad . \quad . \quad . \quad . \quad . \quad . \quad . \quad (17)$$

where $P(E, \theta, \nu)$ is given approximately by eqn. (10) for $\nu<\nu_1$.

If $\rho(\nu)$ is the density of r.f. radiation at a point, it follows from Einstein's radiation laws that the probability of stimulated emission or absorption in unit time is equal to

$$\frac{c\rho(\nu)}{4\pi}B(E, \theta, \nu)$$

where

$$B(E, \theta, \nu)=\frac{c^2}{2h\nu^3}A(E, \theta, \nu). \quad . \quad . \quad . \quad . \quad . \quad . \quad (18)$$

A plane wave frequency ν traversing a medium containing a relativistic electron gas with energies distributed according to the law of eqn. (1) will be attenuated since the number of electrons absorbing energy from the wave is larger than the number that are stimulated to emit. An exact calculation is complicated by the need to allow for the direction and magnitude of the magnetic field at each point in the radio source, but an approximate value for the attenuation can be found by giving $\sin\theta$ its r.m.s. value of 0·707. If the energy carried by the plane wave is then attenuated as $\exp-\alpha z$ we have

$$\alpha(\nu)=\int_{E_1}^{\infty}\frac{\theta E}{E_0}[N(E-h\nu)-N(E)]\frac{B(E, \pi/4, \nu)}{4\pi}h\nu$$

where E_1 is defined by eqn. (11) with $\theta=\pi/4$.

From eqn. (1), (17), (18) we get that

$$\alpha(\nu)=\frac{0{\cdot}87 n_0\bar{\nu}_H{}^{2\cdot4}}{\nu^{3\cdot4}}\times10^{-6}.$$

The attenuation of a plane wave traversing the source along a diameter is

$$\Delta=\alpha D \text{ nepers.}$$

Eliminating $n_0\bar{\nu}_H{}^{1\cdot9}D$ by means of eqn. (13) and using the numerical results of eqn. (15) we get

$$\Delta=3{\cdot}51\frac{\bar{\nu}_H{}^{0\cdot5}}{\nu^{3\cdot4}}10^{21} \text{ nepers}$$

which does not depend explicitly upon the actual distance of the source.

With a magnetic field of 4×10^{-3} gauss

$$\Delta\approx5\times10^{-4} \text{ nepers}$$

at $\nu=80$ Mc/sec, which is negligible. However Δ varies as $\nu^{-3\cdot4}$ and becomes equal to 1 when

$$\nu=\nu_\alpha=10{\cdot}1 \text{ Mc/sec.}$$

If the regions in which appreciable radio power is generated are concentrated into a volume l^{-3} of that occupied by the source as a whole, than the critical frequency at which $\Delta = 1$ is raised by a factor* at least as large as $l^{-0 \cdot 12}$. At frequencies somewhat lower than the critical frequency the power spectrum of the signal received at the earth would be varying as $\nu^{5/2}$, assuming that the power generated in the source was still increasing as $\nu^{0 \cdot 9}$, at least as long as one can neglect or allow for the effects of absorption in the interstellar gas and in the ionosphere.

This critical frequency ν_x is virtually independent of parameters such as D, ν_c or ν_H so that the absence of such an effect in the power spectrum of the radio source in Cassiopeia would be a decisive disproof of the theory developed in this paper.

§ 6. DISCUSSION AND COMPARISON WITH ALTERNATIVE THEORIES

The theory of the discrete radio sources given above requires magnetic fields much larger than those originally proposed by Alfvén and Herlofson (1950) and indeed almost up to the theoretical limit imposed by energy considerations.† Given the existence of such fields a flux of relativistic electrons is not perhaps so implausible. Riddiford and Butler (1952) have given a theory for the production of relativistic particles during the growth of sunspots, and the combination of large scale induction fields and low matter density would seem to favour the operation of their mechanism in the radio source. Furthermore the r.f. power spectrum of the signal received from the source arises naturally when the electron energy spectrum is similar to that observed in the cosmic radiation.

In the model adopted in this paper we have assumed a very high value for the kinetic energy of an individual ion, and even then the total kinetic energy in the source is not much greater than the total magnetic energy. Hutchinson (1952) has considered a model where the particle density is around $10^{15}/\mathrm{m}^3$ and has imposed as an upper limit on the magnetic field the arbitrary condition that the radius of gyration of electrons in thermal motion be large compared to their mean free path. He concludes that appreciable magnetic fields $\sim 10^{-1}$ gauss, might be found in such regions if the electron temperature was $\sim 10^{2 \cdot 7}$ °K. In this case however the magnetic energy density is some ten times greater than the total kinetic energy in the gas, assuming that the ion temperature is not higher than the electron temperature, so the use of this alternative criterion seems invalid. Furthermore to explain the observed radiation intensities, the magnetic fields would have to be of the order of 0·2 gauss if the total mass in the source is to remain comparable with that of the sun. In this case the critical frequency at which resonant reabsorption becomes significant is ~80 Mc/sec, which is inconsistent with the data already available.

---

* This was found assuming that l is so large that no two radiating regions in the source lie in the same line of sight, and that the ratio of the energy stored in the magnetic field to that stored in the relativistic electron gas is kept constant and independent of l.

† There is as yet no direct evidence for the existence of such fields, but in the case of the Cassiopeia nebulosity the interval motion in the individual filaments is so violent that they would be torn to pieces within a few years unless held together by forces which would presumably be magnetic.

A final objection to the hypothesis that the radiating regions are concentrated into a very small fraction of the total volume of the source is that the lifetime of the relativistic particles becomes excessively short. In the case where the matter density is uniform and equal to 10^9 protons/m^3 the radiation at 80 Mc/sec is provided largely by electrons with energies ~30 MeV. The rate of energy loss due to r.f. radiation is then somewhat larger than that due to inelastic collisions, and appreciably greater than that due to bremsstrahlung, and the lifetime of electrons of this energy is of the order of magnitude of 10^3 years. If the matter density in the radiating regions is as high as 10^{15} particles/m^3 the rate of energy loss due to collisions is increased by 10^6 while the particle energy is decreased by 10, assuming that the ratio of the energy stored in the magnetic field to that in the relativistic electron gas is kept constant. Under these conditions the lifetime of a relativistic particle is of the order of magnitude of one hour and the fraction of the energy lost by r.f. radiation is negligible.

The possibility that the radiation from the discrete sources might be thermal in origin has recently been revived by Hoyle (1953) who suggested that charge separation in the ionized gas might enable one to explain the frequency spectrum of the radiation. From the relative velocities of individual filaments of the nebulosity in Cassiopeia it seems plausible that the electron temperature could be 10^8 °K which is still somewhat larger than the effective radiation temperature of $7\cdot10^7$ °K at 80 Mc/sec. However, recent results by Hey and Hughes (private communication) have shown that the noise powers received from the discrete sources in Cassiopeia and Cygnus in unit frequency band are still rising with wavelength at 22 Mc/sec. From this data the true electron temperature in the Cassiopeia source would have to be at least as high as 10^{10} °K which seems incredible.

The remaining alternative is that the radiation is due to some organized phenomenon such as plasma oscillations. This is by far the most attractive theory from the energy point of view, though it would seem to require that the ionized matter be concentrated in regions where the density is ~10^{14} electrons/m^3 if appreciable radiation* is to be produced at frequencies ~100 Mc/sec. Up to the present however no quantitative theory of radiation from such oscillating plasmas has been evolved so that the hypothesis cannot as yet be tested directly against experiment.

It must be admitted that the radio source in Cassiopeia has been identified with a very peculiar object, quite different from that associated with the Crab nebula source in Taurus and even less akin to the source in Cygnus, which is thought to be two colliding extra galactic nebulae

---

* The plasma resonance frequency is approximately equal to $10N^{1/2}$ where N is the number of free electrons per cubic metre.

(Baade and Minkowski). Furthermore there is no reason to believe that the majority of the discrete sources are of either of these types. Nevertheless it is quite possible that the basic mechanism in all these cases is the one discussed in this paper. This seems especially plausible in the case of the Cygnus source, from which the power received on the earth is $1{\cdot}3\times10^{-22}$ watts/cycle/m^2 at a frequency of 80 Mc/sec. This source can be represented as an ellipse with angular axes of 1′ and 4′ of arc respectively so that its effective black body temperature at 80 Mc/sec $\sim 2{\cdot}6\times10^{8}$ °K while at 20 Mc/sec this effective temperature has risen to $1{\cdot}6\times10^{10}$ °K assuming that the power output increases as ν^{-1}. Since the true electron temperature would have to be considerably greater still the black body mechanism would seem to be completely ruled out. Furthermore the average density of the residual interstellar gas in the colliding galaxies is likely to be far too small to allow one to attribute the r.f. radiation to coherent plasma oscillations. It is not easy to estimate the thickness of the radiating region in the Cygnus source without which one cannot calculate the average magnetic flux density. However the lowest possible value for the critical frequency at which resonant reabsorption becomes important is virtually independent of the thickness of the source and since the absolute brilliance of the source in Cygnus is about four times that of the source in Cassiopeia the lowest value of the critical frequency is about $4^{(1/3\cdot4)}\approx1{\cdot}5$ times greater in the former case, and is therefore 15 Mc/sec as opposed to 10 Mc/sec for the Cassiopeia source.

§ 7. CONCLUSIONS

If the r.f. radiation from the discrete sources within our own galaxy is to be attributed to the interaction of a relativistic electron gas with a local magnetic field we have shown that the energy stored in the latter cannot be negligible compared with the total kinetic energy of the ionized gas in the radio source. Assuming that the magnetic flux density in the source is randomly distributed with no preferred orientation in space we have shown that the r.f. power spectrum is determined by the energy spectrum of the electron gas. The experimental data can be met if the differential energy spectrum is proportional to $(E/E_0)^{-2\cdot8}dE/E_0$ where E_0 is the rest energy, which is approximately the same as the spectrum of the primary cosmic radiation in the neighbourhood of the sun.

A crucial test of the theory is that the frequency power spectrum, of the radiation received at the earth should reach a maximum somewhere in the range 10–20 Mc/sec and thereafter decrease rapidly with decreasing frequency at least as fast as $\nu^{5/2}$ and faster still if additional absorption is taking place in the ionosphere or in interstellar gas clouds. If the frequency power spectrum does not vary in the manner predicted by the theory discussed in this paper one would seem to be forced to look for a coherent mechanism as the origin of the radiation from the discrete sources.

ACKNOWLEDGEMENT

Acknowledgement is made to the Admiralty for permission to publish this paper.

REFERENCES

ALFVÉN, H., and HERLOFSON, N., 1950, *Phys. Rev.*, **78,** 616.
BAADE, W., and MINKOWSKI, R., *Astrophysical Journal* (in publication).
GINSBURG, V. L., 1951, *Doklady Akad. Nauk, S.S.S.R.*, **76,** 377.
HANBURY-BROWN, R., and HAZARD, C., 1953, *Phil. Mag.*, **44,** 939.
HANBURY-BROWN, R., JENNISON, R. C., DAS GUPTA, M. K., MILLS, B. Y., and SMITH, F. G., 1952, *Nature, Lond.*, **170,** 1061.
HEY, J. S., and HUGHES, V. A., private communication.
HOYLE, F., 1953, *Nature, Lond.*, **172,** 296.
HUTCHINSON, G. W., 1952, *Phil. Mag.*, **43,** 847.
RIDDIFORD, L., and BUTLER, S. T., 1952, *Phil. Mag.*, **43,** 447.
RYLE, M., 1950, *Reports on Progress in Physics*, 218.
SCHWINGER, J., 1949, *Phys. Rev.*, **75,** 1912.
UNSÖLD, A., 1949, *Nature, Lond.*, **163,** 489.

XXX. *Special Mechanisms in the Reaction* ^{7}Li(pγ)^{8}Be

By D. H. Wilkinson
Cavendish Laboratory, Cambridge†

[Received December 29, 1953]

Abstract

The course of the reaction ^{7}Li(pγ)^{8}Be is an unusual one: above the strong resonance at $E_p=440$ kev the cross section shows a background that, apart from weak resonances, increases steadily with increasing proton energy until at least $E_p=5\cdot2$ Mev. It is suggested that this background has two origins: at the lower values of E_p it is due to direct radiative transitions between a free proton state and a bound state of ^{8}Be—no compound nucleus is formed; at the higher values of E_p it is due to a process inverse to the familiar 'giant resonances' of photodisintegration. The first contribution is calculated for a variety of conditions in LS and in *jj* coupling; the second is deduced from the known properties of neighbouring photodisintegration cross sections. The two processes together give a good account of the experimental results; there is some suggestion that the 'radius' of ^{8}Be may be about $3\cdot2\times10^{-13}$ cm.

§ 1. Excitation Functions

The reaction ^{7}Li(pγ)^{8}Be ($Q=17\cdot24$ Mev) has been known for many years to be resonant at a proton energy of 440 kev with the production of hard gamma-rays that lead to the ground state (0+) and first excited state ((2+) at 3·0 Mev) of ^{8}Be. This resonance of width 12 kev is shared by ^{7}Li(pp)^{7}Li and is (1+) (see Ajzenberg and Lauritsen (1952), also Devons (1953)). It behaves in every way like a normal resonance and represents conventional compound nucleus formation. However it has also been known for many years that above this resonance the yield of gamma-rays is substantially greater than may be explained in terms of this resonance alone. With increasing proton energy E_p the cross section $\sigma_{p\gamma}$ passes through a shallow minimum at about $E_p=700$ kev (where it has about 1·5% of its value at the peak) through weak resonances at $E_p=1\cdot05$ Mev (known also from ^{7}Li(pp)^{7}Li and ^{7}Li(pp$'$)^{7}Li*) and at $E_p=2\cdot0$ Mev (seen possibly in ^{7}Li(pp)^{7}Li). Above 2·5 Mev the cross section increases ever more rapidly until $E_p=5\cdot2$ Mev, the highest energy so far used; in this range there are certainly no resonances of relative strength comparable with those displayed by ^{7}Li(pp)^{7}Li and ^{7}Li(pn)^{7}Be at 2·22 Mev by ^{7}Li(pα)^{4}He at 3·0 Mev or by ^{7}Li(pn)^{7}Be at 4·9 Mev. The course of ^{7}Li(pγ)^{8}Be above $E_p=500$ kev is illustrated in fig. 1 where is also shown the calculated contribution at higher energies from the E_p=440 kev resonance.* (The curve up to E_p=600 kev is that due to Bonner and Evans (1948) with the cross section scale of Fowler and Lauritsen (1949) (a small correction has been applied on account of the finite target thickness in the work of Bonner and Evans); above 2·5 MEV the curve is that of Bair, Willard, Snyder, Hahn, Kington and Green (1952); the link between the two has been supplied by P. C. Price in this laboratory—though it was earlier clear from the work of Hudson, Herb and Plain (1940) and Hill and Shoupp (1948) that no strong resonances exist in this region.†)

---

† Communicated by the Author.

Fig. 1

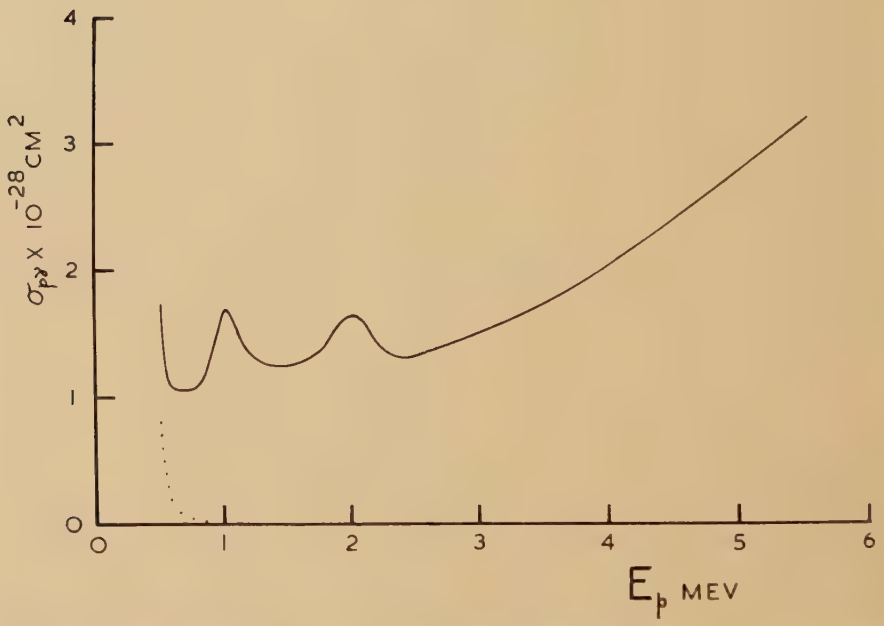

The total cross section $\sigma_{p\gamma}$ for the production of hard radiation in the reaction ^{7}Li(pγ)^{8}Be above the 440 kev resonance (peak cross section 66×10^{-28} cm^2). The dotted curve shows the calculated contribution from the resonance at 440 kev.

---

* We have used a peak cross section of 6·6 mb and a width of 12·2 kev (Hunt 1952) with Coulomb wave functions for p-wave protons and a nuclear radius of $3{\cdot}2\times10^{-13}$ cm (other radii in the range $2{\cdot}8\times10^{-13}$ cm to $4{\cdot}4\times10^{-13}$ cm considered later in this paper give contributions that differ by less than 15% from that shown in fig. 1).

† The local measurements were made in bad geometry at 0° and 90° to the proton beam with an NaI(Tl) crystal biased at 12 MEV; the excitation functions differ only slightly between these positions. But it is known (Devons and Hine 1949; Stearns and McDaniel 1951) that the gamma radiation shows quite strong anisotropy in this range of E_p and so we may only take the $\sigma_{p\gamma}$ of fig. 1 as an approximate indication that is, however, amply good enough for our present purpose. We must also ignore in our estimate of $\sigma_{p\gamma}$ the differing effects of the two strong components of the hard radiation on the measuring instruments employed by the various workers.

It is clear from fig. 1 that the resonance at $E_p=440$ kev is quite inadequate to explain the background radiation at say $E_p=700$ kev; nor are the contributions from the weak resonances at 1·05 MeV and 2·0 MeV nearly enough to explain the background. The course of $\sigma_{p\gamma}$ above 2·5 MeV is also rather curious: it displays no strong resonances of its own nor does it appear to share strongly those displayed by other reactions. It is always, of course, possible to explain an excitation function such as the present one by the hypothesis of several broad overlapping compound nucleus resonances. This explanation is not universally attractive and it is the purpose of this note to see whether $\sigma_{p\gamma}$ may be explained in an alternative fashion that does not involve *ad hoc* hypothesis.

§ 2. DIRECT TRANSITIONS

Broadly speaking there seem to be two ways by which nuclear reactions may proceed: via the formation of a compound nucleus (two-stage processes involving most naturally the product of two matrix elements) or without compound nucleus formation (direct or one-stage processes described by a single matrix element). Among the heavy nuclei the two-stage process is that almost always considered although direct processes are occasionally contemplated (e.g. Courant (1951)) and recent developments have opened the possibility of an extension of essentially ‘single-particle’ ideas to free nucleon states (Feshbach, Porter and Weisskopf 1953). But in the very lightest nuclei direct processes appear to be the rule (e.g. ^{2}H(γp)n--the classic example; ^{2}H(pγ)^{3}He—Wilkinson (1952); ^{3}H(pγ)^{4}He—Flowers and Mandl (1951); the D–D reactions—Konopinski and Teller (1948)). We must then expect to find traces of direct processes in light nuclei in general, perhaps most clearly in the lightest where the density of compound nucleus states is not great and where single particle behaviour in free states is strongest.

We shall then envisage the possibility that the background radiation in ^{7}Li(pγ)^{8}Be is not due to compound nucleus formation but is due rather to a one-stage process in which a free proton makes a direct transition to the ground state or to an excited state of ^{8}Be. Such a direct transition would not show sharp resonances but only the broad ones characteristic of a particle moving in a central field of force to which we would approximate our system ^{7}Li+p (free state) or ^{8}Be (bound state).

It is probable that a one-stage process is seen also in the interaction of fast *neutrons* with ^{7}Li. The total cross section rises slowly and steadily towards a value of about 2 barns at $E_n=4$ MeV (Bockelman, Miller, Adair and Barschall 1951) which value seems rather large unless it is supposed that many broad compound nucleus states overlap—in fact the course of the cross section for ^{7}Li(nn)^{7}Li looks remarkably like that for ^{7}Li(pγ)^{8}Be. However, if one assumes that the neutrons are simply scattered by a square potential well whose radius is that determined from the neutron cross section at higher energies (see § 5) and whose depth is adjusted to give the correct binding energy for the last ($1p_{3/2}$) neutron in ^{8}Li, a theoretical cross section is obtained whose form and absolute magnitude are in excellent agreement with experiment (all partial waves must be taken into account). The observation of one-stage nuclear effects in ^{7}Li(pp)^{7}Li is more difficult because of the existence of Coulomb scattering and because the Coulomb barrier greatly diminishes their absolute importance. It appears that some potential scattering may be found (see Ajzenberg and Lauritsen (1952)).

We shall therefore compute the cross section expected for a direct radiative transition in ^{7}Li(pγ)^{8}Be to see to what degree it may contribute to the background radiation. One advantageous circumstance is that an s-wave proton which will be able most easily to penetrate the Coulomb barrier will be able to make an E1 transition to its final $1p_{3/2}$ state in ^{8}Be and so the direct transition will be a stronger one than if magnetic or higher order electric radiation were involved.

In order to make the calculation a model is required. Here, at the beginning of the problem, we must admit that we cannot hope to make a very realistic computation since we have so little to guide our choice of the effective potential within which we imagine these happenings to take place. In view of this ignorance—and to simplify the algebra—we fall back on the notion of a square well of radius r_0 and depth V and suppose that the same parameters apply as well to the initial state of s-wave proton plus ^{7}Li as to the final bound states of ^{8}Be. (We shall ignore d-wave effects since even at $E_p=5$ the penetrability of the barrier for $l=2$ protons is not large.)

The first step in the computation is to work out the ‘ single particle ’ cross section $\sigma'_{p\gamma}$ corresponding to the capture of an s-wave proton into a 1p state of a featureless well. (In $\sigma'_{p\gamma}$ we ignore the spin of the proton but allow for the finite mass of the ‘ well ’ by using the reduced mass of $\frac{7}{8}$ nucleon masses ; we also ignore the fact that the ‘ well ’ is charged—we use for $\sigma'_{p\gamma}$ the full proton charge instead of the effective charge.) We must note that the actual direct cross section $\sigma_{p\gamma}$ is not $\sigma'_{p\gamma}$ but rather

$$\sigma_{p\gamma}=K\sigma'_{p\gamma}, \qquad \ldots \ldots \ldots \quad (1)$$

where K is the factor modifying the ‘ single particle ’ cross section on account of the facts : (i) that we are only interested in those s to p transitions that lead to a final $1p_{3/2}$ state ; (ii) that the effective proton charge is less than e ; (iii) that the real reaction carries a different statistical weight factor from the ‘ single-particle ’ model ; (iv) that in the real system several equivalent $1p_{3/2}$ nucleons are involved so that care must be taken that initial and final state wave functions are properly antisymmetrical ; (v) that the ‘ single particle ’ system is of $T=\frac{1}{2}$ whereas the real system may be formed initially in $T=0$ or $T=1$

states. (The excited (2+) state at 3 Mev* in ^{8}Be which we must consider is also regarded as belonging to the same configuration of four $1p_{3/2}$ nucleons as the ground state.)

K will depend on the coupling scheme adopted. It appears (Christy 1953, Inglis 1953) that, in the lightest nuclei, LS coupling may be a more realistic approximation than *jj*. We adopt LS coupling in order to give an explicit discussion, although the results are not very sensitive to the coupling scheme. In this scheme the ^{7}Li ground state belongs to ^{22}P which may couple to the approaching s-wave proton to give ^{31}P, ^{13}P, ^{11}P and ^{33}P states. The states of ^{8}Be to which E1 transitions are to be made are taken as ^{11}S and ^{11}D. Such transitions from the initial ^{33}P and ^{13}P states are forbidden by the LS coupling rule on E1 transitions: $\Delta S=0$. E1 transitions from the ^{11}P state are forbidden by the isotopic spin rule independent of coupling scheme†: $\Delta T=\pm 1$ (which would also forbid those from the ^{13}P states).

The only term contributing to the present capture process is therefore ^{31}P (i.e. $J=(1-)$, $T=1$, $L=1$, $S=0$). K may be written as $\frac{3}{16}C$ which contains the statistical weight factor of $\frac{3}{8}$, another factor of $\frac{1}{2}$ because only the $T=1$ states are allowed to radiate by the isotopic spin rule, and where C takes care of points (i), (ii) and (iv) above; C may be computed following the procedure of Lane and Radicati (1953)—see Appendix—and is $\frac{1}{9}$ for transitions to the (0+) ground state and $\frac{7}{18}$ for those to the (2+) excited state of ^{8}Be. This means that, neglecting effects due to the small energy difference between the two transitions, we should find $\frac{7}{2}$ times as many gamma-rays leading to the excited state as to the ground state. In the same approximation, if $\sigma_{p\gamma}$ represents the combined cross section for transitions to both states we may set $C=\frac{1}{2}$.‡

The calculation of $\sigma'_{p\gamma}$ is complicated by the need to take into account the Coulomb distortion of the incident proton wave. The complication is the greater when it is remarked that, as is common in light elements, the larger contribution to the matrix element for the transition comes from the region outside the potential well. However, as will be seen, our ignorance of the most appropriate value for r_0 introduces considerable uncertainty into $\sigma'_{p\gamma}$ and it is perhaps not too gross an approximation to compute the cross section $\sigma'_{p\gamma 0}$ for a chargeless proton and relate it to $\sigma'_{p\gamma}$ by means of the expression for barrier penetrability

---

* It has been suggested (Erdös, Scherrer and Stoll 1953) that in fact this state at 3 Mev is multiple. This does not appear to be incontrovertibly established and we shall regard the state for the present purpose as single: provided the states belong to the $(1p_{3/2})^4$ configuration our general conclusions will be little altered.

We should perhaps also notice that our present considerations are essentially in terms of an independent-particle central-field model and that if the low-lying states of ^{8}Be involved are better represented by, say, alpha-particle wave-functions the present computation—though not the general thesis—must be abandoned.

We may also say here that we ignore the weak transitions that may take place to higher excited states of ^{8}Be (Nabholtz, Stoll and Wäffler 1951, Inall and Boyle 1953).

† This may well not be a very potent rule in practice at such high excitation.

‡ In *jj* coupling the ratio of the two transitions, to the excited state and to the ground state is $\frac{3}{2}$ and the composite $C=\frac{5}{18}$—see Appendix.

$$\sigma'_{p\gamma}=\sigma'_{p\gamma 0}\frac{1}{F^2+G^2}, \qquad \qquad (2)$$

where F and G have their usual meanings. This procedure is not by any means unexceptionable but is adequate in view of the considerable uncertainties residing elsewhere.* In defence of this rough procedure it may be said that the 'distance travelled' by the incident proton in a region of negative kinetic energy is, in the range of E_p of interest here, very much less than one wavelength for all values of r_0 that we shall consider† and that in any case F^2+G^2 is rather small (less than 2 for $E_p=1$ MeV and the values of r_0 considered here).

The calculation of $\sigma'_{p\gamma 0}$, the 'single particle' cross section for a chargeless proton, proceeds along familiar lines. It is convenient to define some symbols :

$|W|$=binding energy ;

$E=\hbar\omega-|W|$=energy of the system in centre-of-mass space$=\frac{7}{8}E_p$;

$$a^2=\frac{2m}{\hbar^2}|W| ; \qquad ar_0=\zeta-1 ;$$

$$b^2=\frac{2m}{\hbar^2}(V+E) ; \qquad br_0=\phi ;$$

$$c^2=\frac{2m}{\hbar^2}(V-|W|) ; \qquad cr_0=\nu ;$$

$$k_p{}^2=\frac{2m}{\hbar^2}E ; \qquad k_pr_0=\xi ;$$

$$\frac{V}{|W|}-1=\chi.$$

---

* Thomas (1952) has discussed the external contribution to (pγ) reactions with correct allowance for the external Coulomb wave functions. To apply this treatment in the present case would hardly be justifiable ; it demands knowledge of the relevant reduced widths, knowledge that, in terms of our model is equivalent to knowledge of r_0 to which, as we have remarked, the results of the present computation are rather sensitive. At least the ground state and first excited state reduced widths may ultimately be forthcoming from ^{7}Li(dn)^{8}Be or even ^{7}Be(dp)^{8}Be stripping and a more realistic account of the external wave-functions may then be desirable.

† For $E_p=1$ MeV and $r_0=3{\cdot}2\times10^{-13}$ cm the region of negative kinetic energy extends only 0·04 free space wavelengths ; substantially larger values of r_0 may be operative in practice as will be seen.

(Note that $a^2+k_p{}^2=b^2-c^2$ and that $\nu=(\zeta-1)\chi^{1/2}$.) The radial wave functions for initial and final states are :

$$\begin{aligned} R_i &= Xj_0(br) && r\leqslant r_0 \\ &= \left(\frac{2mk_p}{\pi\hbar^2}\right)^{1/2}\frac{\sin\,(k_pr+\epsilon)}{k_pr}, && r\geqslant r_0 \\ R_f &= Yj_1(cr) && r\leqslant r_0 \\ &= Z\,\frac{1+ar}{r^2}\,\mathrm{e}^{-ar} && r\geqslant r_0 \end{aligned}$$

where m is the reduced mass of the system and ϵ, X, Y and Z are to be adjusted in the usual way to secure both continuity at $r=r_0$ and the normalization :

$$\int_0^\infty R_f{}^2r^2\,dr=1.$$

(R_i is already normalized 'per unit energy'.)

For a given well radius r_0 the well depth V is given in terms of the binding energy $|\,W\,|$ by

$$\nu\cot\nu=1+\zeta\chi.$$

We now use the standard result

$$\sigma'_{\mathrm{p}\gamma 0}=24\,\frac{\pi^2}{k_p{}^2}\,\frac{\omega^3}{c^3}\,|\,M\,|^2,$$

in which we have summed over the final substates of the 1p particle. M, the matrix element for the transition, is given by

$$M=e\int\psi_i z\psi_f\,d\tau,$$

where ψ_i is to be normalized 'per unit energy' as above.

Integration over the angle variables gives the selection rule $\Delta m=0$ and we find (the angular wave-functions are normalized to unity over the sphere)

$$\sigma'_{\mathrm{p}\gamma 0}=\frac{8}{3}\,\frac{\pi^2}{k_p{}^2}\,\frac{\omega^2}{c^2}\,\frac{e^2}{\hbar c}\,\hbar\omega\left\{\int_0^\infty R_iR_fr^3\,dr\right\}^2.$$

The evaluation of the overlap integral is elementary and we find

$$\sigma'_{\mathrm{p}\gamma 0}=\frac{32\pi}{3}\,\frac{e^2}{\hbar c}\,\frac{V^2}{mc^2\hbar\omega}\,r_0{}^2\,\frac{\chi^2\zeta^2}{\xi(\xi^2+\phi^2\cot^2\phi)\{\nu^2\operatorname{cosec}^2\nu+(1+\zeta)\chi^2+\zeta\chi-1\}},$$

which we relate to $\sigma_{\mathrm{p}\gamma}$ using (1) and (2).

We must now decide what value is appropriate for $|\,W\,|$. The natural choice for the binding energy may seem to be that of the last proton in ^{8}Be namely 17·24 MEV. It may, however, properly be argued that we should use rather some value representative of the mean binding of the four equivalent 1p$_{3/2}$ nucleons. But within the rather limited aims of the present calculation it is not necessary to consider this refinement and we set $|\,W\,|=17{\cdot}24$ MEV. Similarly we do not consider it worthwhile to perform a new computation for transitions to the 3 MEV state of ^{8}Be but rather take the same $\sigma'_{\mathrm{p}\gamma 0}$ to apply to them also.

One reason for our neglect of these details is that the predicted cross section is rather sensitive to our choice of r_0 and we have little to guide us in making this choice. Figure 2 shows $\sigma_{p\gamma}$ as a function of r_0 within the range $2{\cdot}8\times10^{-13}$ cm to $4{\cdot}4\times10^{-13}$ cm for $E_p=870$ kev. It is seen that within this range of r_0, $\sigma_{p\gamma}$ passes through quite a sharp maximum owing largely to the maximizing of the overlap integral (the vanishing of cot ϕ) and that the theoretical prediction of $\sigma_{p\gamma}$ must therefore be subject to considerable uncertainty. Figure 3 presents the total calculated direct cross section $\sigma_{p\gamma}$—including transitions to both final states of ^{8}Be—as a function of E_p for $r_0=3{\cdot}2\times10^{-13}$ cm.*

Fig. 2

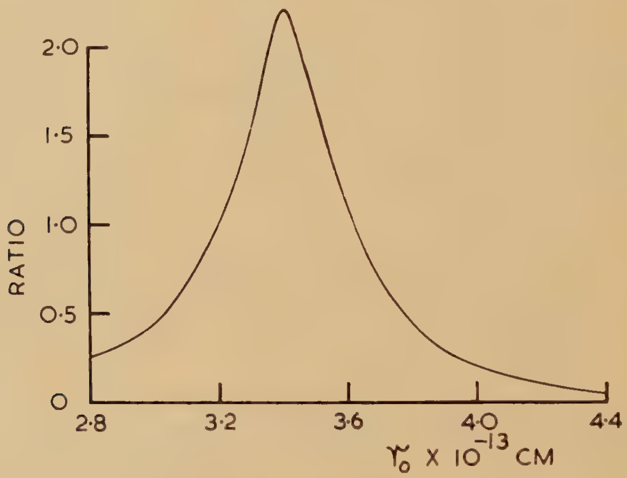

The variation of the direct transition cross section $\sigma_{p\gamma}$ (in LS coupling) with the well radius r_0 at a proton energy of $E_p=870$ kev. $\sigma_{p\gamma}$ is normalized to unity at $r_0=3{\cdot}2\times10^{-13}$ cm.

If we compare fig. 3 with fig. 1 two points are clear: one is that the direct transitions appear amply able to explain the background radiation immediately above the 440 kev resonance; the other is that they are unable to explain the magnitude and form of the cross section at higher proton bombarding energies.† $\sigma_{p\gamma}$ as calculated for a direct transition inevitably falls rather rapidly as E_p becomes large because of the decrease in the proton wavelength; the experimental curve shows just the opposite effect—a persistent and ever-more-rapid rise of $\sigma_{p\gamma}$ with increasing E_p. Figure 2 shows that a theoretical direct cross section in agreement with the experimental background radiation at low values of E_p may easily be obtained within the range of r_0 considered.

---

* This value of r_0 has been chosen approximately to maximize the cross section at $E_p=5$ Mev, i.e. such that $\phi\sim\frac{3\pi}{2}$ at high E_p values.

† The inclusion of d-wave transitions does not modify this general conclusion nor does the inclusion of transitions of higher multipole order.

Another piece of evidence that may be adduced in favour of this suggestion of direct transitions is the energy spectrum of the capture radiation above the 440 kev resonance. At this resonance the transitions to the ground state of ^{8}Be outweigh those to the 3 Mev state by roughly 2 : 1 (Walker and McDaniel 1948). It was noticed by Tangen (1947) that above resonance the proportion of the lower energy component increases and Stearns and McDaniel (1951) showed that at E_p=1 Mev* the softer radiation predominates by a factor of order 2 or more. As we have seen above, on LS coupling, the expected ratio of transitions to excited and ground states is 7 : 2 and on *jj* coupling it is 3 : 2.† We must remark that Stearns and McDaniel's work includes the 1·05 Mev resonance ; however, even allowing for the possibility that the whole of this resonant contribution is to the excited state it appears that the remaining background radiation also favours the excited state. These workers also found a fairly strong angular distribution at E_p=1 Mev for both components. If our present suggestion is correct the background radiation alone should be largely isotropic although one must be prepared to find interference effects due to relatively weak underlying resonances. Such interference effects are well known at low values of E_p from the work of Devons and Hine (1949) who observed interference between

Fig. 3

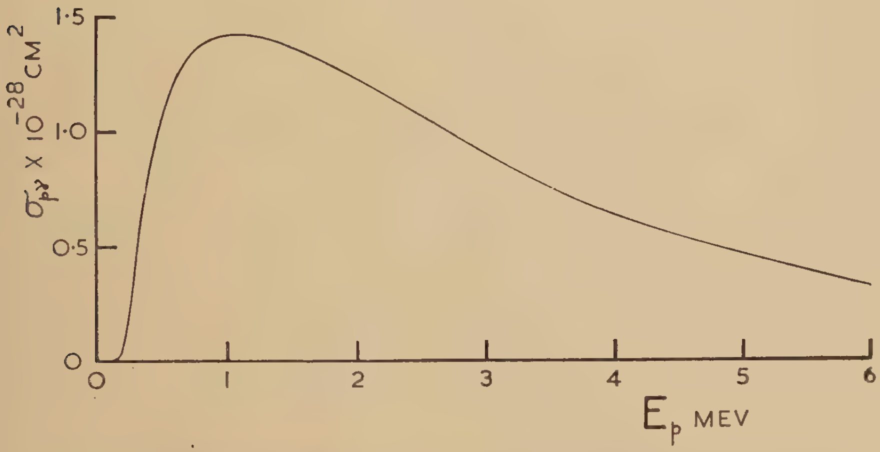

The total direct cross section $\sigma_{p\gamma}$ (in LS coupling) as a function of E_p for a well radius r_0=3·2×10^{-13} cm.

---

* E_p=1·15 Mev and a target of thickness 250 kev.

† Another possible contributing factor to the preference of the radiation for the excited state is that the latter may indeed be multiple—a possibility noticed in § 2.

the 440 kev level (now known to be (1+)) and a broad background of opposite parity. It appears that the presently-suggested direct transition may well supply the interference since it involves a parity change. Again we should notice that although we may reasonably neglect the contribution to the total $\sigma_{p\gamma}$ of direct d-wave proton capture their interference terms may still be quite strong and cause a significant departure of the background radiation itself from isotropy.

We may summarize our discussion of direct capture by saying that it seems well able to explain the background radiation at not-too-high values of E_p, has the correct parity to produce the interference effects above $E_p=440$ kev and predicts correctly that the 3 MEV state should be favoured in the non-resonant regions but appears inadequate to explain the smooth and persistent increase in the capture cross section towards high values of E_p.

A more detailed account than the present one appears to be unjustified at present owing to our ignorance of the effective well shape and size, the considerable sensitivity of the theoretical cross section to the latter and also, it must be said, the approximation involved in representing the behaviour of the incident proton within the well by a free-particle wave function. A more detailed calculation should certainly replace the present procedure of the use of the penetration function by one in which proper Coulomb wave functions are used in the evaluation of the overlap integral.

§ 3. THE GIANT RESONANCE

The relatively smooth and uneventful increase in the capture cross section at high proton energies may, of course, be explained by the usual *deus ex machina* of broad resonances. It does seem most unlikely at all events that it is due to a single conventional compound nucleus resonance. $\sigma_{p\gamma}$ at $E_p=5$ MEV is about 3×10^{-28} cm^2 and is still rising. We suppose that the radiation is E1 ; the resonance is $(1-)\,T=1$ so that the gamma-ray transition is allowed while the alpha-particle break-up is in any case forbidden by the symmetry rules. The smallest value of Γ_p consistent with the smooth excitation function is 2–3 MEV ; $\Gamma_p=3$ MEV corresponds to $\Gamma_\gamma>20$ kev or $(2J+1)\,|\,M\,|^2>4{\cdot}8$ in Weisskopf units (Weisskopf 1951). This value of $(2J+1)\,|\,M\,|^2$ is 10 times greater than any other found in light nuclei for E1 transitions (Wilkinson 1953) and shows that a single conventional resonance level is of no use and, indeed, that several would be needed.

An alternative explanation that does not involve an *ad hoc* hypothesis is that we are indeed dealing with a level of the compound nucleus but one of an unusual kind ; that we are seeing here the inverse process to the famliar ‘ giant resonance ’ of photodisintegration.

Throughout the periodic table from the lightest to the heaviest elements ‘ giant resonances ’ are found in (γn), (γp) and other photo-processes. The gamma-ray energy at which these resonances are found varies slowly and smoothly and with little local fluctuation from about 24 MEV for light elements to about 13 MeV for heavy elements (see, for example, Montalbetti, Katz and Goldemberg (1953)). Furthermore, the widths of the resonances do not show great variation and the values of the integrated cross section across the 'giant resonance' vary smoothly and regularly with atomic weight (see, for example, Jones and Terwilliger (1953)). Since all nuclei so far investigated show without exception the same behaviour it seems reasonable that the reaction ^{8}Be(γp)^{7}Li should fit into the same general scheme.*

Many 'giant resonances' are known in light nuclei but perhaps the most realistic procedure for predicting the behaviour of ^{8}Be(γp)^{7}Li is to select the nearest one in a nucleus resembling ^{8}Be in having high binding energies for neutron and proton. The nearest are ^{12}C(γn)^{11}C and ^{12}C(γp)^{11}B; the respective peak energies E_m are 22·9 and 21·5 MeV with widths Γ_g of 2·8 and 1·7 MeV and the cross sections integrated across the resonances are 46 MeV-mb and 63 MeV-mb† (Katz and Cameron 1951, Halpern and Mann 1951). According to the dipole sum rule the integrated cross section should vary as NZ/A (Levinger and Bethe 1950) and this suggests, using the mean of the ^{12}C(γn)^{11}C and ^{12}C(γp)^{11}B results, an integrated cross section of 38 MeV-mb over the resonance for ^{8}Be(γp)^{7}Li. This may be compared with the 22 MeV-mb suggested by the empirical formula of Jones and Terwilliger (1953), namely that the integrated cross section up to $\hbar\omega=27\cdot5$ Mev for neutron production* is $5\cdot2\times10^{-4}\times A^{1\cdot8}$ Mev-barns.

---

* It is known that these 'giant resonances' involve co-operative motion between the nucleons (perhaps of an extreme kind—see Goldhaber and Teller (1948)) and represent a fair fraction of the entire available dipole sum. This means that we may expect in them to find a value of $|M|^2$ considerably greater than unity.

† It does not appear certain that E_m and Γ_g are significantly different for the two reactions. If they are indeed different a breakdown of charge-independence is not necessarily implied since the thresholds for the two reactions (18·71 MeV for ^{12}C(γn)^{11}C and 15·95 MeV ^{12}C(γp)^{11}B) are sufficiently different and sufficiently close to E_m in the (γn) case to give quite a strong 'phase space' preference to the proton-producing reaction; this argument applies even more strongly to transitions to the first excited states (1·85 MeV in ^{11}C; 2·14 MeV in ^{11}B). It thus appears quite possible that the true Γ_g is somewhat larger than either of the values for the individual reactions and that the different values exhibited by (γp) and (γn) are due to the increasingly successful neutron competition at higher gamma-ray energies. In support of this suggestion we may note that the integrated cross section for the (γp) reaction is reported to be the higher of the two by about 50%. We should then, roughly speaking, add to the observed Γ_g the difference of the E_m values giving a true Γ_g of about 3·5 MeV. In fact the Γ_g values for ^{12}C(γn)^{11}C and ^{12}C(γp)^{11}B are by far the smallest displayed by any nucleus, the usual run being 4–6 MeV, though this effect may be a consequence of the unusually tight nucleon binding in ^{12}C.

A similar but not such extreme case is presented by ^{8}Be(γn)^{7}Be and ^{8}Be(γp)^{7}Li (respective binding energies 18·89 and 17·24 MeV) and we are probably safe in ignoring the difference between the (γn) and (γp) integrated cross sections. It may be, however, that we should use a rather larger value of Γ_g than that given by the individual reactions in carbon for the reasons just stated. Because of the uncertain experimental situation we do not feel justified in modifying Γ_g and shall use the experimental values as they stand, noting that they may be too small for our application.

We therefore adopt as the hypothetical constants for the ^{8}Be(γp)^{7}Li reaction: $E_m=22\cdot2$ Mev; $\Gamma_g=2\cdot3$ Mev; integrated cross section 30 Mev-mb (the mean of the two estimates). For E_m and Γ_g we have again used the mean of the carbon values. We may have confidence that these predicted values are accurate to about ±1 Mev in the energies† and perhaps $\pm50\%$ in the integrated cross section.

We may now relate this $\sigma_{\gamma p}$ to the desired $\sigma_{p\gamma}$ by detailed balance provided we have some idea about the proton spectrum from the ^{8}Be(γp)^{7}Li reaction. The second excited state of ^{7}Li at 4·61 Mev only becomes energetically available to ^{8}Be(γp)^{7}Li above the equivalent E_p value of 5·27 Mev and so may be ignored in the present discussion. The two available states in ^{7}Li are the ground state ($\frac{3}{2}-$) and the ($\frac{1}{2}-$) state at 0·478 Mev; the 'giant resonance' is ($1-$) so we may suppose that half the 'giant resonance' $\sigma_{\gamma p}$ represents transitions to the ground state of ^{7}Li, it and the alternative state being reached by s-wave transitions of almost the same energy.‡ So now

$$\sigma^0{}_{p\gamma}=\sigma_{\gamma p}\frac{1}{4}\frac{k_\gamma{}^2}{k_p{}^2},$$

where $\sigma^0{}_{p\gamma}$ represents that part of the 'giant resonance' capture that leads to the ground state of ^{8}Be and $\sigma_{\gamma p}$ is one half of that 'giant resonance' photodisintegration cross section derived above.

We must also anticipate 'giant resonance' capture to the first excited state of ^{8}Be at 3 Mev. The photodisintegration cross section we must assume to take the same course as that from the ground state of ^{8}Be when

$$\sigma^3{}_{p\gamma}=\sigma_{\gamma p}\frac{5}{4}\frac{k_\gamma{}^2}{k_p{}^2},$$

where $\sigma^3{}_{p\gamma}$ represents that part of the 'giant resonance' capture that leads to the first excited state of ^{8}Be.

Again we expect a preference to be shown in the capture radiation for the excited state of ^{8}Be.§

---

* In the present case the outgoing particles are charged; the s-wave protons are of sufficiently high energy for the Coulomb barrier to have little effect on the integrated cross section; higher partial waves experience a more substantial barrier but it is largely centrifugal and so almost the same as that experienced by the corresponding neutrons in the (γn) reaction.

† But see earlier footnote.

‡ This assumption of the same reduced width for the two competing transitions is a reasonable one since both states of ^{7}Li are P states. s- and d-wave reduced widths are all large in p-shell nuclei (A. M. Lane, unpublished).

§ The more so when it is noticed that ($1-$), ($2-$) and ($3-$) 'giant resonance' contributions are now possible and so there should be a greater preference for the ground state of ^{7}Li in the ^{8}Be*(γp)^{7}Li reaction. This effect should increase $\sigma^3{}_{p\gamma}$ somewhat.

$\sigma^0{}_{p\gamma}$ and $\sigma^3{}_{p\gamma}$ have been computed by inserting the above constants for E_m and Γ_g into a Breit-Wigner expression* and using the relations of detailed balance given above. The result of this computation is shown in fig. 4 ($\sigma^0{}_{p\gamma}$ and $\sigma^3{}_{p\gamma}$ have been added so fig. 4 is directly comparable with figs. 1 and 3).

This cross section is of the right order and form to make up the difference between the direct interaction cross section that is adequate at low energies and the total experimental cross section of fig. 1.

Fig. 4

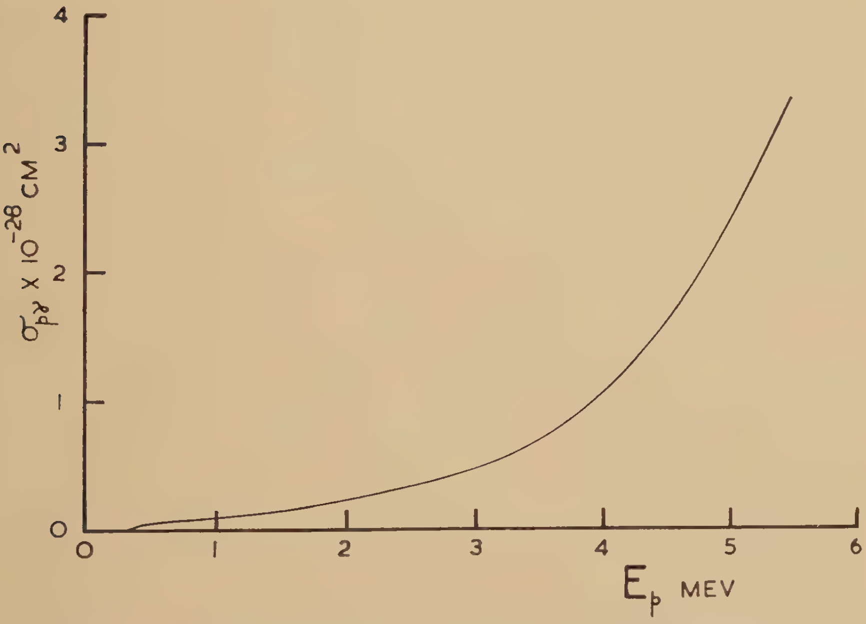

The total calculated 'giant resonance' capture cross section $\sigma_{p\gamma}$.

If this suggestion of an inverse 'giant resonance' is correct we must expect $\sigma_{p\gamma}$ to pass through a broad maximum centred at a proton energy of between 5·5 and 7 MEV, little above the range of proton energy so far examined.

§ 4. The Total Cross Section

We may make a crude comparison of theory with experiment by subtracting from the experimental curve of fig. 1 the effects of the three known resonances. This gives the dashed curve of fig. 5. Since the theoretical direct interaction cross section is so sensitive to r_0 (see fig. 2) it has been adjusted such that when it is added to the small contribution from the

---

* A rough allowance has been made for the small contribution from d-wave protons; this causes $\sigma_{p\gamma}$ to rise rather more steeply than it would on the basis of s-wave capture alone. The same reduced widths have again been taken for s-wave and d-wave contributions.

'giant resonance' the theoretical and experimental curves agree at $E_p=1$ MeV. To get this value for the direct interaction cross section we must take well radii of $3{\cdot}1\times10^{-13}$ or $3{\cdot}7\times10^{-13}$ cm in LS coupling and $3{\cdot}3\times10^{-13}$ or $3{\cdot}6\times10^{-13}$ cm in *jj* coupling; say $r_0\sim3{\cdot}2\times10^{-13}$ or $3{\cdot}6\times10^{-13}$ cm. The direct interaction cross sections for the two mean radii are shown by the dotted lines in fig. 5.* The theoretical direct interaction and 'giant resonance' cross sections are now added to give the full lines of fig. 5. The agreement displayed in fig. 5 is sufficiently

Fig. 5

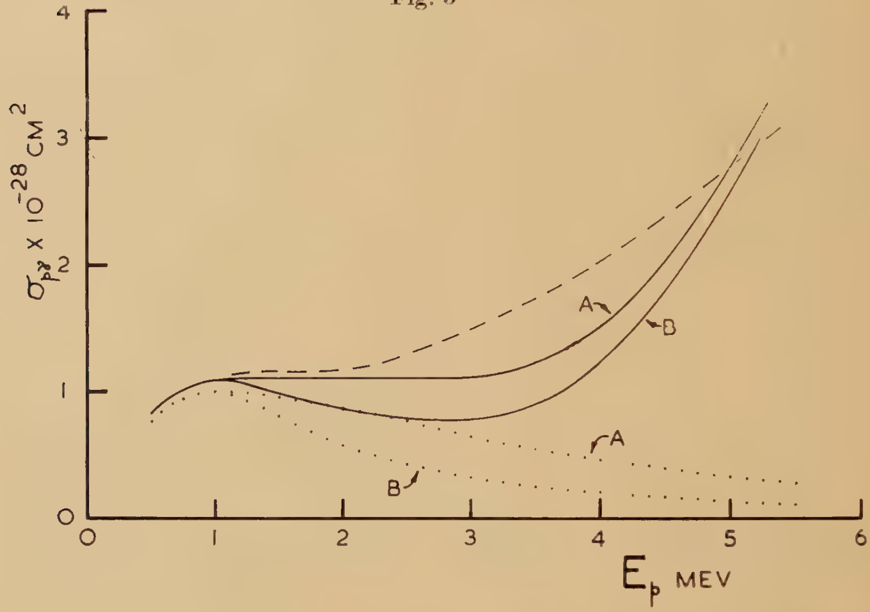

The total experimental 'non-resonant' capture cross section (dashed curve) compared with the sum of the theoretical direct interaction cross section and the 'giant resonance' cross section (the full curves are this sum). The direct interaction cross section (dotted curves) have been taken for well radii $r_0\sim3{\cdot}2\times10^{-13}$ cm (curves A) or $3{\cdot}6\times10^{-13}$ cm (curves B) in order that the experimental and theoretical (sun) curves fit at $E_p=1$ MeV.

---

* That for large r_0 is seen to fall rather more rapidly with increasing E_p than that for small r_0. This is largely because, for $r_0\sim4\times10^{-13}$ cm $\phi>\frac{3\pi}{2}$ and so cot ϕ increases with E_p while for $r_0\sim3\times10^{-13}$ cm $\phi<\frac{3\pi}{2}$ for low E_p and $\sim\frac{3\pi}{2}$ at $E_p=5$ MeV so cot ϕ decreases with increasing E_p.

There is little difference between the direct interaction cross section curves for $r_0=3{\cdot}1\times10^{-13}$ cm in LS coupling and $r_0=3{\cdot}3\times10^{-13}$ cm for *jj* coupling or between those for $r_0=3{\cdot}6\times10^{-13}$ cm in *jj* coupling and $r_0=3{\cdot}7\times10^{-13}$ cm in LS coupling so we have simply plotted curves for $r_0\sim3{\cdot}2\times10^{-13}$ cm (curve A) and $r_0\sim3{\cdot}6\times10^{-13}$ cm (curve B).

good* to suggest that the two mechanisms discussed here may indeed be responsible for much of the apparently non-resonant background radiation in ^{7}Li(pγ)^{8}Be.

§ 5. DISCUSSION

It is tempting to take seriously the values of r_0 that appear to be needed to explain the magnitude of the direct interaction cross section. This must not be done without caution, however, since the assumption of a square well must be very crude, the approximate account of the Coulomb force is inadequate, the assumption of a free-particle wavefunction for the incident particle inside the nucleus is questionable and the results are further slightly dependent on the coupling scheme adopted and, within that scheme, to our choice of a unique parent for the initial state—see Appendix. It is, however, interesting to compare our value of r_0 with that given for neighbouring nuclei by methods that also concern themselves largely with the radial extent of the wavefunction. Thus Coon, Graves and Barschall (1952) in a study of fast neutron scattering find for ^{6}Li, ^{7}Li and ^{9}Be r_0 values of 3·8, 3·9 and $4{\cdot}1 \times 10^{-13}$ cm respectively. ‘Stripping radii’ of 5·0, 5·3 and $5{\cdot}7 \times 10^{-13}$ cm are required for the same three nuclei (Holt and Marsham 1953).

These remarks might be taken to favour the larger of our alternative pairs of radii for ^{8}Be: 3·6(jj) or 3·7(LS) $\times 10^{-13}$ cm. However, as may be seen from fig. 5 a distinctly better account of the experimental curve at the lower values of E_p is given by the lower pair of radii: 3·1(LS) or 3·3(jj) $\times 10^{-13}$ cm. So the internal evidence may be held to favour the radius $r_0 \sim 3{\cdot}2 \times 10^{-13}$ cm—which, it may be remarked is close to the ‘conventional’ radius $1{\cdot}5 \times A^{1/3} \times 10^{-13}$ cm. It should also be noticed that ^{8}Be is rather different from its neighbours ^{6}Li, ^{7}Li and ^{9}Be referred to above in that it is very stable against nucleon emission. In this respect it closely resembles ^{12}C as has already been remarked in § 3 and it is perhaps noteworthy that the radius of ^{12}C as determined by the fast neutron and stripping results just quoted is $3{\cdot}6 \times 10^{-13}$ cm (fast neutron) or $4{\cdot}0 \times 10^{-13}$ cm (stripping), much closer to its ‘conventional’ radius ($3{\cdot}44 \times 10^{-13}$ cm) than is the case for ^{6}Li, ^{7}Li and ^{9}Be.

If the two mechanisms that we have proposed are acknowledged to be operative—and it seems difficult to deny them a rôle of the order calculated here—we must conclude that no more conventional resonances of any strength are needed to explain the ^{7}Li(pγ)^{8}Be cross section below E_p=5·5 Mev. However, as remarked in § 2, we must expect there to be conventional resonances at work as well and these may exert by their interference with the background radiation a profound influence on the angular distribution of gamma-ray emission though not on the total cross section for gamma-ray production. At low values of E_p the angular distributions associated with both our special mechanisms should be predominantly isotropic although the contribution of d-wave protons in both processes will give some anisotropy. Angular distribution measurements aimed at elucidating the characteristics of the 1·05 Mev and 2·0 Mev resonances will be complicated by the presence of the background radiation but, on the other hand, this background may aid the interpretation since its character is understood and the phase relationships are only slowly varying and are calculable. Angular distribution measurements over the whole range of E_p are also desirable in order to obtain more accurate estimates of the total cross section.

---

* The ‘giant resonance’ contribution seems to be too small around $E_p = 3$–4 MEV and to rise too rapidly at high values of E_p. This may be because our choice of Γ_g is too small for the reasons stated in a footnote to § 4. Use of the value of Γ_g there suggested would give a substantially better fit over the whole range of E_p; it would also imply a somewhat smaller direct interaction cross section though some would still be needed. If we choose to regard Γ_g as a free parameter (though not so the integrated cross section) as close a fit as may be desired can be obtained everywhere.

Both the special mechanisms suggest that transitions to the excited state of ^{8}Be should be favoured by the background radiation. This is in agreement with experiment up to E_p=1 Mev but it would be of great interest to extend the experimental investigation to higher proton energies. In any case a separation of the gamma-ray components is highly desirable if angular distribution measurements are to be interpreted unambiguously.

ACKNOWLEDGMENTS

I am indebted to Mr. A. M. Lane and Dr. L. A. Radicati for an account of their unpublished work, to Mr. Lane for further valuable and illuminating discussions on it and to Mr. P. C. Price for the measurement of the excitation function.

REFERENCES

AJZENBERG, F., and LAURITSEN, T., 1952, *Rev. Mod. Phys.*, **24**, 321.

BAIR, J. K., WILLARD, H. B., SNYDER, C. W., HAHN, T. M., KINGTON, J. D., and GREEN, F. P., 1952, *Phys. Rev.*, **85**, 946.

BOCKELMAN, C. K., MILLER, D. W., ADAIR, R. K., and BARSCHALL, H. H., 1951, *Phys. Rev.*, **84**, 69.

BONNER, T. W., and EVANS, J. E., 1948, *Phys. Rev.*, **73**, 666.

CHRISTY, R. F., 1953, *Phys. Rev.*, **89**, 839.

COON, J. H., GRAVES, E. R., and BARSCHALL, H. H., 1952, *Phys. Rev.*, **88**, 562.

COURANT, E. D., 1951, *Phys. Rev.*, **82**, 703.

DEVONS, S., 1953, *Report to Birmingham Conference.*

DEVONS, S., and HINE, M. G. N., 1949, *Proc. Roy. Soc.* A, **199**, 56, 73.

ERDÖS, P., SCHERRER, P., and STOLL, P., 1953, *Helv. Phys. Acta*, **26**, 207.

FESHBACH, H., PORTER, C. E., and WEISSKOPF, V. F., 1953, *Phys. Rev.*, **90**, 166.

FLOWERS, B. H., and MANDL, F., 1951, *Proc. Roy. Soc.* A, **206**, 131.

FOWLER, W. A., and LAURITSEN, C. C., 1949, *Phys. Rev.*, **76**, 314.

GOLDHABER, M., and TELLER, E., 1948, *Phys. Rev.*, **74**, 1046.

HALPERN, J., and MANN, A. K., 1951, *Phys. Rev.*, **83**, 370.

HILL, J. E., and SHOUPP, W. E., 1948, *Phys. Rev.*, **73,** 931.
HOLT, J. R., and MARSHAM, T. N., 1953, *Proc. Phys. Soc.* A, **66,** 1032.
HUDSON, C. M., HERB, R. G., and PLAIN, G. J., 1940, *Phys. Rev.*, **57,** 587.
HUNT, S. E., 1952, *Proc. Phys. Soc.* A, **65,** 982.
INALL, E. K., and BOYLE, A. J. F., 1953 (in press).
INGLIS, D. R., 1953, *Rev. Mod. Phys.*, **25,** 390.
JONES, L. W., and TERWILLIGER, K. M., 1953, *Phys. Rev.*, **91,** 699.
KATZ, L., and CAMERON, A. G. W., 1951, *Can. J. Phys.*, **29,** 518.
KONOPINSKI, E. J., and TELLER, E., 1948, *Phys. Rev.*, **73,** 822.
LANE, A. M., and RADICATI, L. A., 1953 (in press).
LEVINGER, J. S., and BETHE, H. A., 1950, *Phys. Rev.*, **78,** 115.
MONTALBETTI, R., KATZ, L., and GOLDEMBERG, J., 1953, *Phys. Rev.*, **91,** 659.
NABHOLTZ, H., STOLL, P., and WÄFFLER, H., 1951, *Phys. Rev.*, **82,** 963.
STEARNS, M. B., and MCDANIEL, B. D., 1951, *Phys. Rev.*, **82,** 450.
TANGEN, R., 1947, *Thesis*, Trondheim.
THOMAS, R. G., 1952, *Phys. Rev.*, **88,** 1109.
WALKER, R. L., and MCDANIEL, B. D., 1948, *Phys. Rev.*, **74,** 315.
WEISSKOPF, V. F., 1951, *Phys. Rev.*, **83,** 1073.
WILKINSON, D. H., 1952, *Phil. Mag.*, **43,** 659 ; 1953, *Ibid.*, **44,** 450.

APPENDIX

THE CALCULATION OF THE FACTOR C

The treatment given here is that of Lane and Radicati (though note that some of their phase factors are omitted).

The initial state of spin J (also L and S in LS coupling) consists of a core plus $n-1$ equivalent nucleons of orbital angular momentum l (of the j shell in jj coupling) plus an l_0 nucleon (of the j_0 shell). The transition is made by electron dipole radiation to the final state of spin J' (L' and S') consisting of the same core plus the same $n-1$ equivalent nucleons plus an l_1 nucleon (of the j_1 shell).

In LS coupling

$$C=[n\sum_p U(1l_1LL_p,\, l_0L')U(1L'JS,\, LJ')\langle\alpha_p\,|\}\,\alpha\rangle\langle\alpha_p\,|\}\,\alpha'\rangle\mathcal{T}_p]^2$$

and in jj coupling

$$C=[n\sum_p U(1j_1JJ_p,\, j_0J')U(1l_1j_0\tfrac{1}{2},\, l_0j_1)\langle\alpha_p\,|\}\,\alpha\rangle\langle\alpha_p\,|\}\,\alpha'\rangle\mathcal{T}_p]^2$$

if the selection rules are complied with. The summation is carried out over all parent states p. α, α' and α_p represent the initial, final and parent states and the $\langle|\}\rangle$ are the relevant fractional parentage coefficients.

$\mathcal{T}_p$ is the isotopic spin factor that evaluates the overlap integral in isotopic spin space and allows for the effective charge, i.e. allows for the charge on the rest of the nucleus that constitutes the ‘ well ’ for the ‘ single particle ’ motion.

$$(-)^{2T_p-T-T'}\mathcal{T}_p=\frac{\sqrt{3}}{2}U(1\,\tfrac{1}{2}\,TT_p,\,\tfrac{1}{2}\,T')C^{1\,T'\,T}_{0\,M_T\,M_T}$$

$$U(abcd,\, ef)=\sqrt{(2e+1)(2f+1)}\,W(abcd,\, ef).$$

We must now decide on the parent of the states concerned. Since the initial states are of mixed configuration we make the usual assumption that they have a unique parent (the ground state of ^{7}Li in the present case) and so a fractional parentage coefficient of $n^{-1/2}$. Since the final states are of a single configuration in the present case the fractional parentage coefficients are independent of the details of the nuclear forces in the two extreme coupling schemes and are given in the standard tabulations.

As noted in the text in LS coupling only the ^{31}P initial state complies with the selection rules in its transitions to the ground ^{11}S and first excited ^{11}D states. The parent in ^{7}Li is ^{22}P. If now C^0 and C^3 are the values of C for transitions to the $(0+)$ ground state and $(2+)$ first excited state of ^{8}Be,

$$C^0{}_{LS}=\left[4U(1111,\,00)U(1010,\,10)\frac{1}{\sqrt{4}}\,1\,\frac{1}{2}\right]^2=\frac{1}{9},$$

$$C^3{}_{LS}=\left[4U(1111,\,02)U(1210,\,12)\frac{1}{\sqrt{4}}\sqrt{\frac{7}{10}}\,\frac{1}{2}\right]^2=\frac{7}{18}.$$

In jj coupling only that $(1-)\,T=1$ state contributes that has as parent the ^{7}Li ground state

$$C^0{}_{jj}=\left[4U(1\,\tfrac{3}{2}\,1\,\tfrac{3}{2},\,\tfrac{1}{2}\,0)U(1\,1\,\tfrac{1}{2}\,\tfrac{1}{2},\,0\,\tfrac{3}{2})\frac{1}{\sqrt{4}}\,1\,\frac{1}{2}\right]^2=\frac{1}{9},$$

$$C^3{}_{jj}=\left[4U(1\,\tfrac{3}{2}\,1\,\tfrac{3}{2},\,\tfrac{1}{2}\,2)U(1\,1\,\tfrac{1}{2}\,\tfrac{1}{2},\,0\,\tfrac{3}{2})\frac{1}{\sqrt{4}}\sqrt{\frac{3}{5}}\,\frac{1}{2}\right]^2=\frac{1}{6}.$$

Note that the isotopic spin factor $\mathscr{T}_p$ is here just the classical effective charge factor $N/A=\frac{1}{2}$.

XXXI. *A λ-Anomaly in the Specific Heat of Solid Hydrogen*

By R. W. Hill and B. W. A. Ricketson
The Clarendon Laboratory, Oxford*

[Received December 23, 1953]

Abstract

The specific heat of solid hydrogen has been measured as a function of the ortho/para concentration in the temperature range from 1·15°K to the triple point. It has been shown that the specific heat contribution of the ortho molecules is anomalous throughout this region, and that the anomaly assumes a cooperative character at the lowest temperatures for specimens rich in orthohydrogen. The temperature of the maximum of the cooperative anomaly is at 1·6°K in normal hydrogen, but shifts rather rapidly to lower temperatures with falling orthohydrogen concentration. Considerations of the entropy show that the entire anomalous behaviour can be associated with the ordering of the rotations of the ortho molecules.

§ 1. Introduction

The orthohydrogen molecule in its ground state is 9-fold degenerate, being 3-fold degenerate with respect to both the molecular rotation and the nuclear spin; ortho/para hydrogen mixtures show, of course, an additional mixing contribution to the entropy. The value of the chemical constant of hydrogen (Simon 1923) proves that these additional disorder terms must be the same in hydrogen gas and in solid hydrogen at 10°K (Simon and Wohl 1930). While, probably, no demixing of ortho and para molecules can be expected to take place in the solid phase with falling temperature, the degeneracy of the ortho molecule should be lifted, and this should manifest itself in an anomalous specific heat. The contribution due to the nuclear term can very probably not be expected to occur above about 10^{-3}°K, while that due to the molecular rotation term may occur at very much higher temperatures. Simon, Mendelssohn and Ruhemann (1930, 1931) first showed that the specific heat is in fact anomalous below 10°K, and strongly dependent on orthohydrogen concentration. They have also shown that the anomaly cannot be due to demixing of the ortho and para molecules, and attributed it therefore to the splitting of the molecular rotation term.

The present paper is a brief account of an amplification of their work, and of its extension to lower temperatures where cooperative behaviour has been found in samples rich in orthohydrogen.

---

* Communicated by Professor F. Simon, F.R.S.

§ 2. EXPERIMENTAL

The apparatus used for these experiments has been described elsewhere (Hill 1953) and will not be discussed here, but some mention must be made of the experimental difficulties which are peculiar to solid hydrogen, since these have rather severely limited the scope of the experiments carried out so far. These difficulties arise from the instability of the orthohydrogen molecule at low temperatures, homogeneous conversion to parahydrogen taking place in the solid state at a rate dependent on orthohydrogen concentration (Cremer and Polanyi 1933). This conversion liberates substantial quantities of heat which limit the lowest temperature obtainable by pumping over liquid helium in thermal contact with the specimen, and which also cause the sample to warm up rather rapidly at liquid helium temperatures ; in normal hydrogen, for example, the rate of liberation of heat is 0·056 cals mole^{-1} min^{-1}, causing a rate of rise of temperature of 0·1 deg. min^{-1} at 4°K. In addition, the net change of concentration is not negligible over a period of a few hours, and experiments must be carried out as rapidly as possible.

In our first experiments, as in those of the earlier authors, the first of these factors restricted the experimental range to that above 2°K, the lower limit of temperature depending on the concentration of the specimen, and a fairly complete study has been made in this temperature range as a function of concentration. Our observations in this range have established that the rate of evolution of heat is temperature independent, at least between 1·8° and 4·5°K. With a redesigned calorimeter it has been found possible to reach temperatures below 2°K, and the range up to 2°K has been explored simply by taking a temperature–time curve as the sample warms up due to the heat liberated by conversion. Very marked inflections have been found in the curves for samples rich in orthohydrogen, showing that the specific heat rises to a very high value over a narrow range of temperature.

§ 3. RESULTS

If the assumption is made that the rate at which heat is liberated in the hydrogen remains unchanged at temperatures through and below the cooperative anomaly, the heating curves can be translated into specific heat versus temperature curves. The heating curves are shown in fig. 1 and the specific heat curves, including the higher temperature data, in figs. 2 and 3. Part of the higher temperature data has been reported briefly elsewhere (Hill 1951). It is estimated that the specific heat rises to a maximum value of about 15 cals mole^{-1} deg.$^{-1}$ for 74% orthohydrogen, and about 6 cals mole^{-1} deg.$^{-1}$ for 66% orthohydrogen. It is clear that the specific heat values given by the slope of the heating curve are not very accurate, but this is of no great importance, since the factors of principal interest are—at least at the moment—the dependence of the ‘ λ-point ’ temperature on concentration, and the values of the entropy changes due to the anomaly. This latter factor can be obtained without first evaluating the specific heat, for

$$dS = \frac{\alpha\, dt}{T}$$

and

$$S_2 - S_1 = \alpha \int_{t_1}^{t_2} \frac{1}{T} \cdot dt$$

where α is the heating rate, t is the time and T the absolute temperature. Entropy values can therefore be obtained by integrating under the reciprocal of the temperature–time graph. These values will, of course, be erroneous if the heating rate changes in this temperature range. While the possibility of this cannot at the moment be excluded, the *total* anomalous entropy, given later, is not likely to be very greatly affected.

Fig. 1

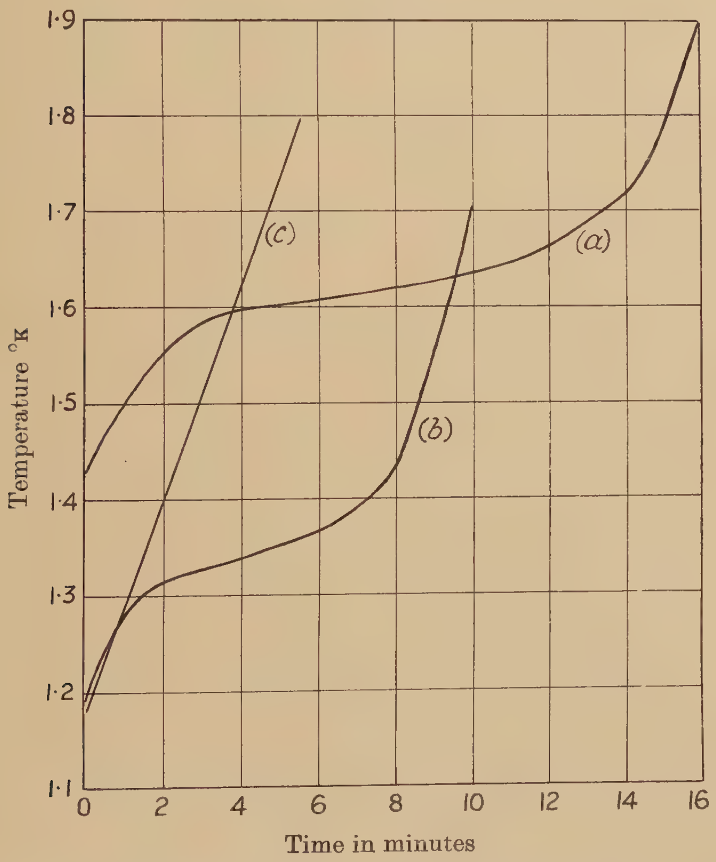

Heating curves for three hydrogen specimens.
(*a*) 74%, (*b*) 66%, (*c*) 56% orthohydrogen.

§ 4. DISCUSSION OF RESULTS

The most striking result is the existence of the cooperative anomaly, and the sharp dependence of its temperature on concentration. In hydrogen of approximately normal composition the specific heat maximum occurs at 1·6°K, while in 66% orthohydrogen it is shifted to 1·35°K. In 56% orthohydrogen no such anomaly could be found above 1·15°K. The question arises whether the cooperative behaviour disappears in hydrogen of sufficiently low ortho concentration, the whole anomaly

Fig. 2

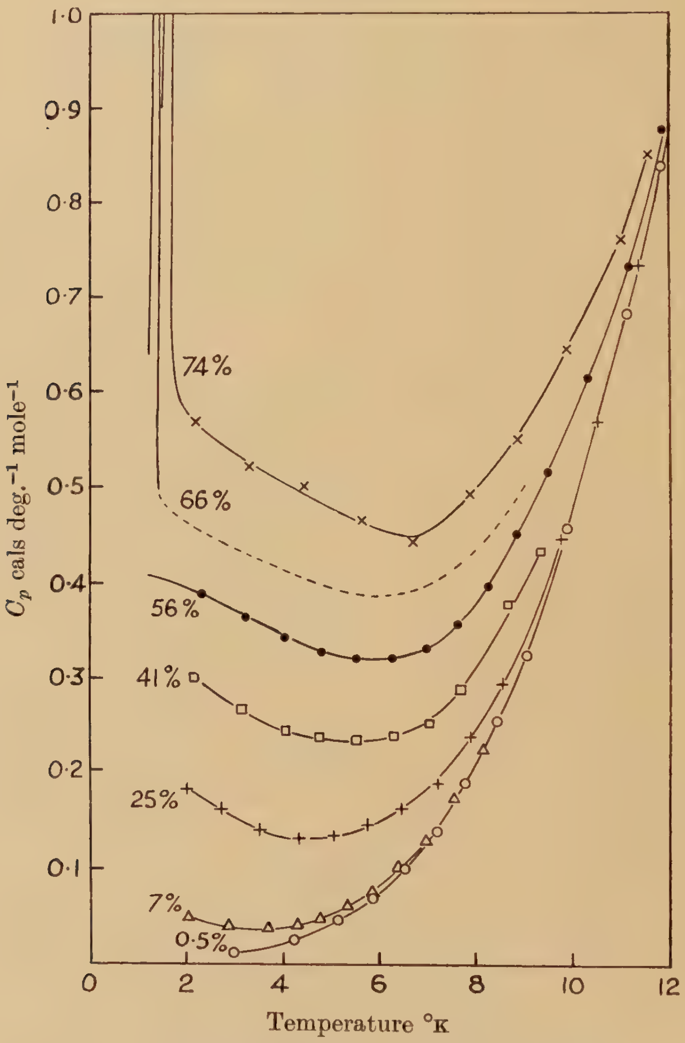

The specific heat of solid hydrogen.
The dotted curve is interpolated.

being then more of the Schottky type, or whether the 'λ-point' merely shifts to lower temperatures. Experiments below 1°K will be needed to elucidate this point, and these will be undertaken very shortly. The existence of the 'λ-point', in normal hydrogen at least, is consistent with the changes in the nuclear resonance spectrum reported by Hatton and Rollin (1949) and by Reif and Purcell (1953). It would now be of great interest if the resonance experiments could be repeated at other orthohydrogen concentrations.

Fig. 3

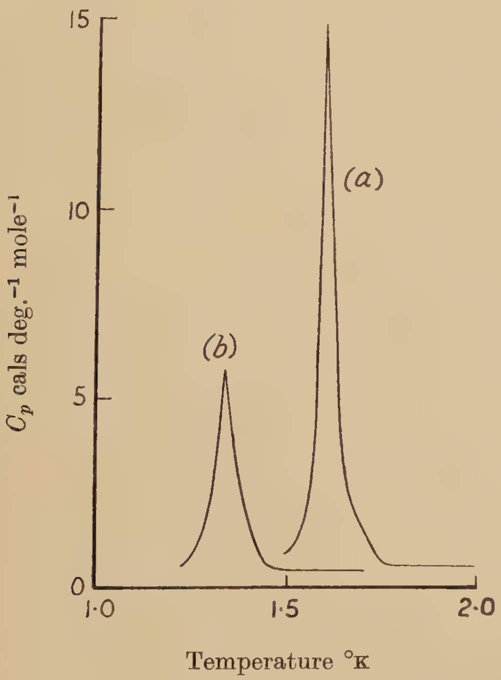

The λ-anomalies in solid hydrogen.
(*a*) 74%, (*b*) 66% orthohydrogen.

The total *anomalous* entropy, evaluated from the lowest temperature of measurement up to the triple point, has been found to be a few tenths of an entropy unit less than $R \log 3$ per mole of orthohydrogen (=1·63 E.U.). This is the value which would be expected if the entire anomaly is due to the ordering of molecular rotation. Even when allowance has been made for the possibility of error in connection with the heating rate, there is no *a priori* need to invoke the other possible contributions to the entropy in order to explain the present results. Attention must, however, be drawn to the fact that the anomalous specific heat above the maximum seems to decrease more slowly, and in a rather different manner, than is normally encountered.

A considerable amount of work is still required before the investigation can be completed. Apart from the further experiments indicated above, the question of the constancy of the heating rate will have to be settled before the exact form of the entropy curve can be given. Also the hysteresis found by Reif and Purcell may manifest itself in the specific heat, and time effects will therefore have to be studied. In view of the interesting nature of the results obtained so far and their bearing on the nuclear resonance experiments, it was thought worth while to publish this interim report, which gives a reasonably complete account of the specific heats above 1°K.

ACKNOWLEDGMENTS

The authors are greatly indebted to Professor F. E. Simon, F.R.S., for his invaluable advice and encouragement throughout this work. They also wish to express their thanks to the University of Oxford for the award of an I.C.I. Fellowship, and the Department of Scientific and Industrial Research for a grant respectively.

REFERENCES

CREMER, E., and POLANYI, M., 1933, *Zeits. Phys. Chem.* B, **21**, 459.
HATTON, J., and ROLLIN, B. V., 1949, *Proc. Roy. Soc.* A, **199**, 222.
HILL, R. W., 1951, *Report of the International Conference of Low Temperature Physics* (Oxford); 1953, *J. Sci. Instrum.*, **30**, 331.
MENDELSSOHN, K., RUHEMANN, M., and SIMON, F. E., 1931, *Z. Phys. Chem.* B, **15**, 121.
REIF, R., and PURCELL, E. M., 1953, *Phys. Rev.*, **91**, 631.
SIMON, F. E., 1923, *Z. f. Physik*, **15**, 307.
SIMON, F. E., MENDELSSOHN, K., and RUHEMANN, M., 1930, *Naturwiss.*, **18**, 34.
SIMON, F. E., and WOHL, K., 1930, *Ergebn. Exact. Naturw.*, **9**, 264ff.

XXXII. *Magnetic Behaviour of Thin Single-Crystal Nickel Films*

By L. E. Collins and O. S. Heavens
University of Reading*

[Received December 15, 1953]

Summary

The coercivity of monocrystalline films of nickel, grown epitaxially on the (100) face of rocksalt, has been studied as a function of thickness over the range 200 Å to 1000 Å. Films grown in this way do not exhibit the granularity characteristic of films deposited on cold, inactive substrates; electron micrographs show continuity over distances of the order several microns. The behaviour of such a film is expected to be simpler than that of a polycrystalline film, in which the magnetic properties depend on crystallite boundaries, crystallite size distribution, orientation, etc.

Spontaneous magnetization of the films is observed, with the magnetization vector in the plane of the film. The high coercivity characteristic of a single domain structure is observed and the maximum value agrees roughly with that calculated from the anisotropy constants. As is expected, the behaviour of monocrystalline films differs markedly from that of polycrystalline specimens.

§ 1. Introduction

The magnetic properties to be expected in ferromagnetic materials in the form of very thin films have been described, on the basis of Domain Theory, by Kittel (1946). Calculations are given of the domain boundary, magnetic and anisotropy energies for various shapes of particle. From these considerations it is shown that for particles whose smallest dimension is comparable with the domain size (or, more strictly, the Bloch wall thickness), a single domain structure is expected. Estimates are made for this critical particle size and indicate that for iron, nickel and cobalt it is of the order 10^{-5} cm. In a single domain structure, changes in direction of magnetization are possible only by simultaneous rotation of all the magnetization vectors. For this process, large anisotropy forces have to be overcome and a high coercivity is observed. This behaviour in small particles is well-known.

Little work has been reported on thin films of ferromagnetics. Drigo and Pizzo (1949) have studied the properties of films of Fe, Co and Ni of thicknesses ranging from 30 Å to 10 000 Å. The films were prepared by electrolytic deposition on copper discs. The crystal structures were not examined. Films so deposited would be expected to be polycrystalline, with more or less randomly-oriented crystallites. Qualitative agreement with the predictions of Domain Theory was obtained. Large coercivities were observed, the maximum values being :

---

* Communicated by Professor R. W. Ditchburn.

Iron	380 œ at 90 Å.
Cobalt	375 œ at 130 Å.
Nickel	260 œ at 600 Å.

The lower figure for nickel is consistent with its small anisotropy energy. Crittenden, Olsen and Hoffmann (1951) studied evaporated films of nickel and observed a single domain structure at small thicknesses. Ferromagnetism in these films disappeared at thicknesses of the order 20 Å. A similar figure is reported by König (1948) for evaporated iron films. The dependence on temperature of the intensity of magnetization of evaporated nickel films (Crittenden and Hoffmann 1953) has been found to be in agreement with the predictions of the spin-wave theory as developed by Klein and Smith (1951).

The polycrystalline film is a complicated system however, in which such features as the crystallite orientation (which may not be random) and the range of crystallite sizes present combine to make any but the most approximate calculations impossible. The growth of films on single-crystal substrates by epitaxy provides a method of making specimens in which some of the objections of polycrystalline films are avoided. Specimens of nickel prepared by this method have been examined by electron diffraction and electron microscopy and appear to be highly suitable for the study of magnetic properties in thin layers. The single-domain structure and high coercivity are observed. The coercivity *vs.* thickness curves differ significantly from those obtained for polycrystalline films.

§ 2. PREPARATION AND EXAMINATION OF SPECIMENS

The films are deposited, by evaporation in vacuum, on single-crystal slabs of rocksalt heated to 450°c. They are prepared in an electron diffraction camera so that their structure may be examined before removal from the vacuum. Slight oxidation, extending to a small number of layers, is observed on films after removal. Films grown in this way on a (100) rocksalt face have the (100) plane of nickel parallel to the plane of the film and are found on removal to show some distortion together with (111) twinning. The films are removed from the rocksalt by dissolving the latter, are picked up on a $\frac{1}{2}$ in. diameter $\times 0{\cdot}018$ cm quartz coverslip and are heated in vacuum ($<10^{-6}$ mm Hg) for 1 hour at 650°c. Electron diffraction examination of the films showed that this treatment removes both strain and twinning. The lower limit to the thickness of film which could be dealt with in this way is set by the mechanical strength of the film, which must withstand removal from the rocksalt. Films of thickness down to 200 Å were examined.

Electron micrographs of films grown by this method were compared with those of films deposited on unheated rocksalt, under which condition epitaxy does not occur and a polycrystalline layer results. The micrographs (fig. 1, Pl. 3) show a much less granular structure for the epitaxially grown film than for the polycrystalline one and suggest that the behaviour of the former film might be expected to approximate more nearly to the parallel-sided ideal of a thin film than to the aggregated form usually observed.

The thicknesses of the films were determined by measuring their transmittance for mercury green light. The relation between transmittance and thickness was first obtained for films deposited on quartz, the thickness measurements being made by multiple-beam Fizeau fringes. (An attempt to determine the film thickness while the film lay on the rocksalt was unsuccessful since the cleaved rocksalt surface is not sufficiently flat for Fizeau fringe measurements to be possible.) The accuracy of the thickness measurements made on the specimen films depends on the validity of the assumption that the optical constants of the epitaxially grown films do not differ widely from those of the polycrystalline films. The optical constants of films are certainly structure-sensitive at small thicknesses and the assumption is certainly not valid at thicknesses around 100 Å. The scanty and conflicting results available in this connection (see, e.g. Mayer 1950) suggest that for films above 200–300 Å in thickness, the error is unlikely to be serious.

§ 3. MAGNETIC MEASUREMENTS

Measurements were made at first using a magnetometer of the type used for the determination of ferromagnetic impurity. The specimen, in the form of a disc, is suspended from a fine suspension in a horizontal magnetizing field so that the direction of the field lies initially in the plane of the disc. A known twist is applied at the suspension head and the resulting rotation of the specimen is measured. If the intensity of magnetization vector I_p lies in the plane of the film, then the couple C required to hold the specimen, of volume v, at an angle ϕ to the field, H, is given by

$$C = HI_p v \sin\phi. \qquad \qquad (1)$$

If, however, the vector I_p rotates out of the plane of the specimen, application of eqn. (1) yields the apparent intensity of magnetization I_p' (Sucksmith, Potter, and Broadway 1928). The true intensity is given by

$$I_p = \tfrac{1}{2} I_p' + \left\{ \frac{I_p'^2}{4} + \frac{HI_p'}{N_2 - N_1} \right\}^{\frac{1}{2}}, \qquad \qquad (2)$$

where N_1, N_2 are the demagnetizing factors respectively in and perpendicular to the plane of the film. Considering a flat circular disc as an ellipsoid with $a = b \gg c$, we have $N_1 = 0$ and $N_2 = 4\pi$ so that

$$I_p = \tfrac{1}{2} I_p' \left\{ 1 + \left(1 + \frac{H}{\pi I_p'} \right)^{\frac{1}{2}} \right\}. \qquad \qquad (3)$$

The behaviour of a specimen when examined in a magnetometer of this types gives an indication of the nature of the domain structure. For if a specimen is not in the form of a single domain, then rotation of I_p out of the plane of the film will occur and application of eqn. (1) will yield I_p' which decreases with increasing field when saturation is reached. Figure 2 shows the magnetization curves obtained with a polycrystalline film. The normal magnetization curve obtained by the use of eqn. (3) shows that appreciable rotation of I_p out of the specimen plane occurs.

Fig. 2

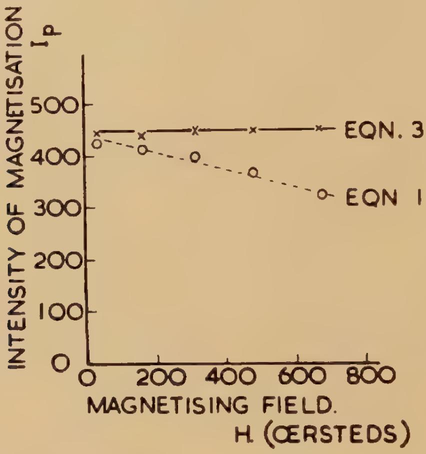

Magnetization curves for polycrystalline specimen using measured deflection method.

Similar experiments made with the (100) single crystal films yielded curves such as that of fig. 3 in which the intensity of magnetization is calculated *from equation* (1). The fact that a normal magnetization curve is obtained indicates that for these specimens there is no rotation of I_p out of the specimen plane for fields of the order a few hundred oersteds. With very much stronger fields, the value of I_p calculated from eqn. (1) was found to fall below the value obtained for smaller fields indicating that some rotation of I_p from the plane of the disc can be produced. Fields of strength many times that required for saturation are needed. It will be observed that the coercive force for the specimen described by fig. 3 is very large compared with the value normally observed for bulk nickel.

Owing to the uncertainty in the direction of the I_p vector in the method described above, subsequent investigations were made with the magnetometer designed by Bate, Schofield and Sucksmith (1952) in which the specimen, in a horizontal plane, is held at one end of a counterbalanced beam suspended by a torsion wire. Superposed on the magnetizing field is a field gradient from a pair of Helmholtz coils connected in reverse. The specimen is set symmetrically with respect to the zero-field position of these coils. On passing current, the specimen moves and is restored to its original position by rotation of the torsion head. The possibility of rotation of the magnetization vector is thus excluded by ensuring that the magnetizing field and specimen plane are parallel throughout. A series of measurements with this magnetometer was made on (100) single crystal films of thicknesses from 200 Å to 1000 Å. Measurements were made with the magnetizing field in various azimuths relative to the [001] direction of the (100) plane. No significant difference in the behaviour with direction was detected. Although the [011] is an easier direction of magnetization than the [001] the difference is at most a few per cent, as shown by the results on bulk specimens by Sucksmith, Potter and Broadway. The variation of coercive force with thickness is given in fig. 4 on which is also shown the curve obtained by Drigo and Pizzo for electrolytically deposited films of nickel.

Fig. 3

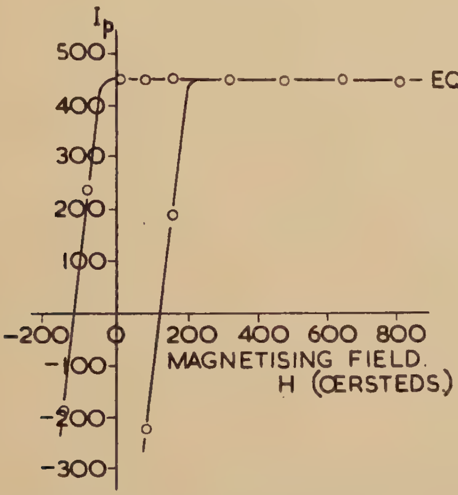

Typical curve for monocrystalline film. (100) plane parallel to specimen plane.

§ 4. Discussion

The evidence for the hypothesis that epitaxially grown nickel films are single domains of considerable extent for thicknesses in the neighbourhood of a few hundred angstrom units is supported by (*a*) the electron micrographs, (*b*) the behaviour of specimens in the first type of torsion magnetometer and (*c*) the large increase in coercive force observed as the thickness is reduced. Films of this type are of considerable interest since their behaviour is not complicated by the presence of small crystallites, as in the polycrystalline films, and by domain boundaries, as in thicker films or in bulk specimens. In a single-domain specimen, the observed coercivity depends on three factors: (*a*) the magnetocrystalline (anisotropy) energy, (*b*) the shape factor and (*c*) the strain energy. If the effect of the last two factors is small, then the maximum coercivity would be expected to be of the order $2K/I_s$ (Kittel 1949) where K is the anisotropy constant and I_s the saturation intensity. (This is calculated for a uniaxial crystal whose principal axis is an easy direction and is therefore only an approximate formula for nickel.) For a (100) single crystal of nickel, this gives a coercivity of ≈200 œ. For a film which is small in only one dimension, so that the demagnetization factors for directions in the plane are small, the shape effect would be expected to be small. Little can be said of the strain term for, although the electron diffraction patterns from the films indicated freedom from strain, quite large strains are required to show strain broadening in a diffraction pattern. The curve in fig. 4 indicates that the maximum coercivity is attained at a thickness below 200 Å. It was found impossible

Fig. 4

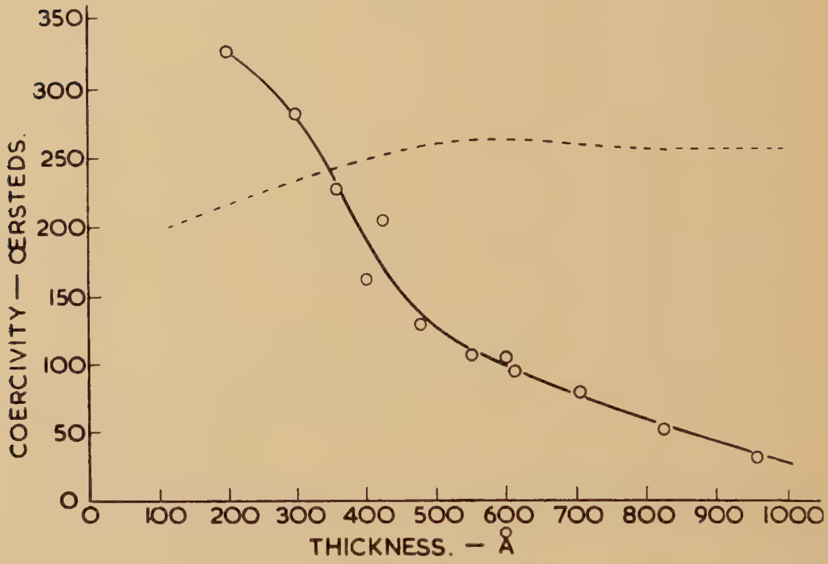

Results of coercivity measurements on (100) monocrystalline films. Dotted curve : results of Drigo and Pizzo for electrolytically deposited films.

to deal with specimens thinner than this owing to their fragility. Since the coercivity curve must descend to zero for very small thicknesses (where ferromagnetism no longer exists), and since there is an indication that the curve is turning over, it would appear likely that the maximum coercivity is of the order 350 œ. This is appreciably higher than the value obtained from the anisotropy constant and may indicate some residual strain in the specimens, although they were annealled until magnetic equilibrium was reached. Also it was found to make no difference to the magnetic properties of the films whether they were cooled slowly (several hours) or rapidly (∼10 minutes) after annealling.

It is, however, by no means certain that the values of anisotropy constants derived from bulk crystals will apply closely to films of the order 50 atoms thick.

The different behaviour of the polycrystalline films examined by Drigo and Pizzo is to be expected since these films probably contain crystallites whose size covers a wide range. The marked dependence of coercivity on the size and shape of particles leads one to expect that coercivity curves for polycrystalline specimens will be sensitive to the crystallite-size distribution. The use of epitaxially-grown films removes some of the difficulties associated with thin film investigations of this nature.

REFERENCES

BATE, L., 1952, *Ph.D. Thesis*, Sheffield.
CRITTENDEN, E. C., and HOFFMANN, R. W., 1951, *Rev. Mod. Phys.*, **25,** 310.
CRITTENDEN, E. C., OLSEN, L. D., and HOFFMANN, R. W., 1951, *Phys. Rev.*, **83,** 870.
DRIGO, A., and PIZZO, M., 1949, *Nuovo Cim.*, **6,** 827.
KITTEL, C., 1946, *Phys. Rev.*, **70,** 965 ; 1949, *Rev. Mod. Phys.*, **21,** 541.
KLEIN, M. J., and SMITH, R. S., 1951, *Phys. Rev.*, **81,** 378.
KÖNIG, H., 1948, *Optik*, **3,** 101.
MAYER, H., 1950, *Physik Dünner Schichte* (Stuttgart).
SUCKSMITH, W., POTTER, H. H., and BROADWAY, L., 1928, *Proc. Roy. Soc.* A, **117,** 471.

XXXIII. *Thermal Expansion of Simple Solids at Low Temperatures and Grüneisen's Law*

By D. Bijl and H. Pullan
Clarendon Laboratory, Oxford*

[Received December 28, 1953]

Abstract

Experimental results on the thermal expansion of copper, aluminium. and iron are discussed in relation to Grüneisen's law. This law is shown to break down at temperatures below about $0{\cdot}3\theta$, the thermal expansion becoming bigger than the values predicted by Grüneisen's law. A possible explanation is given.

In view of the importance of a detailed knowledge of the thermal expansion for the equation of state of solids, surprisingly few measurements at low temperatures have been carried out. For instance, there appears to be no detailed data on the temperature dependence of the thermal expansion of any cubic solid below 90°K. It is obviously of interest to have more experimental data at low temperatures and we therefore decided to study the thermal expansion of a number of simple solids as a function of temperature between room temperature and 20°K. Detailed results will be published in due course together with a description of the experimental method, which is based on the measurement of the change of capacity of a condenser produced by a change in length of the specimen. In this note we shall discuss only the results so far obtained for the cubic metals copper, aluminium and iron and their relation with Grüneisen's law. All specimens were polycrystalline.

According to Grüneisen's theory of the equation of state of solids there is the following relation between the volume change relative to the volume V_0 at the absolute zero, $\Delta V/V_0$, and the thermal energy E :

$$\delta = \Delta V/V_0 = A\gamma \frac{E}{1-bE}, \quad . \quad . \quad . \quad . \quad . \quad . \quad . \quad . \quad (1)$$

where A, b and γ are constants ; γ is a measure of the dependence of the frequencies of the lattice waves on the volume (Grüneisen 1926). Except for the highest temperatures in our range the term bE can be neglected and according to (1) δ/E should then be independent of temperature, i.e. Grüneisen's law should be satisfied.

In fig. 1 we have plotted $\gamma_{\text{eff}}/\gamma_c (=(\delta/E)/(\delta/E)_c)$ as a function of T/θ_0 ; $(\delta/E)_c$ and γ_c are the constant values of δ/E and γ respectively at the highest temperatures and θ_0 is the Debye temperature near the absolute zero. Both E and δ are calculated relative to 20°K ; E was obtained by integration of the specific heat values taken from the literature. At the lower temperatures δ and E are very small which explains the considerable scatter of points in this temperature range. The curves in all cases show a similar deviation of Grüneisen's law which can be expressed as an increase of γ with decreasing temperature. It should be remarked that our present experimental results are somewhat provisional, but we do not think that this affects our qualitative conclusion. Measurements with an improved apparatus are in course of preparation.

---

* Communicated by Professor F. Simon, F.R.S.

We also carried out preliminary measurements on a polycrystalline specimen of beryllium. The results showed an even larger increase of γ with decreasing temperatures than the other metals. The accuracy of the measurements is, however, low because the thermal expansion of beryllium is very small owing to its high Debye characteristic temperature. These results are therefore not included in the figure.

Fig. 1

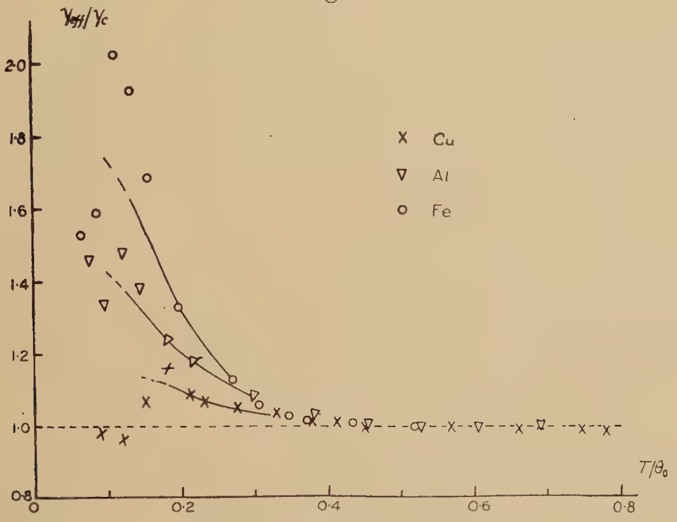

Experimental values of $\gamma_{\text{eff}}/\gamma_c$ as a function of T/θ_0. $\theta_0 = 335$, 419, 462°K for Cu, Al and Fe respectively.

After we had carried out the check on Grüneisen's law discussed above, we found indications of an increase of γ in the experimental data of Buffington and Latimer (1926) on Cu and Al, Keesom (1927) on Cu and Ag, and Nix and McNair (1941) on Fe. This effect apparently has escaped notice, except in Keesom's paper. Keesom, however, only states that the experimental value of γ of copper and silver between 20°K and 90°K is slightly larger than the value calculated from (1); no further comment is given.

In looking for an explanation for the deviation from Grüneisen's law one has to consider the possibility that the conduction electrons in metals are responsible; in actual fact such deviations can be expected in the direction we observed (Visvanathan 1951). This effect, however, can very probably only occur at temperatures where the electronic and lattice specific heats are of comparable magnitude, i.e., appreciable deviations can only be expected at much lower temperatures than we were able to use. A possible exception is iron, the electronic specific heat of which becomes noticeable at temperatures near 20°K.

Thus our results must be due to a breakdown of Grüneisen's simplified picture. This is suggested by the fact that the strongest variation of γ with temperature occurs at roughly the same values of T/θ_0 for all three metals. A discussion of the equation of state given by Slater (1939) is illuminating. Treating the lattice as a system of harmonic oscillators, Slater shows that Grüneisen's equation of state only holds if the quantities $\gamma_i(=-d \ln \nu_i/d \ln V)$ (where ν_i is the frequency of the ith mode of vibration) are all equal. This condition is fulfilled by a Debye type frequency spectrum, but as the frequency spectrum of actual solids deviates appreciably from this, it seems unlikely that Grüneisen's law can be strictly valid. A thorough discussion of the situation would be extremely involved, so we shall confine ourselves to a much simplified treatment. We shall neglect the zero-point energy as this is unlikely to cause a deviation from Grüneisen's law. This point will be discussed in a separate note (Bijl 1953).

Let us regard a crystal of N identical particles as an elastic isotropic continuum in which N longitudinal and $2N$ transverse waves are possible. Assuming the same cut-off wavelength for both types of waves, we find for each Debye spectrum with characteristic temperatures given by

$$\theta_l=\frac{hv_l}{k}\left(\frac{3N}{4\pi V}\right)^{1/3} \qquad \theta_t=\frac{hv_t}{k}\left(\frac{3N}{4\pi V}\right)^{1/3},$$

where V is the volume of the crystal and v_l and v_t are the velocities of propagation of the longitudinal and transverse waves respectively (Brillouin 1946). If ρ is the density, χ the volume compressibility and σ Poisson's ratio we have

$$v_l=\left\{\frac{3(1-\sigma)}{\chi\rho(1+\sigma)}\right\}^{1/2} \qquad v_t=\left\{\frac{3(1-2\sigma)}{2\chi\rho(1+\sigma)}\right\}^{1/2} \quad . \quad . \quad . \quad . \quad . \quad (2)$$

It is easily seen that $\gamma_l(=-d \ln v_l/d \ln V)$ and $\gamma_t(=-d \ln v_t/d \ln V)$ are in general not equal, unless $d\sigma/dV=0$. In fact, there is reason to infer that $d\sigma/dV>0$ (Slater 1939, p. 240), from which it follows that $\gamma_t>\gamma_l$ (compare (2)). Furthermore, because the frequency of a transverse wave is smaller than that of a longitudinal wave of the same wavelength, relatively more transverse waves will be excited at low temperatures. Consequently, we can expect an increase of effective γ with decreasing temperature.

For the model adopted in this paper the thermal energy is given by

$$E=RT[D(\theta_l/T)+2D(\theta_t/T)] \quad D(x)=\frac{3}{x^3}\int_0^x \frac{\xi^3\, d\xi}{(\exp \xi)-1}.$$

Instead of eqn. (1) we now have (neglecting the term bE)

$$\delta=A[\gamma_l D(\theta_l/T)+2\gamma_t D(\theta_t/T)].$$

The effective γ, γ_{eff}, is then determined by

$$\frac{\gamma_{\text{eff}}}{\gamma_c}=\frac{3}{1+2(\gamma_t/\gamma_l)}\,\frac{D(\theta_l/T)+2(\gamma_t/\gamma_l)D(\theta_t/T)}{D(\theta_l/T)+2D(\theta_t/T)} \quad . \; . \; . \; . \; . \quad (3)$$

where γ_c is the limiting value of γ_{eff} at high temperatures. According to (3) $\gamma_{\text{eff}}/\gamma_c=1$ for all temperatures if $\gamma_l=\gamma_t$, or $\theta_l=\theta_t$ (Debye's case). For an actual calculation of $\gamma_{\text{eff}}/\gamma_c$ we require γ_t/γ_l which could only be calculated if $d\sigma/dV$ were known. The best we can do is to calculate $\gamma_{\text{eff}}/\gamma_c$ for chosen values of γ_t/γ_l. For metals we have very nearly $\sigma=\frac{1}{3}$, so that we can take $\theta_l=2\theta_t$.

In fig. 2 we have plotted the values of $\gamma_{\text{eff}}/\gamma_c$ derived from (3) as a function of T/θ_0 for different values of γ_t/γ_l; θ_0 is given by $3/\theta_0{}^3=1/\theta_l{}^3+2/\theta_t{}^3$. The simple theory predicts a Grüneisen law for high and low temperatures, but with a larger value of γ at the low temperatures. At intermediate temperatures a marked deviation from Grüneisen's law must be expected. The theoretical curves seem to describe the salient features of our experimental results, but only qualitative agreement is found. This is not surprising in view of the crudeness of our theoretical considerations and the somewhat provisional character of our experiments.

Fig. 2

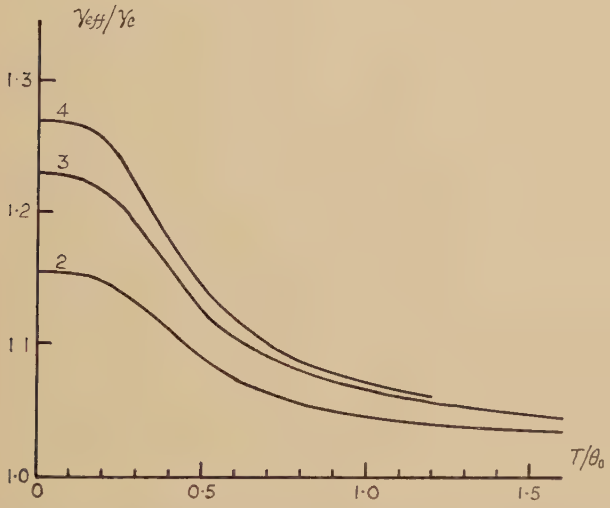

Theoretical values of $\gamma_{\text{eff}}/\gamma_c$ as a function of T/θ_0 for different values of γ_t/γ_l, which are indicated by the numbers near the curves at the left-hand side of the figure.

We would like to thank Professor F. E. Simon for his stimulating interest. One of the authors (D. B.) is indebted for the award of a Pressed Steel Company Ltd. research fellowship, the other (H. P.) for a maintenance grant from the Department of Scientific and Industrial Research, during the time this work was carried out.

REFERENCES

BIJL, D., 1953, to be published.
BRILLOUIN, L., 1946, *Wave Propagation in Periodic Structures* (New York), Ch. VII.
BUFFINGTON, R. M., and LATIMER, W. M., 1926, *J. Amer. Chem. Soc.*, **48,** 2305.
GRÜNEISEN, E., 1926, *Handbuch der Physik*, **10**, 1 (Berlin).
KEESOM, W. H., 1927, *Z. f. phys. Chemie*, **130,** 658.
NIX, F. C., and MCNAIR, D., 1941, *Phys. Rev.*, **60,** 597.
SLATER, J. C., 1939, *Introduction to Chemical Physics* (New York), Ch. XIII, XIV.
VISVANATHAN, S., 1951, *Phys. Rev.*, **81,** 626.

XXXIV. *The Correction of Elasticity Measurements on Slightly Anisotropic Materials*

By H. Pursey and H. L. Cox
National Physical Laboratory, Teddington*

[Received December 23, 1953]

Summary

Expressions are derived for the average elastic constants of a polycrystalline bar, having circular symmetry about its principal axis, and composed of material with cubic crystal symmetry. It is shown that the differences between these and the corresponding constants obtained for a material with completely random orientation depend in each case on the same function of the crystal orientation distribution, and therefore the complete elastic behaviour of the material may be determined from measurements of three independent quantities. In particular, it is shown how the true elastic constants of an isotropic specimen may be determined from the results of a series of longitudinal and torsional resonance tests, or from three measurements of travel-time of high-frequency pulses of mechanical energy through the material.

When the orientation distribution is expressed in terms of zonal harmonics it is found that elastic anisotropy is caused solely by the presence of the component $P_4(\cos\theta)$. Stereographic charts are included showing the texture corresponding to this and three higher harmonics, thereby establishing a relation between the elastic behaviour of cubic materials and the results of x-ray measurements.

§1. Introduction

In a recently published paper (Bradfield and Pursey 1953) the authors described the way in which small degrees of anisotropy can influence the results of a series of elasticity measurements on polycrystalline bars, and a method was outlined whereby the true elastic moduli of the material in its isotropic form could be obtained from longitudinal and torsional resonance tests on slightly anisotropic specimens, provided the single-crystal constants of the material were known approximately. The purpose of the present paper is to give a detailed account of the method of deriving the corrections, which are applicable for specimens having circular elastic symmetry about the axis of vibration, and made from a material whose crystalline structure has cubic symmetry.

The elastic constants of the polycrystalline material have been derived both by averaging the elastic constants c_{pq}, and also the moduli of compliance s_{pq}, similar expressions being obtained in each case for the anisotropy corrections.

---

* Communication from the National Physical Laboratory.

§ 2. METHOD OF AVERAGING THE ELASTIC CONSTANTS

Let the elastic constants of a single-crystal of the material be c_{11}, c_{12} and c_{44}, and let $c=c_{11}-c_{12}-2c_{44}$. Then if the direction cosines between the cube edges X', Y', Z' and the specimen axes X, Y, Z are given by the matrix below,

$$\begin{array}{c|ccc|} & X & Y & Z \\ X' & l_1 & m_1 & n_1 \\ Y' & l_2 & m_2 & n_2 \\ Z' & l_3 & m_3 & n_3 \end{array}$$

we find that the elastic constants referred to the specimen axes are given by

$$c_{11}'=c_{11}-2c\sum_{123} l_2^2 l_3^2, \qquad c_{22}'=c_{11}-2c\sum_{123} m_2^2 m_3^2, \qquad c_{33}'=c_{11}-2c\sum_{123} n_2^2 n_3^2,$$

$$c_{44}'=c_{44}+c\sum_{123} m_1^2 n_1^2, \qquad c_{55}'=c_{44}+c\sum_{123} n_1^2 l_1^2, \qquad c_{66}'=c_{44}+c\sum_{123} l_1^2 m_1^2,$$

$$c_{23}'=c_{12}+c\sum_{123} m_1^2 n_1^2. \qquad c_{31}'=c_{12}+c\sum_{123} n_1^2 l_1^2, \qquad c_{12}'=c_{12}+c\sum_{123} l_1^2 m_1^2,$$

$$c_{24}'=c\sum_{123} m_1^3 n_1, \qquad c_{25}'=c\sum_{123} l_1 m_1^2 n_1, \qquad c_{26}'=c\sum_{123} l_1 m_1^3,$$

$$c_{14}'=c\sum_{123} l_1^2 m_1 n_1, \qquad c_{15}'=c\sum_{123} l_1^3 n_1, \qquad c_{16}'=c\sum_{123} l_1^3 m_1,$$

$$c_{34}'=c\sum_{123} m_1 n_1^3, \qquad c_{35}'=c\sum_{123} l_1 n_1^3, \qquad c_{36}'=c\sum_{123} l_1 m_1 n_1^2,$$

$$c_{45}'=c_{36}', \qquad c_{56}'=c_{14}', \qquad c_{46}'=c_{25}'.$$

Now suppose that the crystal is rotated through an angle ϕ about the Z (specimen) axis. Then the direction cosine matrix becomes

$$\begin{array}{c|ccc|} & X & Y & Z \\ X' & l_1\cos\phi-m_1\sin\phi & l_1\sin\phi+m_1\cos\phi & n_1 \\ Y' & l_2\cos\phi-m_2\sin\phi & l_2\sin\phi+m_2\cos\phi & n_2 \\ Z' & l_3\cos\phi-m_3\sin\phi & l_3\sin\phi+m_3\cos\phi & n_3 \end{array}$$

The elastic constants referred to the specimen axes are now given by expressions such as

$$c_{11}'=c_{11}-2c\sum_{123}(l_2\cos\phi-m_2\sin\phi)^2(l_3\cos\phi-m_3\sin\phi)^2,$$

and if these are now written in the form of a term independent of ϕ plus a series of Fourier components, the constant terms will be the mean elastic constants of an aggregate of crystals randomly oriented with respect to ϕ, and hence having circular symmetry about the Z axis.

Using the relations which exist between the direction cosines, we find that the average elastic constants can all be expressed in terms of the function $\sum_{123} n_1^2 n_2^2$. We then obtain

$$\overline{c_{11}'}=\overline{c_{22}'}=c_{11}-\frac{c}{4}\left(1+3\sum_{123} n_1^2 n_2^2\right),$$

$$\overline{c_{33}'}=c_{11}-2c\sum_{123} n_1^2n_2^2,$$

$$\overline{c_{44}'}=\overline{c_{55}'}=c_{44}+c\sum_{123} n_1^2n_2^2,$$

$$\overline{c_{66}'}=c_{44}+\frac{c}{4}\,(1-\sum_{123} n_1^2n_2^2),$$

$$\overline{c_{23}'}=\overline{c_{31}'}=c_{12}+c\sum_{123} n_1^2n_2^2,$$

$$\overline{c_{12}'}=c_{12}+\frac{c}{4}\,(1-\sum_{123} n_1^2n_2^2).$$

The average elastic constants of any aggregate of cubic crystals having circular symmetry about the Z-axis may now be found by inserting in the above equations the average value of $\sum_{123} n_1^2n_2^2$ corresponding to a given distribution. In spherical polar co-ordinates we have

$$n_1=\cos\psi\sin\theta,\qquad n_2=\sin\psi\sin\theta,\qquad n_3=\cos\theta,$$

and the average value of $\sum_{123} n_1^2n_2^2$ is given by

$$\overline{\sum_{123} n_1^2n_2^2}=\frac{1}{4\pi}\int_0^{2\pi}d\psi\int_0^{\pi}\sin\theta\,d\theta(\cos^2\theta\sin^2\theta+\sin^4\theta\cos^2\psi\sin^2\psi)f(\theta,\psi).$$

where $f(\theta,\psi)$ is the distribution function of the crystallites, and is subject to the normalization condition

$$\frac{1}{4\pi}\int_0^{2\pi}d\psi\int_0^{\pi}d\theta f(\theta,\psi)\sin\theta=1.$$

Since we assume circular symmetry, and hence random distribution with respect to ψ, this integration may be carried out immediately. We then obtain

$$\overline{\sum_{123} n_1^2n_2^2}=\frac{1}{2}\int_0^{\pi}(\cos^2\theta\sin^2\theta+\frac{1}{8}\sin^4\theta)f(\theta)\sin\theta\,d\theta$$

$$=\frac{1}{10}\int_0^{\pi}\{P_0(\cos\theta)-P_4(\cos\theta)\}f(\theta)\sin\theta\,d\theta,$$

where $P_0(\cos\theta)$ and $P_4(\cos\theta)$ are zonal harmonics, given in terms of trigonometric functions by

$$P_0(\cos\theta)=1,\qquad P_4(\cos\theta)=\frac{1}{64}\,(35\cos 4\theta+20\cos 2\theta+9).$$

Putting $x=\cos\theta$ and $g(x)=f(\theta)$ we have

$$\overline{\sum_{123} n_1^2n_2^2}=\frac{1}{10}\int_{-1}^{+1}\{P_0(x)-P_4(x)\}g(x)\,dx.$$

and the normalization condition becomes

$$\int_{-1}^{+1}g(x)\,dx=2.$$

Provided $g(x)$ may be expanded as a series of zonal harmonics, we may write

$$g(x)=P_0(x)+\sum_{n=1}^{\infty}a_nP_n(x),$$

the amplitude of the first term being unity to satisfy the normalization condition above. Therefore, since the zonal harmonics constitute a set of orthogonal functions,

$$\overline{\sum_{123} n_1^2 n_2^2} = \frac{1}{10}\int_{-1}^{+1} [\{P_0(x)\}^2 - a_4\{P_4(x)\}^2]\, dx = 1/5 - a_4/45.$$

It follows that, when the distribution is expressed in this way, we need only know the amplitude of the fourth zonal harmonic component. Evidently, for a completely random distribution of crystallites, $a_4=0$ and $\overline{\sum_{123} n_1^2 n_2^2}=1/5$. We may define the 'elastic anisotropy index', γ of the specimen as the fractional difference between 1/5 and $\overline{\sum_{123} n_1^2 n_2^2}$. Then $\gamma = a_4/9$, and

$$\overline{\sum_{123} n_1^2 n_2^2} = (1-\gamma)/5.$$

We then obtain for the average elastic constants in terms of γ and the single-crystal constants

$$\overline{c_{11}'} = \overline{c_{22}'} = c_{11} - 2c/5 + 3\gamma c/20, \qquad \overline{c_{33}'} = c_{11} - 2c/5 + 2\gamma c/5,$$

$$\overline{c_{44}'} = \overline{c_{55}'} = c_{44} + c/5 - \gamma c/5, \qquad \overline{c_{66}'} = c_{44} + c/5 + \gamma c/20,$$

$$\overline{c_{23}'} = \overline{c_{31}'} = c_{12} + c/5 - \gamma c/5, \qquad \overline{c_{12}'} = c_{12} + c/5 + \gamma c/20.$$

We find therefore that the above averaging process gives for the elastic constants of an isotropic material

$$\overline{c_{11}} = c_{11} - 2c/5, \qquad \overline{c_{12}} = c_{12} + c/5, \qquad \overline{c_{44}} = c_{44} + c/5,$$

and we may therefore write :

$$\overline{c_{11}'} = \overline{c_{22}'} = \overline{c_{11}} + 3\gamma c/20, \qquad \overline{c_{33}'} = \overline{c_{11}} + 2\gamma c/5, \qquad (1), (2)$$

$$\overline{c_{44}'} = \overline{c_{55}'} = \overline{c_{44}} - \gamma c/5, \qquad \overline{c_{66}'} = \overline{c_{44}} + \gamma c/20, \qquad (3), (4)$$

$$\overline{c_{23}'} = \overline{c_{31}'} = \overline{c_{12}} - \gamma c/5, \qquad \overline{c_{12}'} = \overline{c_{12}} + \gamma c/20. \qquad (5), (6)$$

§3. APPLICATION TO RESONANCE TESTS ON BARS

From a series of longitudinal and torsional resonance tests on a round bar, having circular elastic symmetry about its axis, the following quantities may be determined :

(i) An apparent Young's modulus E'.

(ii) An apparent Modulus of Rigidity G'.

(iii) A value of Poisson's ratio σ_z, derived from observations of the dispersion of longitudinal wave velocities.

From E' and G' may be derived the quantity $\sigma' = (E'/2G' - 1)$, equal to Poisson's ratio in the case of an isotropic material. The fractional difference between σ' and σ_z is a useful measure of the elastic anisotropy of the material, and will be denoted by α. Thus

$$\alpha = \sigma'/\sigma_z - 1.$$

In terms of the average elastic constants $\overline{c_{11}'}$ etc., we find that E', G' and σ_z are given by

$$E'=\{\overline{c_{33}'}(\overline{c_{11}'}+\overline{c_{12}'})-2\overline{c_{31}'^2}\}/(\overline{c_{11}'}+\overline{c_{12}'}),$$

$$G'=\overline{c_{44}'},$$

$$\sigma_z=\overline{c_{31}'}/(\overline{c_{11}'}+\overline{c_{12}'}),$$

and from eqns. (1) to (6)

$$E'=(\overline{c_{11}}+2\overline{c_{12}})(\overline{c_{11}}-\overline{c_{12}}+0{\cdot}60\gamma c)/(\overline{c_{11}}+\overline{c_{12}}+0{\cdot}20\gamma c),$$

$$G'=\overline{c_{44}}-0{\cdot}20\gamma c,$$

$$\sigma_z=(\overline{c_{12}}-0{\cdot}20\,\gamma c)/(\overline{c_{11}}+\overline{c_{12}}+0{\cdot}20\gamma c).$$

It follows from the above equations that

$$\alpha=\gamma c(\overline{c_{11}}+2\overline{c_{12}})/(\overline{c_{12}}-0{\cdot}20\gamma c)(\overline{c_{11}}-\overline{c_{12}}-0{\cdot}40\gamma c)$$
$$\approx\gamma c(\overline{c_{11}}+2\overline{c_{12}})/\overline{c_{12}}(\overline{c_{11}}-\overline{c_{12}}),$$

and therefore

$$E'=(\overline{c_{11}}+2\overline{c_{12}})(\overline{c_{11}}-\overline{c_{12}})/(\overline{c_{11}}+\overline{c_{12}})+0{\cdot}40\gamma c(\overline{c_{11}}+2\overline{c_{12}})^2/(\overline{c_{11}}+\overline{c_{12}})^2$$
$$=E\{1+0{\cdot}40\gamma c(\overline{c_{11}}+2\overline{c_{12}})/(\overline{c_{11}}-\overline{c_{12}})(\overline{c_{11}}+\overline{c_{12}})\}$$
$$=E(1+0{\cdot}40\alpha\sigma_c),$$

where $$\sigma_c=\overline{c_{12}}/(\overline{c_{11}}+\overline{c_{12}}).$$

Similarly, $$G'=G\{1-0{\cdot}40\alpha\sigma_c/(1+\sigma_c)\}.$$

Rearranging these expressions to obtain the isotropic constants in terms of measurable quantities, and neglecting terms in α^2 and higher powers of α we have :

$$E=E'(1-0{\cdot}40\alpha\sigma_c),\qquad G=G'\{1+0{\cdot}40\alpha\sigma_c/(1+\sigma_c)\}.\qquad (7),\ (8).$$

In the above expressions, σ_c is the value of Poisson's ratio of the isotropic material obtained by averaging the single-crystal constants c_{11}, c_{12} and c_{44}, which is equivalent to assuming constant strain throughout the material (Voigt 1928). A similar analysis may be carried out by averaging the moduli of compliance s_{11}, s_{12} and s_{44}, which assumes constant stress in the material (Reuss 1929). The results so obtained are identical in form with eqns. (7) and (8) after replacing σ_c by σ_s where

$$\sigma_s=-\overline{s_{12}}/\overline{s_{11}},$$

$$\overline{s_{11}}=s_{11}-2s/5,\qquad \overline{s_{12}}=s_{12}+s/5,\qquad \overline{s_{44}}=s_{44}+4s/5,\qquad s=s_{11}-s_{12}-s_{44}/2.$$

Careful measurements have shown that the true elastic constants and Poisson's ratio of the isotropic material lie between the values obtained by these two methods, and that σ_z is nearly equal to the true Poisson's ratio. Therefore, no significant error is introduced by using σ_z (a measurable quantity) in place of σ_c or σ_s in the above expressions for E and G.

§4. CALCULATION OF BULK MODULUS AND $\bar{c}_{11}$

The bulk modulus, K, of the material may be calculated from the above results by means of the expression

$$K=EG/3(3G-E). \quad . \quad . \quad . \quad . \quad . \quad . \quad . \quad . \quad (9)$$

The result so obtained is, however, liable to considerable error, since the difference between $3G$ and E is generally quite small. A better method is to obtain a value of $\overline{c_{33}'}$ by measurements of travel time of short high-frequency pulses along the axis of the bar. (See, for example, Bradfield 1950.) Now

$$\begin{aligned} K&=\overline{c_{11}}-4\overline{c_{44}}/3 \\ &=\overline{c_{33}'}-4G'/3-4\alpha G'\sigma_c/3(1+\sigma_c). \end{aligned}$$

Using this expression, the bulk modulus may be obtained with considerably more accuracy than from (9) above.

Similar difficulties are encountered in deriving $\overline{c_{11}}$ from E and G, and greater accuracy may be obtained by using values of $\overline{c_{33}'}$ and G'. From eqns. (2) and (3) we find on eliminating γ

$$\overline{c_{33}'}+2\overline{c_{44}'}=\overline{c_{11}}+2\overline{c_{44}}.$$

Rearranging and using eqn. (8) we obtain

$$\begin{aligned} \overline{c_{11}}&=\overline{c_{33}'}+2(G'-G) \\ &=\overline{c_{33}'}-0\cdot 80\alpha G'\sigma_c/(1+\sigma_c). \end{aligned}$$

It will, of course, make little difference whether G or G' is used in the last formula, and as before we may replace σ_c by the measurable quantity σ_z.

§5. APPLICATION TO MEASUREMENTS BY HIGH-FREQUENCY PULSE METHODS

By propagation of both shear and irrotational high-frequency pulses along several directions sufficient information may be obtained to calculate the isotropic elastic constants without using any of the results of resonance measurements. The values of $\overline{c_{11}}$, $\overline{c_{12}}$, $\overline{c_{44}}$ and K are obtained by eliminating γ from suitable pairs of eqns. (1) to (6). For example, knowing $\overline{c_{11}'}$, $\overline{c_{33}'}$ and $\overline{c_{44}'}$ we find

$$\begin{aligned} \overline{c_{11}}&=(8\,\overline{c_{11}'}-3\,\overline{c_{33}'})/5, \\ \overline{c_{12}}&=(16\,\overline{c_{11}'}-11\,\overline{c_{33}'})/5-2\,\overline{c_{44}'}, \\ \overline{c_{44}}&=\overline{c_{44}'}+4\,(\overline{c_{33}'}-\overline{c_{11}'})/5, \\ K&=\overline{c_{11}'}-4\,\overline{c_{44}'}/3+5\,(\overline{c_{11}'}-\overline{c_{33}'})/3. \end{aligned}$$

Measurements by this method are generally less precise than those made by resonance techniques, but are useful in yielding additional information about the specimen. For example, any appreciable departure from circular symmetry can be detected, and indicates to what accuracy the foregoing analysis may be valid.

§6. RELATION BETWEEN ELASTIC ANISOTROPY AND TEXTURE AS REVEALED BY X-RAYS

Since the three axes of a cubic crystal are indistinguishable from one another, the texture (see Barrett 1943) of the polycrystalline material relative to the specimen axis will be represented by the sum of three distribution functions of the type considered in this paper, formally identical with each other, but having each of the three crystallographic axes as their respective axes of symmetry. Since the sense of each axis is also indeterminate, all odd-order harmonics vanish, and the texture corresponding to the jth zonal harmonic is given by

Fig. 1

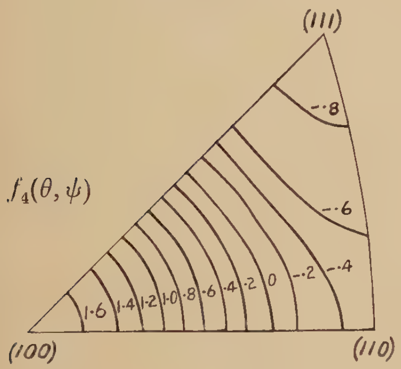

Fig. 2

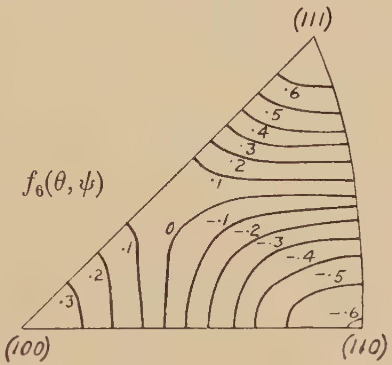

Fig. 3

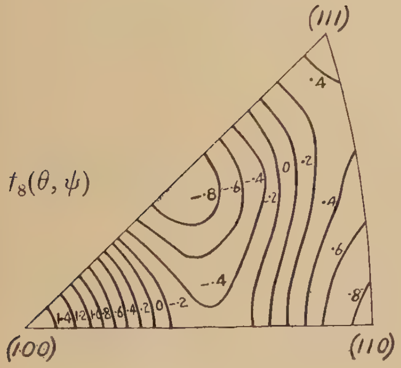

Fig. 4

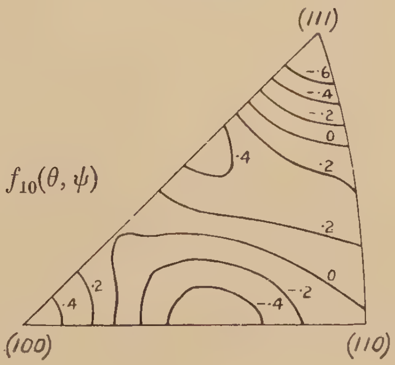

$$f_j\,(\theta, \psi) = P_j\,(n_1) + P_j\,(n_2) + P_j\,(n_3),$$

where n_1, n_2 and n_3 are the direction cosines of the specimen axis relative to the three cube edges, and j is any even integer. Now $f_0\,(\theta, \psi)$ is a constant, corresponding to random orientation, and we find the texture corresponding to the second zonal harmonic vanishes as follows :

$$f_2(\theta,\psi)=P_2(\cos\psi\sin\theta)+P_2(\sin\psi\sin\theta)+P_2(\cos\theta)$$
$$=\frac{1}{2}(3\cos^2\psi\sin^2\theta-1+3\sin^2\psi\sin^2\theta-1+3\cos^2\theta-1)$$
$$=0.$$

Therefore, the texture is given by

$$F(\theta,\psi)=1+\sum_{r=2}^{\infty}a_r f_{2r}(\theta,\psi).$$

As has already been shown, the only term contributing to the elastic anisotropy will be the one corresponding to $r=2$. This, and the next three terms, are shown in figs. 1 to 4 as contour maps in stereographic projection.

It will be apparent from the above analysis that a material may be isotropic in its elastic behaviour, but may nevertheless show anisotropy in other physical properties. In the case of materials whose texture may be represented to a reasonably close approximation by a combination of not more than two of the above components, it should be possible to predict the elastic behaviour from the results of a series of x-ray measurements, and an investigation of this is being planned.

ACKNOWLEDGMENTS

The authors wish to acknowledge helpful discussions with their colleagues Mr. G. Bradfield and Dr. E. A. Calnan. The work described above has been carried out as part of the research programme of the National Physical Laboratory, and this paper is published by permission of the Director of the Laboratory.

REFERENCES

BARRETT, C. S., 1943, *The Structure of Metals* (New York : McGraw-Hill).
BRADFIELD, G., 1950, *Nuovo Cim.*, Suppl. No. 2, Vol. 7, Series 9, p. 162.
BRADFIELD, G., and PURSEY, H., 1953, *Phil. Mag.*, **44**, 437.
REUSS, A., 1929, *Zeits. ang. Math. Mech.*, **9**, 49.
VOIGT, W., 1928, *Lehrbuch der Kristallphysik*, p. 962.

XXXV. *Red Shifts in the Spectra of Celestial Bodies*

By E. Finlay-Freundlich*
The University Observatory, St. Andrews†

[Received January 2, 1954]

Abstract

The red shift of the spectral lines of B-stars belonging to the Orion Nebula group, relative to the lines of the spectrum of the Nebula itself, is shown to be about ten times larger than the red shift which the theory of relativity predicts on the basis of the known values of their masses and radii. A similar discrepancy is found in the case of O-stars. It is suggested that the red shift may be due to a loss of energy in the radiation field of the star. If $\Delta\nu$ is the change of frequency of the line and ν its original frequency, the following formula is proposed.

$$\Delta\nu/\nu = -A \,.\, T^4 \,.\, l \qquad \text{(A)}$$

when A is a constant, T the temperature of the radiation field and l the length of path traversed through the radiation field.

It is shown that formula (A) represents not only the observations on O- and B-stars, but also on A-stars, the Sun, supergiant M-stars, Wolf–Rayet stars and on the so-called cosmological red shift.

In addition to the red shift given by formula (A) the data from the Sun and from white dwarfs seem to suggest that there exists an additional gravitational red shift which is, however, only a fraction (about 1/5) of the red shift predicted by the theory of relativity.

§ 1. Introduction

The fact that the lines in the spectra of certain classes of stars reveal a systematic displacement towards the red end of the spectrum—a so-called ‘ red shift ’—became evident as soon as the number of apparent measured radial velocities was large enough to make statistical investigations of the observational material possible. The effect is particularly pronounced for stars of high surface temperature, that is, stars of spectral type B or O ; in all stellar statistical discussions it has been called the K-effect.

The study of this red shift has developed into an extremely complicated problem, and we know now that the red shift is of a very complex nature. The fact that the B-stars embedded in the Orion Nebula show a pronounced red shift relative to the lines in the spectrum of the nebula itself (Freundlich 1919, Struve and Titus 1944, Struve 1945), that the O-stars in numerous stellar clusters reveal a red shift relative to the

---

* A brief account of the main points of the present paper has been published (Freundlich 1954).

† Communicated by P. M. S. Blackett, F.R.S.

B-stars belonging to the same cluster (Trumpler 1935), and other facts, including solar observations, leave no doubt that a physical effect exists producing displacements (red shifts) of the spectral lines. The discovery, on the other hand, that the K-effect depends on the galactic longitude and passes twice through a maximum and minimum along the periphery of the galactic plane (Freundlich and v. d. Pahlen 1923), makes it clear that another effect, probably of dynamical character (v. d. Pahlen and Freundlich 1928) is in operation too and partly responsible for the observed red shifts.

The present paper is concerned only with the red shifts of purely physical character, that is, with those red shifts which cannot be interpreted as Doppler effects. We mention the other red shifts, the K-effect, in order to make understandable why this complex problem has so far resisted all attempts to find a satisfactory explanation.

A solution of the problem of the physical red shifts appeared near at hand when the general theory of relativity predicted a systematic red shift of all spectral lines originating at a value of the gravitational potential which is lower than its value on the earth's surface. This shift should be $\Delta\lambda/\lambda = \Delta\phi/c^2$ where $\Delta\phi$ is the difference in gravitational potential, λ the wave length of the line, $\Delta\lambda$ the change of wavelength and c the velocity of light. Since the stars showing most clearly a systematic red shift were the stars of greatest masses, it appeared natural to interpret the observed red shift as a gravitational red shift. We shall see, however, that this interpretation is untenable. In the case of the Sun, where measurements of the displacement of lines in the spectrum are at least a hundred times more accurate than corresponding observations in stellar spectra and where, moreover, a detailed analysis along the disc is possible, all attempts to prove the existence of a general constant red shift as predicted by the theory of relativity have ended without any conclusive and convincing results. A small red shift seems indicated, but its value changes along the disc. Neither the reduced absolute value nor the increase of the red shift towards the limb can be brought in agreement with the theory of relativity unless special *ad hoc* assumptions are made.

It will be shown in this paper that the observed red shifts of the solar and stellar lines are of a different nature from the red shifts predicted by the theory of relativity. The observations reveal a new effect which is probably of the greatest importance.

In the next section we shall first rediscuss the evidence from stellar spectra. After that we will draw some general conclusions which will lead to a new hypothesis about the red shift which we shall apply to the whole of the relevant observational material in the remaining sections.

§ 2. DISCUSSION OF THE RED SHIFT IN B- AND O-STARS

The main difficulty in proving the existence of a physical red shift in stellar spectra lies in the separation of this effect from genuine Doppler effects. Strictly speaking, every observed line shift can be interpreted as a Doppler effect, and only independent evidence of a different character permits one to decide whether or not an observed line-shift is probably a Doppler effect.

The fact that the B-stars embedded in the Orion Nebula reveal a strong red shift was discovered early (Freundlich 1919). Using the latest observations and restricting the discussion to those 16 B-stars and 2 O-stars which constitute in a narrower sense the Orion Nebula group, the value of this red shift has been redetermined by Miss B. Middlehurst and Mr. T. B. Slebarski. Earlier, all stars had been discussed for which the right ascension α and declination δ were within the limits

$$5^{\mathrm{h}}\,13^{\mathrm{m}} < \alpha < 5^{\mathrm{h}}\,40^{\mathrm{m}}, \quad -9^\circ < \delta < 5^\circ,$$

as this group of B-stars had been defined by Kapteyn as the stars connected with Orion Nebula. Later investigations (Markowitz 1949) have, however, shown that in this wide range not all stars can be considered as organically connected with the nebula. The Orion Nebula group in the true sense is restricted to the area

$$5^{\mathrm{h}}\,30^{\mathrm{m}} < \alpha < 5^{\mathrm{h}}\,36^{\mathrm{m}}, \quad -6^\circ < \delta < -4^\circ.$$

In table 1 we have collected all data pertaining to 16 B-stars in this area belonging to the Orion Nebula.* Expressing the red shift in terms of a

Table 1

1	2	3	4	5	6	7
HD36959	29·2	11·7	B1k	12·0	6·5	1·18
HD36960	28·1	10·6	B1sk	15·5	9·9	1·00
HD37016	31·4	13·9	B2sk	10·8	4·4	1·44
HD37017	29·2	11·7	B2	10·1	3·9	1·65
HD37018	27·7	10·2	B2	13·4	12·4	0·69
HD37020	34·3	16·8	B2	8·0	3·9	1·31
HD37021	24·0	6·5	B2	6·1	2·4	1·65
HD37023	32·4	14·9	B0	9·2	3·4	1·74
HD37040	30·5	13·0	B3	8·7	5·8	0·98
HD37042	28·5	11·0	B1sk	9·3	4·2	1·41
HD37058	26·8	9·3	B3sk	6·6	3·6	1·18
HD37129	25·5	8·0	B3k	7·3	4·2	1·09
HD37209	29·4	11·9	B1s	10·4	7·9	0·83
HD37303	29·8	12·3	B3n	10·1	7·4	0·86
HD37334	28·3	10·8	B3	6·7	3·7	1·16
HD37356	29·1	11·6	B3sk	8·6	5·7	0·95

Column 1 gives the catalogue number of the star, Col. 2 the observed red shift v_{B} in km/sec, Col. 3 the residual red shift ($v_{\mathrm{B}}-v_{\mathrm{N}}$; $v_{\mathrm{N}}=17{\cdot}5$ km/sec=red shift of the nebula itself) in km/sec, Col. 4 the spectral type of the star, Col. 5 its mass in solar masses as unit, Col. 6 its radius in solar radii as unit, Col. 7 the expected relativistic red shift in km/sec.

---

* A separate paper discussing the astronomical data in more detail is in preparation.

Doppler effect, that is in km/sec, we find for the mean red shift of the B-stars with respect to the nebula itself the equation*

$$\overline{v_B}-\overline{v_{\mathrm{Neb}}}=+11{\cdot}4\pm0{\cdot}2\ \mathrm{km/sec},$$

which is larger than the predicted gravitational red shift by a factor of the order ten. The mean gravitational red shift is +1·2 km/sec, while the individual values range from 0·7 to 1·7 km/sec. The uncertainties in the masses and radii cannot bridge the gap between the observational and the theoretically predicted red shift. In our earlier investigation (Freundlich 1919), using stars in the larger area, the existence of this effect was equally unambiguous; the resulting value was +6 km/sec. The investigation by Struve and Titus (1944), which was confined to the two O-stars and three B-stars in the Trapezium of the Orion Nebula, gives a red shift of the O-stars which is even as large as +15 km/sec. It will be shown below that this increase is probably real.

Figure 1 gives the distribution of the observed red shifts as ordinates plotted against the expected value of the gravitational red shift. The values scatter only moderately around the mean. We could establish no correlation between the observed red shift and the gravitational red shift, the correlation coefficient being 0·17.

Fig. 1

Radial velocity—relativity red shift (calculated).

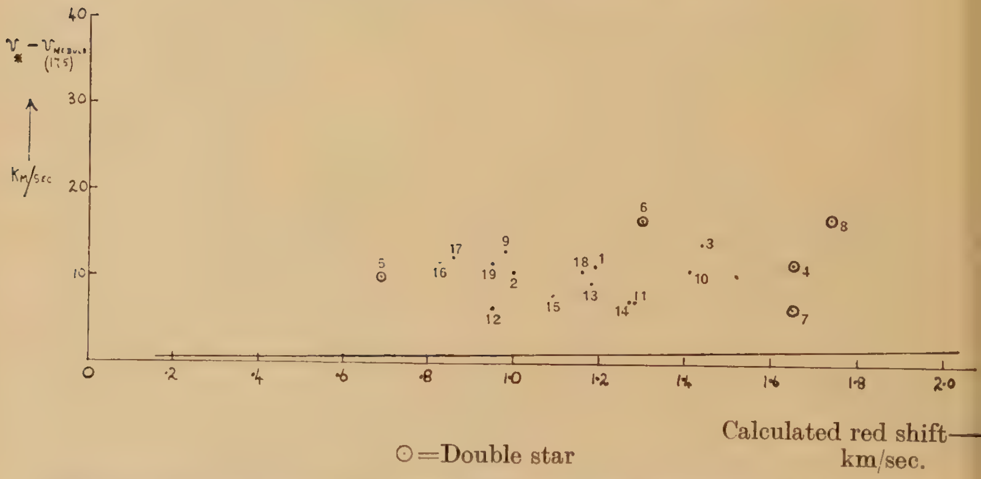

Radial velocities of nineteen B-stars relative to the Orion Nebula, as a function of the relativistic red shift calculated from their masses and radii. If the red shift were purely the gravitational red shift all points should lie on the straight line at the bottom of this figure.

---

* In deriving this equation we excluded five variable B-stars. If these had been included the result would have been +11·3±0·3 km/sec. (All errors are probable errors.)

To insure the reality of the observed effect, we also derived the differences $v_B - v_{Ca}$ (v_{Ca} being the shift of the interstellar Ca lines) for all B-stars in whose spectra the interstellar H and K lines were measurable. The result was

$$\overline{v_B - v_{Ca}} = +10{\cdot}1 \text{ km/sec} \quad \text{or} \quad +8{\cdot}5 \text{ km/sec},$$

the second value resulting, if one or two exceptionally large values are omitted. We have not corrected for the rotation effect of the galaxy; firstly because this correction would be small compared to the scattering of the individually observed values, and secondly because near star groups do not clearly reveal the rotation of the galaxy at all. (Pismis 1938.)

Summarizing the result of this renewed investigation of the B-stars belonging to the Orion Nebula group we have:

The B-stars in the Orion Nebula group show a systematic red shift relative to the lines in the nebula amounting to at least +10 km/sec. This value is, by a factor of the order ten, larger than the red shift predicted by the theory of relativity.

This result confirms previous findings and it also agrees with other results to be considered below.

Let us now consider in more detail the question whether or not these large red shifts can be interpreted as gravitational red shifts. We can do this by comparing the masses calculated on the assumption that the red shift is due to the gravitational effect with the masses obtained from other evidence, especially in the case where the star is a component of a binary system. In the latter case its mass can be estimated from the orbital elements, or at least a limit determined giving the order of magnitude of the mass. For only two of the stars embedded in the Orion Nebula is an estimate of the masses possible by this method, viz., for BM Ori (HD 37021), a B2-star, and HD 37041, an O-star. In both cases the lines of only one component of the binary are observable and thus only a lower limit for the mass of the whole system can be derived. In both cases these limits correspond to the normally expected values for the spectral types in question, viz., $m_1 + m_2 \geqslant 2{\cdot}8\, m_\odot$ for BM Ori, and $m_1 + m_2 \geqslant 12{\cdot}9\, m_\odot$ for HD 37041. Although the red shift of BM Ori is exceptionally small, viz., only about half the mean value of 11·4 km/sec,* the red shift yields a mass for the one component alone of at least $25\, m_\odot$.† The red shift of HD 37041 would indicate a mass of $284\, m_\odot$, while the mass of the whole system is, according to the orbital motion only of the order $13\, m_\odot$.

---

* The star seems in addition to be heavily obscured, for its apparent brightness is by two magnitudes lower than that of the other stars in the group; its radius as derived from its luminosity will, in consequence, come out abnormally small.

† With the normal value for its radius the red shift would give a mass of $55\, m_\odot$.

It is possible to base the proof that these large red shifts may not be interpreted as gravitational effects on a much wider range of observations. Bottlinger (1931) has investigated a few hundred B-stars and he finds, for instance, that of 42 B-stars of which the radial velocities, after being carefully corrected for the motion of the Sun and for the galactic rotation, exceed 10 km/sec, 39 are positive and only 3 negative. He finds the systematic character of the red shift so pronounced that he interprets these red shifts as pure gravitational displacements. The resulting masses range from about 100 to 1200 $m_{\odot}$. Among these stars are six which are members of binary systems and two (μ_2 Sco and Boss 5070) of which the mass can be determined by other means. Table 2 gives the data of these eight stars and it is clear that the masses derived from the red shifts are all too large by a factor of the order 10 to 20.

Table 2

1	2	3	4	5
o Per	B2k	>9·2	10	168
ϕ_1 Per	B0ssk	>5·6	14	180
ζ CMa	B3	>0·8	8	160
τ CMa	O9sk	>14·9	17	250
θ_2 Cru	B3	>0·4	8	126
v Cen	B2	>0·02	10	150
μ_2 Sco	B3nn	24·0	8	115
Boss 5070	B2k	71·0	10	98

Column 1 gives the name of the star, Col. 2 its spectral type, Col. 3 the total mass of the binary system (m_1+m_2), Col. 4 the normal value of mass for the spectral type of the star in which the red shift is found, Col. 5 the mass calculated from the observed red shift, assuming it to be a relativistic red shift. All masses are expressed in solar masses as unit.

A similar contradiction between masses derived from observed red shifts and values derived from other astronomical evidence appears in Trumpler's investigation (1935). In a number of star clusters Trumpler discovered a systematic red shift of the O-stars relative to the B-stars in the same cluster. Interpreting these red shifts as gravitational displacements, he is also led to values for the masses of O-stars which reach a few hundred solar masses, which are quite improbably large. O. Struve (1950) stresses this point, that Trumpler's mass values are fictitious and in contradiction to all other evidence. We shall use Trumpler's data below to fix the mean value of the systematic red shift for the O-stars.

There is a complete similarity of the results obtained by Bottlinger from a statistical discussion of a wide material of B-stars over the whole sphere, by Trumpler from star clusters which, as a whole are partly approaching us, partly receding from us, and finally the results obtained here from the B- and O-stars which form the Orion Nebula group. This similarity makes it obvious that these systematic red shifts cannot be Doppler effects. It is quite improbable that they are produced by a systematic motion of the stars in the Orion Nebula group relative to the nebula itself, or by a systematic motion of the O-stars relative to the B-stars in the same cluster, etc., always indicating a systematic recession inside a group of stars.

We see thus that the large red shifts reveal a physical effect which cannot be interpreted either as a gravitational displacement or as a true recession effect.

To conclude this section, let us consider the data pertaining to O-stars. The material consists of data about six star clusters (Trumpler 1935), Struve and Titus' observations (1944), about the O- and B-stars in the Trapezium of Orion, and the data about the Orion Nebula group. These data are summarized in table 3. From this table we see that while values for $v_{\rm O}-v_{\rm B}$ scatter over a wide range, we get a well defined value for the mean red shift for O-stars, viz., $\overline{v_{\rm O}}=+17{\cdot}6\pm0{\cdot}5$ km/sec. In this determination of $\overline{v_{\rm O}}$ we have excluded the two values where the B-stars were very early B-stars (B0 and B1·5). If they had been included we would have found $\overline{v_{\rm O}}=+18{\cdot}9\pm0{\cdot}7$ km/sec. Our value is larger than the value of 13·8 km/sec derived by Trumpler, the reason being that Trumpler adds as correction for the B-stars simply the relativistic correction, not realizing that the B-stars reveal systematic red shifts exceeding the relativistic effect by a factor of the order 10. Struve and Titus obtained for the red shift of the two O-stars embedded in the Trapezium with respect to the nebula itself, the value +15·0 km/sec. This value also indicates a further increase of the red shift for the O-stars of higher temperature than the B-stars.

Table 3

1	2	3	4	5	6
NGC 2244		6	B2	+13·4	+23·4
NGC 2244	O6			+ 6·4	+16·4
NGC 2244	O9			+ 7·0	+17·0
NGC 2264	O7	11	B7·5	+13·8	+15·6
NGC 2353		5	B8·5	+15·3	+16·6
NGC 2362	O8·5	7	B3	+ 8·7	+14·9
NGC 6871	O9w	3	B1·5	+ 7·8	+20·8
NGC 6871	B0			+13·6	+26·6
NGC 7380	O9	4	B0	+ 3·2	+25·4
NGC 7380	O9	11	B7	+13·8	+16·2
Trapezium	O8	3	B1·7	+ 5·8	+17·8
Trapezium	O8	18	B2	+ 7·4	+17·4

Column 1 gives the catalogue number of the star cluster, Col. 2 the mean spectral type of the O-stars concerned, Col. 4 the mean spectral type of the comparison B-stars, Col. 3 the number of comparison stars, Col. 5 the difference in red shift between the O- and B-stars in km/sec, Col. 6 the red shift of the O-stars in km/sec after correcting for the red shift of the comparison stars. The last two rows pertain to the O-stars of the Trapezium in the Orion-Nebula. The first three comparison B-stars are also Trapezium stars, and in the last column 18 Orion Nebula B-stars are used as comparison stars.

Summarizing the results of this section, we see that *the observations show clearly the existence of a red shift which increases rapidly with the surface temperature of the star. For a* B2-*star of effective temperature* 20 000°K *the new effect amounts to* $\Delta\lambda/\lambda = 3\cdot3\times10^{-5}$ *corresponding to a Doppler effect of* +10 *km/sec.* The red shift is larger than the value predicted by the theory of relativity according to our present knowledge of stellar masses and radii by a factor of the order 10. For O-stars the red shift rises to about +18 km/sec. Since O-stars are rare and the physical conditions at their surface not yet sufficiently understood (their spectra show, e.g., emission lines), their surface temperatures are not yet safely known, but they must be considerably higher than the surface temperature of the B-stars and must exceed 25 000°K. We will therefore base the value of the red shift on the above mentioned value of +10 km/sec for a B2-star of 20 000°K.

§ 3. General Remarks on the Nature of the New Effect

The most essential feature of the new red shift is that it becomes predominant for stars of the highest surface temperatures, when it exceeds widely the relativistic red shift. For the Sun, on the other hand, for which the most detailed and most accurate data concerning line displacements exist, the observed average red shifts fall short of the relativistic prediction. This means that the situation is just the opposite from that for the B- and O-stars. In addition, the red shift reveals along the solar disc a pronounced systematic behaviour by increasing steeply towards the limb in all directions from the Sun's centre. For this limb effect no explanation has been offered up to now.

It seems to me that it is possible to understand all these phenomena if we give up the efforts to explain them as purely gravitational effects. Instead, I propose to introduce as an additional hypothesis that light passing through deep layers of intense radiation fields, loses energy—perhaps due to photon–photon interaction—and that the energy loss is proportional both to the density of the radiation field and to the length of path of the light through the radiation field. Using for the density of the radiation field Stefan–Boltzmann's law, we have thus

$$\Delta\nu/\nu = -A\,.\,T^4\,.\,l, \qquad \ldots\ldots\ldots \quad (1)$$

where A is a constant and l the length of path. We shall assume that light emerging from the surface of a star loses energy chiefly inside the stellar atmosphere, where an intense inward flux of radiation exists. We choose, therefore, tentatively, l equal to the depth down to which we see into the Sun's or the star's atmosphere. For the Sun, the value of l is of the order of magnitude 10^7 cm (Unsöld 1938). The same value of l will be chosen as a first approximation for other stars too, except for super giants, for which the depth of the atmosphere seems to exceed that of a dwarf star by a factor of the order 10^3. It must be stressed that, of course, all these assumptions are of a preliminary nature, until the theory of this new effect is better established.

With $l=10^7$ cm and $\Delta\nu/\nu=-3\cdot3\times10^{-5}$ for a B-star of 20 000°K effective temperature, we get for the constant A,

$$A=2\times10^{-29}\ \text{degrees}^{-4}\ \text{cm}^{-1}. \qquad (2)$$

We have actually used formula (1) to apply the corrections in table 3—and thus to derive from the values of v_O-v_B the mean systematic red shift for O-stars. In this way, we found for this red shift the value $+17\cdot6$ km/sec, mentioned above.

In the following sections it will be shown that formula (1) gives a satisfactory description of the observed red shift along the solar disc, explains the red shift observed in other stellar spectra and may even permit an interpretation of the cosmological red shift other than that of an expanding universe.

§ 4. THE RED SHIFT OF THE SOLAR LINES

(i) *Summary of the Present Situation*

According to the general theory of relativity the solar lines should be displaced relative to corresponding terrestial lines by the amount

$$\Delta\lambda/\lambda=2\cdot12\times10^{-6}.$$

Modern tower telescopes, producing on the slit of the spectrograph an image of the Sun of at least 4 in. to 6 in. in diameter, are able to measure line displacements even considerably smaller than this predicted effect.

St. John (1928) has amassed a huge amount of material of solar observations comprising measurements of over 1500 lines, but only 133 lines were observed near the Sun's limb. Although the existence of a limb effect was known and although Evershed (1935, 1936) was not able to offer any reasonable explanation for it, it was thought that, if the relativistic red shift could be safely established for the central region of the Sun, the limb effect could be disregarded as being only a disturbing effect of secondary importance. However, the observations of the lines near the Sun's centre did not reveal clearly the predicted relativistic shift. Agreement with the theory could only be reached by adding a further, rather artificial, hypothesis about systematic currents in different layers of the solar atmosphere giving rise to violet shifts partly cancelling the expected gravitational red shifts. To characterize the situation, it is sufficient to quote the summary of Hunter's paper (1934) on the solar limb effect :—

" It seems clear that no hypothesis yet put forward will account for all the facts. Until one is forthcoming, the large deviations from the predictions of Einstein will give reason for doubting even the assignment of the major part of the red displacements to the gravitational effect. Any future explanation retaining the relativity shift as valid must account for the excess shift at the limb and the defect at the centre together with the variations in these quantities with line intensity and with epoch, and also for the observed form of the function representing the change in wavelength of a Fraunhofer line across the solar disc."

This is in full agreement with later observations by Miss Adam (1948), which are a most consistent set of observations of solar lines at about 6100 Å. In fig. 2 (taken from Freundlich 1954), the values of the red

Fig. 2

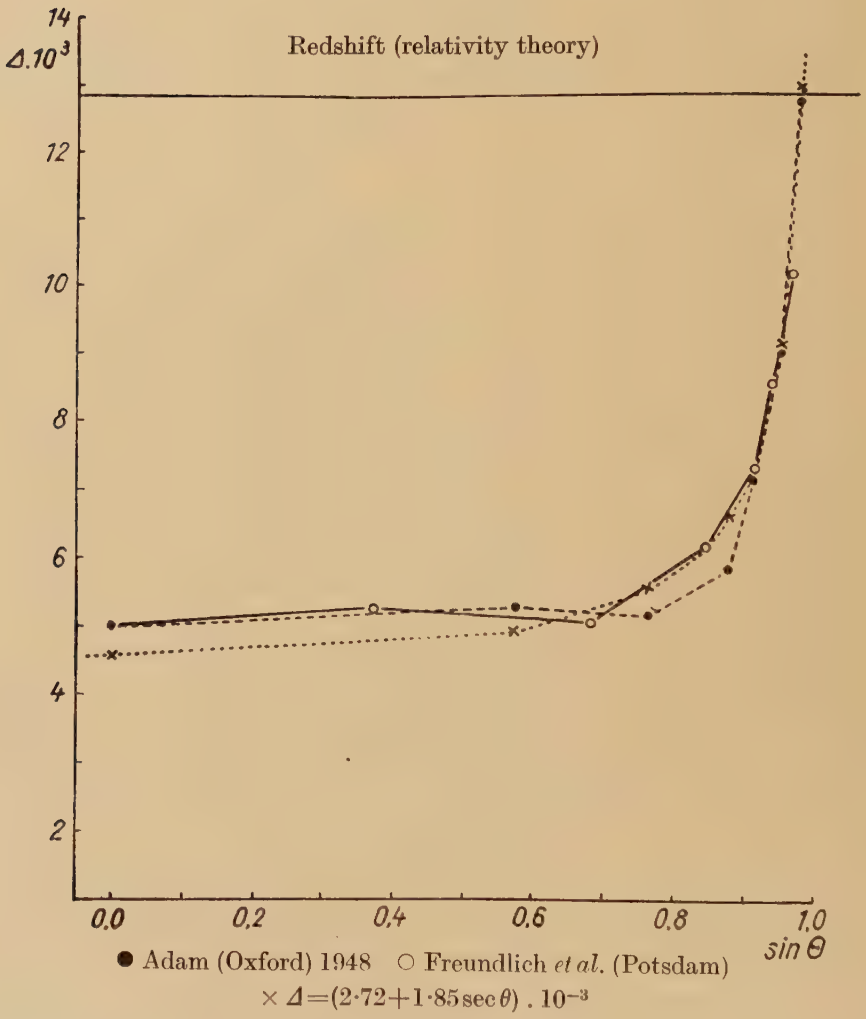

The red-shift Δ of solar lines as a function of the angle θ between the line of sight and the solar radius to the point where the line of sight cuts the solar surface. The horizontal line ($\Delta=0{\cdot}0129$) is the red shift according to the theory of relativity.

shift from the centre of the Sun to the limb (Adam 1948) are shown and compared with observations made by Freundlich, v. Brunn and Brück (1930) in Potsdam. These latter observations gave only relative changes of the red shift when one moved from the centre of the Sun to the limb along 12 radii of the discs. The red shift increases along all radii according to the same law—which, however, at that time could not be explained. The observations of Miss Adam at 6100 Å, which are referred to a terrestrial light source, give absolute values of the red shift. The Potsdam observations which are based on a selected group of solar lines at about 4400 Å have been made to coincide with Miss Adam's observations at 6100 Å at the centre of the disc. The practically complete coincidence of both series demonstrates the accuracy attainable with powerful tower telescopes and emphasizes the general character of the limb effect. We shall base all further discussion on this latest set of observations. Before doing so we wish to quote Miss Adam's summary which is very similar to the one of Hunter's paper (1934) :—" If we assume that the solar lines do suffer an Einstein gravitational displacement, then we must find some mechanism other than radial currents which will effectively neutralise this displacement over 80–90 per cent of the solar disc and yet leave the full Einstein shift near the limb."

(ii) *A New Interpretation*

If what we observe on the Sun is chiefly due to the new effect discussed in the previous section, we would expect to find the following two phenomena.

(1) Taking the Sun's temperature to be 6000°K, we would expect a red shift which is smaller than the one shown by the B2 stars by a factor of the order $(6/20)^4=8{\cdot}1\times10^{-3}$. The shift should thus be of the order of 0·081 km/sec or $\varDelta\lambda/\lambda=2{\cdot}7\times10^{-7}$. The group of lines observed by Miss Adam has the mean wavelength 6100 Å, and we get thus $\varDelta\lambda=1{\cdot}65\times10^{-3}$ Å which should to a first approximation be the red shift at the centre of the Sun, if produced by the effect studied in the present paper.

(2) Moving from the Sun's centre to the limb, we would expect the red shift to increase proportional to $\sec\theta$, θ being the angle between the line of sight and the solar radius to the point where the line of sight cuts the surface, since the length of path through the atmosphere is equal to $l_0\sec\theta$, l_0 being the length of path at the centre.

Accordingly we obtained a least square solution for the quantities x and y in the equation $\varDelta\lambda_{\text{obs}}=x+y\sec\theta$ using Miss Adam's data. The least square solution gives

$$x=(+2{\cdot}72\pm0{\cdot}2)\times10^{-3}\,\text{Å},\quad y=(+1{\cdot}85\pm0{\cdot}1)\times10^{-3}\,\text{Å}.$$

The dotted curve in fig. 2 shows that the red shift along the whole surface of the Sun is well represented by the formula

$$\varDelta\lambda=(2{\cdot}72+1{\cdot}85\times\sec\theta)\times10^{-3}\,\text{Å}.$$

The value of $1\cdot85\times10^{-3}$ Å for the central red shift is in good agreement with the predicted value $1\cdot65\times10^{-3}$ Å. In addition a constant red shift is found, but its value is only about one-fifth of the value predicted by the theory of relativity (see fig. 2). It is of the greatest importance that solar observations are taken up again from this new point of view.

§ 5. Observed Red Shifts of other Stellar Spectra

The red shift effect considered in the present paper decreases so rapidly with decreasing temperature that observable effects are only to be expected for later type stars under very special conditions.

(i) A-*Stars*

The effective temperature for A-stars is about 10 000°K and the red shift should have decreased to about 0·6 km/sec. Various statistical investigations (Gyllenberg 1915) of the K-effect for A-stars give, apart from the dependence on galactic longitude mentioned earlier, a positive mean red shift between 0·1 and 0·9 km/sec. A mean red shift of the right order of magnitude is thus indicated.

(ii) *Super Giant* M-*Stars*

The surface temperature of these stars has decreased to about 3000°K. The characteristic feature of these stars are their very large radii. The mean density of their matter must be extremely low and according to Unsöld (1938) their atmospheres are about two thousand times as extended as the solar atmosphere. The depth at which the stellar lines originate in the stellar body and the depth at which other lines originate in the surface layers of their atmospheres must differ by the great length of path these stellar lines must traverse. It was discovered by Adams and McCormack (1935) that in various of the near and bright supergiants of low temperature (given in table 4) lines which must be produced on the top level of the atmosphere, such as the sodium D_1 and D_2 and Ca^+ H and K lines, show a marked violet shift relative to the stellar lines. They tried to explain these systematic shifts as indicating a general expansion of the atmosphere of such stars, but there is no other evidence to support this hypothesis.

Table 4

1	2	3	4	5
α Orionis	cM2	+3·4	+5·8	460
β Pegasi	M2	+5·3	+8·2	110
α Scorpii	cM2	+5·2	—	160
α′ Herculis	M5	+3·5	—	320

Column 1 gives the name of the star, Col. 2 its spectral type, Col. 3 the red shift in km/sec of the stellar lines with respect to the D_1 and D_2 lines of Na, Col. 4 the red shift in km/sec of the stellar lines relative to the H and K lines of Ca, Col. 5 the stellar radius in solar radii as unit.

According to the ideas developed here we would interpret the observed line displacements as *red shifts* of the stellar lines, coming from great depths, relative to the high level atmospheric lines. Although the surface temperature of these stars is relatively low (3000°K), the length of path l may be 10^3 times as large as in the case of the Sun. Hence red shifts should be expected of the order of $(3/20)^4 \times 10^3 \times 10$ km/sec$\doteqdot 5$ km/sec in full agreement with observations.

The list of stars in Adam's and McCormack's paper contains also β Ori, a cB8 star of $T_{\text{eff}} \sim 13\,000$°K and α Cygni ($T_{\text{eff}} \sim 10\,000$°K). In these two cases very much smaller values for l are, of course, sufficient to explain the observed red shift of low level lines relative to the atmospheric lines.

(iii) *Wolf–Rayet Stars*

The effective temperatures of W–R-stars lie between 40 000°K and 100 000°K, as determined from the ionization potentials of lines in their spectra. These stars should thus, according to formula (1), show red shifts of the order of 100 km/sec or more. These red shifts have, indeed, been found. The most striking cases are those of the binaries HD 193576 (one component a W-R-star and the other component an O-star) and HD 190918 (one component a W–R-star and the other component a B-star). The spectral lines of both components can be observed in both cases and lead to a consistent set of orbital elements (Wilson 1940, 1949). However, the radial velocity of the centre of gravity of the system as determined from the light curve of the W–R component gives a value +90 km/sec resp. +110 km/sec higher than the value determined from the light curve of the other component (compare fig. 3, taken from O. C. Wilson). The W–R component shows thus a red shift relative to the other component. Since these components should show red shifts of 10 km/sec resp. 20 km/sec (see § 2), we see that W–R-stars show red shifts of 110–120 km/sec in agreement with formula (1) with $T = 40\,000$°K.

(iv) *White Dwarfs*

In connection with the problem under consideration the red shift of Sirius B attains special significance. At the surface of white dwarfs, such as Sirius B, the radiation field is so strongly reduced compared to normal dwarf stars, such as the Sun or Sirius A, that the relativistic red shift should become observable quite unimpaired by the new effect due to the radiation field in the stellar atmosphere. It is highly regrettable that the accuracy attainable in measuring the red shift of the lines in Sirius B is so low and that there is still a great uncertainty concerning the mass and radius of Sirius B, so that final conclusions cannot yet be drawn.

The results in Adam's paper (1925) are mainly based on measurements of H_β and H_γ; the other lines which were measured gave results of only very low weight. The measurements of H_β yield a red shift of +26 km/sec, the values scattering between +17 km/sec and +31 km/sec; H_γ gives a red shift of +10 km/sec, values scattering here between +2 km/sec and +17 km/sec. To make these two sets compatible, the red shift obtained for H_γ is corrected by multiplying the observed mean value by a factor 2·1, the assumption being that the blending of the spectrum of Sirius B by the light of Sirius A makes such a radical correction necessary.

Fig. 3

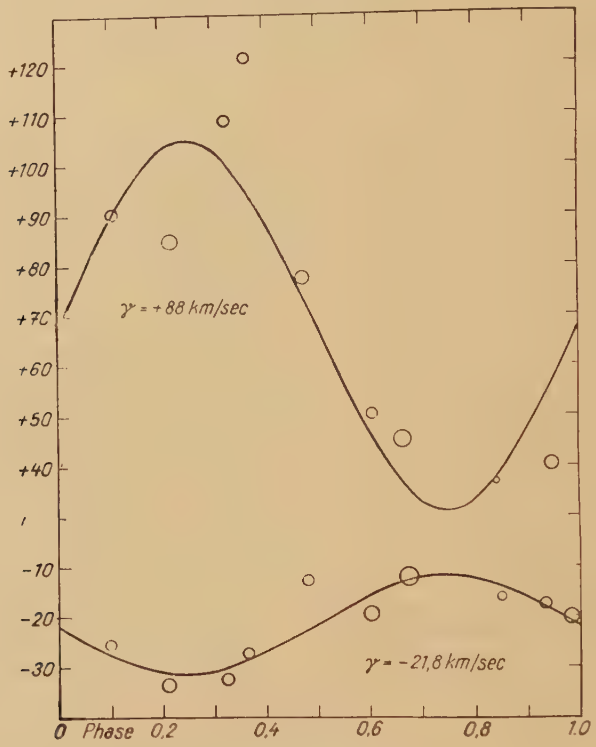

The radial velocity curves of the two components of the binary HD 190918. The upper curve corresponds to the Wolf–Rayet component, the lower one to the B-component. The velocity γ of the centre of gravity of the system following from the upper curve is +88 km/sec and following from the lower curve is —22 km/sec.

The final value of the red shift is +19 km/sec, which agrees well with a second independent determination by Moore (1928) which gave (+21±5) km/sec. From these observations the conclusion can be drawn that Sirius B reveals a systematic red shift, the value of which *most probably lies between* +10 *km/sec and* 30 *km/sec, but no more can be said.*

Since then white dwarfs have been the object of intensive study, and evidence is accumulating that the true values for the mass and radius of Sirius B differ considerably from the values on which the first determination of the gravitational red shift had been based. The mass is apparently very nearly equal to the solar mass and the radius smaller than $0{\cdot}008\, R_{\odot}$. The new values of mass and radius lead to a predicted gravitational red shift much larger than the red shift so far observed.

Kuiper (1941) discusses, for instance, a possible model for Sirius B which would give rise to a gravitational red shift of nearly 80 km/sec, but dismisses this model chiefly because it would contradict the actually observed red shift, taking the agreement of the observed and the theoretically predicted value as absolutely necessary. However, Gamow and Critchfield (1949) are also led to a very similar model for Sirius B :—it has a mass of $0{\cdot}98\, m_{\odot}$ and a radius of $0{\cdot}008\, R_{\odot}$. They state, without giving further references, that these values are consistent with recent observations. From these values of mass and radius a gravitational red shift of nearly +80 km/sec follows.

There is obviously also in the case of Sirius B growing evidence that the observed red shift is considerably smaller than the value predicted by the theory of relativity.

§ 6. THE COSMOLOGICAL RED SHIFT

The fundamental character of the effect under consideration raises, necessarily, the question whether it might not also be the cause of the cosmological red shift which hitherto has been interpreted as a Doppler effect. In this case, the influence of the factor l in formula (1) is given explicitly from observations. The observed red shift $\Delta\lambda/\lambda$ increases for every million parsec ($=3\times10^{24}$ cm) by $0{\cdot}8\times10^{-3}$ which corresponds to a velocity increase of 500 km/sec when interpreted as a Doppler effect. An increase by 10 km/sec—corresponding to the red shift in a B2 star with $T_{\mathrm{B}}=20\,000$°K—would correspond to a path $l_{\mathrm{S}}=1{\cdot}2\times10^{23}$ cm.

As far as the mean temperature T_{S} of intergalactic space is concerned, apart from the knowledge that it must be near the absolute zero, no reliable information is available. If we may interpret the cosmological red shift in the same way as the stellar red shifts, the following equation should hold :

$$T_{\mathrm{S}}{}^4 l_{\mathrm{S}}=T_{\mathrm{B}}{}^4 l_{\mathrm{B}}, \quad \text{or} \quad T_{\mathrm{S}}=T_{\mathrm{B}}(l_{\mathrm{B}}/l_{\mathrm{S}})^{1/4}. \qquad . \quad . \quad . \quad . \quad (3)$$

Equation (3) shows that the value of T_{S} obtained in this way does not depend strongly on the choice of l_{B}. Taking for l_{B} the two extreme values 10^7 cm and 10^9 cm, we get the following two reasonable values

$$T_{\mathrm{S}}=1{\cdot}9\text{°K} \quad \text{and} \quad T_{\mathrm{S}}=6{\cdot}0\text{°K}.$$

In a recent paper Gamow (1953) derives a value for T_{S} of 7°K from thermodynamical considerations assuming a mean density of matter in space of 10^{-30} g/cm^3.

One may have, therefore, to envisage that the cosmological red shift is not due to an expanding universe, but to a loss of energy which light suffers in the immense lengths of space it has to traverse coming from the most distant star systems. That intergalactic space is not completely empty is indicated by Stebbins and Whitford's discovery (1948) that the cosmological red shift is accompanied by a parallel unaccountable excess reddening. Thus the light must be exposed to some kind of interaction with matter and radiation in intergalactic space.

§ 7. Conclusions

It appears that an effect of not yet established nature produces red shifts of the lines in stellar spectra which overshadows the gravitational red shifts predicted by the theory of relativity. This has obviously been the reason for the difficulties which the astronomers encountered in their attempts to test the theory of relativity. There are also indications that where a gravitational red shift occurs (constant term in the solar red shift, Sirius B) this shift is only about one-fifth of the theoretically predicted shift.

The idea suggested here, that light suffers loss of energy in an intense radiation field, perhaps due to photon–photon interactions, must first be incorporated in the theory of the nature and propagation of light before final conclusions can be drawn.

Acknowledgments

I am very much obliged to Miss B. Middlehurst for the assistance she gave me in the detailed discussion of the red shift of the B-stars in the Orion Nebula group and to Mr. T. B. Slebarski for his statistical analysis of the data pertaining to these stars. I wish also to thank Dr. A. Beer, Cambridge, for the valuable information he gave me concerning the masses of binary stars and Professor Z. Kopal for drawing my attention to the binaries of which one component is a Wolf–Rayet star. I am particularly indebted to Dr. D. ter Haar who during my illness revised and amended the manuscript and made possible the publication of this paper without any further delay.

References

Adam, M. G., 1948, *Mon. Not. R. Astro. Soc.*, **108,** 446.
Adams, W. S., 1925, *Proc. Nat. Acad. Sci.*, **11,** 382.
Adams, W. S., and MacCormack, E., 1935, *Ap. J.*, **81,** 119.
Bottlinger, K. F., 1931, *Veröff. Univ. Sternwarte zu Berlin-Babelsberg*, Vol. 8, Part 5.
Evershed, J., 1935, *Mon. Not. R. Astro. Soc.*, **95,** 503 ; 1936, *Ibid.*, **96,** 153.
Freundlich, E. F., 1919, *Phys. Zeits.*, **20,** 561 ; 1954, *Göttinger Nachr.*, No. 7.
Freundlich, E. F., and v. d. Pahlen, E., 1923, *A.N.* **218,** 369.
Freundlich, E. F., v. Brunn, A., and Brück, H., 1930, *Zeit. f. Astrophys.*, **1,** 43.
Gamow, G., 1953, *Dan. Acad. Math.-Phys. Section*, **27,** No. 10.
Gamow, G., and Critchfield, C., 1949, *Theory of Atomic Nucleus and Nuclear Energy-Sources* (Oxford).
Gyllenberg, W., 1915, *Lund. Medd.*, 2.

HUNTER, A., 1934, *Mon. Not. R. Astro. Soc.*, **94,** 594.
KUIPER, G. P., 1941, White Dwarfs in *Actualités Scientifiques et Industrielles.*
MARKOWITZ, W. M., 1948, *Astr. J.*, **54,** 111.
MOORE, J. H., 1928, *P.A.S.P.*, **40,** 229.
V. D. PAHLEN, E., and FREUNDLICH, E. F., 1928, *Publ. Ap. Obs. Potsdam*, **26,** No. 86.
PISMIS, M. P., 1938, *Revue Fac. Sc. Univ. d'Istanbul*, Vol. 3, Part 4.
STEBBINS, J., and WHITFORD, A. E., 1948, *Ap. J.*, **108,** 413.
STRUVE, O., 1945, *Ap. J.*, **102,** 137; 1950, *Stellar Evolution* (Princeton: University Press).
STRUVE, O., and TITUS, J., 1944, *Ap. J.*, **99,** 84.
ST. JOHN, C. E., 1928, *Ap. J.*, **67,** 195.
TRUMPLER, R. J., 1935, *P.A.S.P.*, **47,** 234.
UNSÖLD, A., 1938, *Physik der Sternatmosphären* (Berlin: Springer).
WILSON, O. C., 1940, *Ap. J.*, **91,** 394; 1949, *Ibid.*, **109,** 76.

XXXVI. *On Freundlich's Red-Shift*

By D. ter Haar
St. Salvator's College, University of St. Andrews*

[Received January 2, 1954]

Abstract

Freundlich's data are analysed and it is shown (i) that the energy loss leading to the observed red-shifts is most probably taking place in the stellar atmospheres; (ii) that neither the Compton effect nor photon–photon interaction in the form considered by Euler and Kockel can account for the effect; (iii) that if the red-shifts are due to a photon–photon interaction effect, the cross section is at least of the order of 10^{-23} m^2,† and if they are due to photon–electron interactions the lower limit for the cross section is about 10^{-21} m^2; (iv) that a photon–electron interaction is more likely to be the cause of the red-shift than a photon–photon interaction.

§ 1. Introduction

In the preceding paper Freundlich has shown that red-shifts occurring in various stellar spectra (i) can not be explained by assuming that they are due to a relativistic gravitational effect, (ii) increase strongly with increasing surface temperature of the stars, and (iii) increase with increasing path of the light through the intense radiation field present in the atmosphere. Freundlich also draws attention to the fact that in the case of the white dwarf Sirius B the observed red-shift, which can only be attributed to a gravitational effect, is about one fifth of what one would expect from the mass and radius of this star. A similar reduction of the gravitational red-shift by a factor five seems to be present in the case of the sun, where apart from a contribution proportional to the path length through the solar atmosphere, a constant red-shift is found, which is about one fifth of the predicted relativistic effect. These observational data pose two problems. (i) How can one explain the reduction of the relativistic red-shift in Sirius B (and perhaps in the sun). (ii) Is it possible to find a mechanism active in a hot stellar atmosphere which will cause loss of energy to the photons passing through the atmosphere. It is not the purpose of the present note to suggest possible mechanisms, but only to derive from Freundlich's data some conditions which must be satisfied by the interaction mechanism. We shall base our analysis on the assumption that the red-shifts occurring in O-, B-, A-, G-, and supergiant M-stars are all due to the same effect. Most of our numerical considerations will be based

---

* Communicated by P. M. S. Blackett, F.R.S.

† We use throughout the MKS system of units.

on the data about the solar red-shift, since these data are probably the most reliable. Neglecting for a moment the constant term in the solar red-shift—which should be discussed in connection with the red-shift in Sirius B—the fractional loss of energy in the sun follows the equation

$$\Delta\nu/\nu = -3\times10^{-7}\sec\theta, \quad . \; . \; . \; . \; . \; . \; . \; . \quad (1)$$

where θ is the angle between the line of sight and the solar radius to the point where the line of sight cuts the solar surface.

In the spectra of supergiant M-stars it is found that lines originating from the bottom of the atmosphere are displaced towards the red end of the spectrum with respect to lines produced at the top of the atmosphere. The red-shift in this case corresponded to a recessional velocity of about 5 km/sec, or

$$\Delta\nu/\nu \doteqdot -2\times10^{-5}. \quad . \; . \; . \; . \; . \; . \; . \; . \quad (2)$$

§ 2. Analysis of Freundlich's Data

In order to be able to arrive at a reliable estimate of the cross section for whatever mechanism is responsible for the observed red-shifts, we must first of all make sure that, indeed, the red-shift is produced in the atmospheres of the stars and not somewhere else. As far as the red-shifts of the O- and B-stars are concerned, one might feel that the radiation field outside the stars might well contribute to the red-shifts (we return to this point in § 4), but the variation of the red-shift over the disc of the sun points to the red-shift being produced, if not in the atmosphere itself, then at any rate in a region close to the atmosphere with an extension small compared to the solar radius. The final proof of the fact that stellar atmospheres are responsible for at least a large part of the red-shift follows from the data about the supergiants. Even though outer layers may contribute to the red-shift, the atmosphere of a supergiant must give rise to a red-shift of the order of the one described by eqn. (2).

The temperature of the atmosphere of a supergiant M-star is of the order of 3000°K and the electron density of the order of 10^{16} m^{-3} (Rosseland 1936). The depth of the atmosphere is of the order of 10^8 m. Since the displaced lines in the case of the sun are sharp, at least one hundred scattering processes must have contributed to the production of the red-shift, each giving a red-shift of the order of $|\Delta\nu/\nu| \doteqdot 3\times10^{-9}$. As the basic assumption of our discussion is that the process which produces the solar red-shift also produces the other red-shifts, we get from eqn. (2) that at least about 10 000 scattering processes are required to produce the red-shift in the supergiants. Moreover, from the solar law (1) it follows that the deflection at each interaction process must be extremely small, since otherwise the dependence on θ would not occur. We come thus to the conclusion that in the case of a supergiant the mean free path must be of the order of 10^4 m. If n be the number of scattering agents in the atmosphere per unit volume and $\bar{\sigma}$ the average scattering cross section, we have $n\bar{\sigma} = 10^{-4}$ m^{-1}, and hence

$$\bar{\sigma}_{\mathrm{ep}} \doteqdot 10^{-20}\ \mathrm{m}^2, \ \bar{\sigma}_{\mathrm{pp}} \doteqdot 10^{-22}\ \mathrm{m}^2 \quad . \; . \; . \; . \quad (3)$$

for electron–photon and photon–photon interaction cross sections. To derive the second value we have assumed that the radiation field is a black body field of 3000°K so that $n_p \doteq 10^{18}\ \mathrm{m}^{-3}$.

If we had used the solar red-shifts and assumed that the total effect was produced in the solar atmosphere ($n_e \doteq 10^{18}\ \mathrm{m}^{-3}$, $n_p \doteq 10^{19}\ \mathrm{m}^{-3}$, depth $\doteq 10^5$ m) we would have got

$$\bar{\sigma}_{ep} \doteq 10^{-21}\ \mathrm{m}^2, \quad \bar{\sigma}_{pp} \doteq 10^{-22}\ \mathrm{m}^2, \qquad \qquad (4)$$

which are essentially the same as eqn. (3).

Before we compare eqns. (3) and (4) with the cross sections for known electron–photon and photon–photon scattering processes, we may briefly discuss the requirement for forward scattering which follows from eqn. (1). Since the red-shift can be followed across the solar disc and varies according to eqn. (1), the scattering process must be such that the total angle over which the photon is deflected must be small compared to the angle under which we see the solar disc from the earth (about 0·01 radians). Assuming once again about 100 scattering processes to be responsible for the observed red-shift we get then for the average angle of deflection ϕ the inequality

$$\phi \lesssim 10^{-5}\ \text{radians}. \qquad \qquad (5)$$

§ 3. COMPARISON WITH KNOWN SCATTERING PROCESSES

Both electron–photon and photon–photon scattering processes have been studied. In the first place we have the Compton effect and the second process has been studied by Euler and Kockel (1935). It is easily seen that neither of these two processes can account for the observed red-shifts. Let us first consider photon–photon scattering. The cross section for scattering of light of wave length λ by light of wave length λ' is given by the formula (this is a slight generalization of Euler and Kockel's equation)

$$\sigma_{pp} \doteq r_e^{\,4}\, \lambdabar_C^{\,4}\, \lambda^{-3}\, \lambda'^{-3}, \qquad \qquad (6)$$

where $\lambdabar_C$ is the Compton wavelength divided by 2π and r_e the classical electron radius. With $\lambda \doteq 6000$ Å (the wavelength of the lines studied in the solar spectrum), $\lambda' \doteq 5000$ Å (the wavelength at the maximum of the Planck curve according to Wien's law) we get

$$\sigma_{pp} \doteq 10^{-74}\ \mathrm{m}^2, \qquad \qquad (7)$$

which is clearly far too small to produce the observed effect as can be seen from eqns. (3) and (4).

As far as the Compton effect is concerned, its cross section is given by the Klein–Nishina formula and thus at most equal to the Thomson cross section,

$$\sigma_{ep} \leqslant 8\pi\, r_e^{\,2}/3 \doteq 10^{-28}\ \mathrm{m}^2, \qquad \qquad (8)$$

which is again too small, though not by quite as much as in the case of the photon–photon scattering. However, in this case it is impossible to satisfy condition (5). If the total loss given by eqn. (1) is produced in n scattering processes, the total angle of deflection Φ is equal to $\phi\sqrt{n}$. The average fractional loss of energy is then $\Delta\nu/n\nu$. Such an average fractional loss of energy $\Delta\nu/n\nu$ is accompanied by an average angle of deflection given by the equation (see, for instance, Richtmyer and Kennard 1947)

$$\phi \doteqdot |\Delta\nu/\nu|^{1/2}\,(\lambda/\pi\lambdabar_C)^{1/2}\,n^{-1/2}, \qquad (9)$$

whence

$$\Phi \doteqdot |\Delta\nu/\nu|^{1/2}\,(\lambda/\pi\lambdabar_C)^{1/2} \doteqdot 0{\cdot}2 \text{ radians}, \qquad (10)$$

which is not small compared to the angle under which we see the sun from the earth.

§ 4. DISCUSSION

In § 2 we saw that the main part of the red-shift must be produced in the stellar atmosphere. The question then arises whether or not the corona and even perhaps the immediate surroundings of the star should contribute to the observed red-shifts. We shall discuss separately the two possibilities of photon–photon interaction and photon–electron interaction.

(i) *Photon–Photon Interactions*

If the red-shifts are due to some kind of photon–photon interaction, it follows from the fact that the scattered light is in the visible region and the scattering light also in the visible region ($\lambda_{\max}=5000$ Å for the sun, $\lambda_{\max}=10\,000$ Å for supergiant M-stars) that it must be a process which is active between photons of only moderate energy. For the total fractional energy loss we can write

$$\Delta\nu/\nu = \int dx \int (\delta\nu/\nu)\,\sigma(\nu', \nu)\,\rho(\nu', T, x)\,d\nu', \qquad (11)$$

where $\delta\nu/\nu$ is the fractional energy loss per scattering, $\sigma(\nu', \nu)$ the cross section for scattering between a photon of energy $\boldsymbol{h}\nu$ and a photon of energy $\boldsymbol{h}\nu'$, ν the frequency of the scattered light quantum and $\rho(\nu', T, x)$ the light quanta density per unit volume at x at the temperature T ($\rho(\nu', T, x)$ is supposed to be a Planck density divided by $\boldsymbol{h}\nu'$). For the sake of simplicity we shall assume $\delta\nu/\nu$ to be independent of ν'.*

From eqn. (11) we get eqn. (1) by putting $\delta\nu/\nu \doteqdot -3\times10^{-9}$, $\sigma=\bar{\sigma}\doteqdot 10^{-22}\,\text{m}^2$, $T=6000^\circ$K, and integrating over the depth of the solar atmosphere ($\doteqdot 10^5$ m).

The question now arises what the influence is of the radiation field outside the solar atmosphere. Neglecting the highly diluted high temperature component in the corona, we may assume the radiation field to be given by the formula

$$\rho(\nu', T, x) = \alpha(\nu'\,;\,x)\,(R_0/x)^2\,\rho(\nu', T_0), \qquad (12)$$

where R_0 is the solar radius, x the distance from the centre of the sun, T_0 the solar surface temperature ($T_0 \doteqdot 6000^\circ$K) and where $\alpha(\nu'\,;\,x)$ takes care of possible absorption of the light (for visible light $\alpha(\nu'\,;\,x)\doteqdot 1$).

From eqns. (11) and (12) we then get for the ratio of the red-shift produced in the stellar atmosphere to the red-shift produced between the sun and the earth (putting $\alpha(\nu'\,;\,x)=1$ and taking $\delta\nu/\nu$ to be a constant)

---

* This assumption greatly simplifies the discussion, but is not essential as can easily be verified.

$$[\Delta\nu/\nu]_{\mathrm{Atm}}/[\Delta\nu/\nu]_{\mathrm{S}\rightarrow\mathrm{E}}=l/R_0, \qquad (13)$$

where l is the height of the solar atmosphere.

From eqn. (13) we see that, if we assume the red-shift to be produced by photon–photon interactions in a radiation field, the red-shift produced between the sun and the earth is much larger than the red-shift produced in the solar atmosphere. The same argument applies to the other cases of the red-shifts produced in O-, B- or A-stars. It must be emphasized that most of the $[\Delta\nu/\nu]_{\mathrm{S}\rightarrow\mathrm{E}}$ is produced in the vicinity of the sun ($x \lesssim 5\,R_0$), and both the red-shift in the supergiants and the secant-law (1) are thus of the utmost importance since they show that the effect really occurs in the atmospheres themselves. It seems from this consideration that photon–photon interactions probably cannot be the cause of the observed red-shifts, which to some extent is satisfactory since the discrepancy between the theoretical cross section (7) and the necessary cross section (3) is so enormous.

(ii) *Photon–Electron Interactions*

The situation is slightly more satisfactory in this case. Instead of eqn. (11) we now have

$$\Delta\nu/\nu=\int dx\int(\delta\nu/\nu)\,\sigma(\nu,\mathbf{v})\,n(\mathbf{v},x)\,d\mathbf{v}, \qquad (14)$$

where $n(\mathbf{v},x)\,d\mathbf{v}$ is the number of electrons with velocities between $\mathbf{v}$ and $\mathbf{v}+\mathbf{dv}$ at x. Once again we can use eqn. (14) to investigate the influence of outer solar layers, such as the corona, but the electron density decreases so rapidly (Aller 1953) that $[\Delta\nu/\nu]_{\mathrm{S}\rightarrow\mathrm{E}}$ in this case will at most be of the same order of magnitude as $[\Delta\nu/\nu]_{\mathrm{Atm}}$. Moreover, the difference between the values of eqns. (3) and (4) and the value of eqn. (8) is not as enormous as in the corresponding case of the photon–photon processes. We may therefore tentatively conclude that although no known phenomenon can give rise to the observed red-shifts it seems more likely that the cause is an electron–photon scattering effect than a photon–photon interaction.

ACKNOWLEDGMENT

I should like to express my thanks to Professor E. F. Freundlich for showing me his data before publication and for many stimulating discussions.

REFERENCES

ALLER, L. H., 1953, *Astrophysics* (New York : Ronald Press Cy.), pp. 374 and 379.

EULER, H., and KOCKEL, B., 1935, *Naturwiss.*, **23**, 246.

RICHTMYER, F. K., and KENNARD, E. H., 1947, *Introduction to Modern Physics* (New York : McGraw-Hill Inc.), p. 517.

ROSSELAND, S., 1936, *Theoretical Astrophysics* (Oxford : University Press), p. 180.

XXXVII. *Cohesion of the Alkali Metals in the Thomas–Fermi–Dirac Theory*

By N. H. March
Department of Physics, The University, Sheffield*

[Received December 21, 1953]

Summary

It is pointed out that, contrary to the usual belief, the Thomas–Fermi–Dirac method affords some explanation of metallic binding, and the results predicted by the theory are presented.

The first suggestion that the Thomas–Fermi (TF) method might be useful for dealing with metallic problems was made by Lennard-Jones and Woods (1928). However, to avoid the mathematical difficulties associated with the non-linearity of the fundamental equation, they considered a two-dimensional model. Unfortunately, much of the physical usefulness of the method was thus sacrificed for the mathematical simplicity achieved.

An important advance was, however, made by Slater and Krutter (1935, referred to hereafter as SK) when they pointed out that to a good approximation the many-centre problem could be reduced to that of a single spherical cell, exactly as in the Wigner–Seitz method. The TF equation can then be solved numerically and this was done by SK for a number of cases. They also considered the Thomas–Fermi–Dirac (TFD) method in which exchange is introduced (Dirac 1930, see also Jensen 1934). Their general conclusions were that the methods (both TF and TFD) were inadequate to provide an explanation of metallic cohesion, but should be useful for giving a first approximation to the potential fields, charge distributions and momentum distributions in metals.

It is the purpose of the present note to show that, contrary to the conclusion of SK, the TFD method does in fact give some explanation of metallic binding, and to present the results which the theory predicts.

It will help to clarify the present work if, first of all, we briefly review the existing state of affairs in the TFD theory. From the outset, a difficulty has been present, because a certain maximum radius R_m exists for each atomic number Z, and hence there is no solution of the TFD equation which represents a charge distribution extending to infinity. Furthermore, there is no solution for which the boundary density is zero. Brillouin (1934) initially made the suggestion that the solution corresponding to the radius R_m should be taken to represent the isolated atom in this theory. However, Jensen (1935) then proposed that the radius of the 'atom' should be found by minimizing the energy with respect to the radius, and he derived the expression

$$\frac{dE}{dR}=-4\pi R^2\left[\tfrac{2}{3}\,c_k\{n(R)\}^{5/3}-\tfrac{1}{3}\,c_e\{n(R)\}^{4/3}\right] \quad . \quad . \quad . \quad . \quad . \quad (1)$$

---

* Communicated by the Author.

where E is the total energy, R is the radius of the 'atom', $n(R)$ is the boundary density and c_k and c_e are defined by

$$c_k = \frac{3h^2}{10m}\left(\frac{3}{8\pi}\right)^{2/3}, \quad c_e = \frac{3e^2}{4}\left(\frac{3}{\pi}\right)^{1/3}.$$

Then, according to Jensen, the radius of the isolated atom in the model is taken to be that radius, R_e say, for which $dE/dR=0$. However, both the suggestions of Brillouin and Jensen are really very unsatisfactory, as they lead to 'atoms' of finite radius with a discontinuity of charge density on the boundary.

But, ignoring these interpretations, and looking at (1) in the light of the work of SK, it is clear that plotting E as a function of R there is a minimum at $R=R_e$, and this is in fact what SK were seeking.* Their numerical calculations for Cu, on which their conclusions were based, failed to reveal the minimum† which, as (1) shows, exists beyond doubt. The reason why SK missed the minimum appears to be due to the fact that R_e lies very close to the maximum radius R_m, and in fact outside the range of their solutions (for Cu, $x_m=16{\cdot}3$, $x_e=15{\cdot}5$ whilst their energy curve extends only to $x=12$, x being the customary TF dimensionless variable). It seems quite clear to the writer, therefore, that the TFD method gives some explanation of metallic binding, and that the previous interpretation of the solution corresponding to the radius R_e as representing the isolated atom is incorrect. If we reject it, then of course the difficulties of discontinuity of charge density disappear, the density joining on smoothly to that in the adjacent atomic polyhedra.

We have still to decide, however, what is the most reasonable physical interpretation to attach to the results of the model. We know of course that the TF and TFD methods are not capable of explaining the periodic properties of the elements, and hence the most that can be expected is that the results will apply to one particular group of metals. From the assumptions of the TF theory it seems clear that the model must describe 'alkali-type' metals (see, for example, Seitz 1940). We shall in fact see that the results obtained support this viewpoint.

Now Jensen, Meyer-Gossler and Rohde (1938) have obtained values of R_e, the radius of the isolated atom in Jensen's model, for Ar, Kr and Xe, and in the course of this work we have carried out accurate calculations for Li and Na. The values of R_e for K, Rb and Cs can then be obtained by interpolation. These values will correspond to the lattice constants in our treatment and are shown in the first row of the table, whilst the values obtained from experiment are shown in the second row. In the writer's opinion the agreement is extremely gratifying when one remembers the nature of the model employed, and the relative ease with which the complete alkali series can be discussed.

---

* That there is no minimum in the unmodified TF model can be seen immediately by putting $c_e=0$ in (1). This was of course proved beyond doubt by SK.

† It is of interest to note in passing that in an earlier paper, Slater (1934) had announced the existence of a minimum.

However, the results obtained for the compressibilities are much poorer, and we have not considered it worthwhile to carry through precise calculations, which would be quite laborious. We have made as good an estimate of the compressibilities as possible using existing solutions of the TFD equation, together with some solutions which we have calculated for Li and Na. We find that the compressibilities do not vary very much with atomic number. We cannot say for certain whether the values increase or decrease with increasing Z, though we believe from our estimates that they decrease. However, the compressibilities are all of the order of 50×10^{-12} cm²/dyne, whereas the experimental values range from $(7-50) \times 10^{-12}$ cm²/dyne as we go through the alkali series from Li to Cs.

Lattice Constants for Alkali Metals

	Li	Na	K	Rb	Cs
TFD R_e (Å)	1·86	2·16	2·28	2·39	2·50
Experiment	1·70	2·09	2·58	2·77	2·98

The value for Li is very poor, it is true, but agreement between theory and experiment improves with increasing atomic number which, one might argue, is satisfactory for such a model. That this argument must not be pushed too far, however, is shown by the fact that the same is not true for the lattice constants. In the case of Li, for which the results are certainly the poorest, the ion-core will not be well described by the method, and furthermore, the valence electrons appear to behave considerably differently from free electrons (March 1954). It is not surprising then that the results are particularly poor in this case. Though the compressibilities are rather disappointing, one should bear in mind the fundamental limitations of the method, and the fact that the detailed shape of the energy curve must be given accurately by the theory if a good compressibility is to be obtained.

The third quantity which one would like to calculate from the theory is the cohesive energy. However, an obvious difficulty arises here ; we have at present no really satisfactory isolated atom in this model, and since the cohesive energy is a small difference between two large quantities, it is essential to use the same method to calculate the energy of the metal and of the isolated atom.

Whilst still not satisfactory, the position with regard to the proper isolated atom in this treatment seems to the writer to have been clarified recently. Scott (1952), in his successful calculation of atomic binding energies, suggested that the difficulties of the TFD method could be avoided by using the ordinary TF atom solution to calculate the energy with exchange (that is the total energy first shown by Jensen to lead, when minimized with respect to the electron density, to the TFD equation). The present writer (March 1953) has gone somewhat further than Scott and has shown how the effect of exchange on the charge distribution can be taken into account in an approximate way by using the ordinary TF solution, with a scale factor introduced, as a variational function. These two investigations suggest to the writer that the correct isolated atom in the TFD model (using TFD here in the sense of the model based on the energy expression obtained by Jensen, rather than on the TFD equation) will be given by that function which behaves like the TF density at the origin, is well behaved elsewhere, and tends to zero at infinity, whilst making the total energy a minimum (not an absolute minimum but a minimum for functions which extend to infinity). As yet however, the writer has had no success in dealing with this problem, though work along these lines is still in progress. So, at any rate for the moment, the best that can be done for the energy of the isolated atom is to use the approximation obtained by the writer (March 1953). In order to see whether sensible values of the cohesive energy can be obtained we have taken the lowest energy given by SK for Cu (which we regard as an 'alkali-type' metal lying between K and Rb) and have found the difference between this and the isolated atom energy referred to above. The difference thus obtained is much too large. The explanation seems to us to be clear: the isolated atom energy is not known with sufficient accuracy. For a decrease of less than $\frac{1}{2}$ of an atomic unit in a total energy of 2047 atomic units for Cu would lead to a reasonable value. If the energy of the isolated atom can be calculated to a high degree of accuracy then we believe it possible that the method could lead to sensible values for cohesive energies (we would hope values less than the experimental values, in the sense that one knows that the correlation energy provides a significant contribution to the binding energy).

One final point which has emerged from the present work is worth mentioning here. It concerns the distribution of charge within an atomic sphere. For Na, it is easy to show that the boundary density is reduced by a factor of more than 2 when exchange is introduced (we have referred to this previously in connection with the momentum distribution of electrons in Na (March 1954)). Whilst, physically, such a decrease is what one would expect from the argument that exchange will tend to contract the charge cloud, the effect is surprisingly large. In fact, the boundary density corresponding to a cell radius of 2·16 Å is reduced to a value considerably below that due to one electron uniformly distributed throughout the atomic sphere. It does not appear possible at present to be certain whether such a result is to be taken seriously, or whether it arises from the Dirac method of including exchange.

References

Brillouin, L., 1934, *J. Phys. Radium*, **5,** 185.
Dirac, P. A. M., 1930, *Proc. Camb. Phil. Soc.*, **26,** 376.
Jensen, H., 1934, *Z. Phys.*, **89,** 713 ; 1935, *Ibid.*, **93,** 232.
Jensen, H., Meyer-Gossler, G., and Rohde, H., 1938, *Z. Phys.*, **110,** 277.
Lennard-Jones, J. E., and Woods, H. J., 1928, *Proc. Roy. Soc.* A, **120,** 727.
March, N. H., 1953, *Phil. Mag.*, **44,** 1193 ; 1954, *Proc. Phys. Soc.* A, **67,** 9.
Scott, J. M. C., 1952, *Phil. Mag.*, **43,** 859.
Seitz, F., 1940, *Modern Theory of Solids* (New York : McGraw-Hill), p. 384.
Slater, J. C., 1934, *Rev. Mod. Phys.*, **6,** 209.
Slater, J. C., and Krutter, H. M., 1935, *Phys. Rev.*, **47,** 559.

XXXVIII. *The Anomalous Spin of* ^{47}Ti

By B. H. Flowers
Atomic Energy Research Establishment, Harwell*

[Received January 13, 1954]

Abstract

A general discussion is given of the occurrence of anomalous spins among the odd mass nuclei. It is shown that the spin of ^{47}Ti may be understood on the basis of the independent particle model provided proper account is taken of the charge independence of nuclear forces. ^{49}V is predicted to have spin 5/2.

No completely satisfactory explanation has yet been given of the occurrence of anomalous spins among the odd mass nuclei. I refer to those odd mass nuclei whose ground states are of spin $J=j-1$ and seniority 3, instead of the normal spin $J=j$ and seniority 1, where j is the total angular momentum of the single-particle level being filled. There are three well-established examples of such nuclei, ^{23}Na, ^{55}Mn and ^{79}Se; and in addition ^{47}Ti has recently been quoted as having spin 5/2 instead of the normal spin of 7/2 expected for this nucleus (Walchi 1953). ^{21}Ne is sometimes quoted as being a further anomaly, but its spin is known only to be $\geqslant 3/2$ from spectroscopic measurements (Koch and Rasmussen 1949), and to be 3/2 or 5/2 from stripping reactions (Middleton and Tai); so that the normal spin of 5/2 is not ruled out in this case. ^{43}Ca has recently been shown to be normal (Jeffries 1953), having spin 7/2 instead of 5/2 as previously reported. Finally, there may be further cases among the heavier nuclei, but identification is then much less certain.

Two problems immediately arise. The first is to explain how these anomalous spins can come about at all; the second is to predict precisely which nuclei should be anomalous. These questions, of course, are not necessarily independent, although they are often assumed to be; but in any event, a complete theory of nuclear structure must find solutions to both of them. It is the purpose of the present note to demonstrate that these two problems are indeed interdependent and to provide a complete answer, in the case of one of the anomalous nuclei, ^{47}Ti.

Two suggestions have been made regarding the first problem. In the first place, Kurath (1950) has pointed out that a configuration j^n of an odd number n of like particles (neutrons only, or protons only, apart from closed shells) can exhibit in jj-coupling the anomalous ground state spin of $J=j-1$ provided that the range of the inter-particle forces is sufficiently great, say R; and provided, owing to the exclusion principle, that $j \geqslant 5/2$. This theory, further developed by Talmi (1952), has two shortcomings apart from those inherent in any independent-particle model. The first is that the range R at which the cross-overs take place is much too large to be consistent with what information we have about nuclear forces. The second is that the theory considers like particles only; that is to say, it ignores the important interactions between neutrons and protons. The second point is the more important in view of the first point; for, as shown by Edmonds and Flowers (1952 b), the neutron–proton interaction increases in importance as the range of interaction is increased. Furthermore, those nuclei to which Kurath's argument strictly applies, i.e. those having only neutrons or only protons apart from closed shells, are found to have normal spins. These are ^{43}Ca, ^{51}V and ^{137}Cs, apart from those with $j<5/2$ which are not of interest at present. In this connection, it would clearly be of interest to determine the spins of the β-active nuclei ^{19}O and ^{45}Ca—the former should be $\frac{1}{2}$ or 5/2 if normal, 3/2 if anomalous; the latter 7/2 if normal and 5/2 if anomalous. Mayer, Moszkowski and Nordheim (1951) suggest that ^{19}O is anomalous. This arises from the supposition that the allowed β-transition is to the $\frac{1}{2}+$ ground state of ^{19}F, implying that ^{19}O is $\frac{1}{2}+$ or $3/2+$, but not $5/2+$. It does not seem certain, however, that the β-decay does not lead to the two very low excited states of ^{19}F at 0·11 and 0·19 MeV quoted by Ajzenberg and Lauritsen (1952). Until this point is settled the possibility of $5/2+$ remains; but even if the transition is to the ground state of ^{19}F, it is still possible that ^{19}O has a $\frac{1}{2}+$ ground state.

---

* Communicated by the Author.

The second suggestion, due to Aage Bohr (1952), is that anomalous spins are expected when independent-particle motion is strongly coupled to the collective quadrupole oscillations of the nuclear surface. However, Bohr's theory would predict spins of $j-2$ for 5 like particles (or holes) in a level with $j \geqslant 9/2$. Thus, for example, ^{79}Se with the neutron configuration $g_{9/2}^{5}$ would have spin 5/2 instead of the observed 7/2.

Neither of these theories presents a solution to the second problem; neither predicts precisely which nuclei should be anomalous. More exactly, Kurath's theory appears to say that no nuclei should be anomalous unless some capricious perturbation effects are at work to favour the anomalous ground state for reasonable values of the range of interaction; while Bohr's theory suggests that interparticle forces which favour the normal ground state are in competition with particle-surface couplings favouring the anomalous state. In each case it is left to unknown perturbations to decide which state shall win.

These perturbations most likely arise from configurational interaction, in the language of the independent-particle model, and from the neutron–proton interactions. Thus, in ^{23}Na the $1d_{5/2}$ and $2s_{1/2}$ single-particle levels lie close together, and it is not implausible that the admixture of s-levels to a $d_{5/2}$ configuration should favour the state of lower spin. This question is at present being studied by J. P. Elliott. In ^{55}Mn, the protons are filling the $1f_{7/2}$ level, but the neutrons have already completed this level and are filling the $2p_{3/2}$ level. Owing to the neutron–proton interaction, the coupling between $p_{3/2}$ states and $f_{7/2}$ states may be sufficient to favour the anomalous ground state. In ^{79}Se, neutrons and protons are again filling different levels, and there is also a good chance of considerable configurational interaction at least amongst the neutrons for which the $1g_{9/2}$ and $2p_{1/2}$ levels lie close together. Thus, in three of the anomalous cases there is every reason to suppose that the perturbations called for by the Kurath and the Bohr theories do in fact exist. These make the first problem easier to understand, but the second problem more difficult to solve.

One suggestion has been made towards the solution of the second problem. Schawlow and Townes (1951) suggest that if a nucleus with x neutrons (or protons) is found to be anomalous, that with x protons (or neutrons) should also be anomalous. There is only one pair of nuclei to support their proposition, ^{47}Ti with 25 neutrons and ^{55}Mn with 25 protons. If ^{21}Ne is indeed anomalous, this nucleus with 11 neutrons will pair off with ^{23}Na having 11 protons to form a second example. The counterpart of ^{79}Se, however, is ^{103}Rh which has spin $\frac{1}{2}$. Indeed, if the explanation of anomalous spins is to be looked for in small perturbations, this proposal is likely to be in error for all but the lightest nuclei owing to the slightly different circumstances in which corresponding neutrons and protons find themselves in heavier nuclei.

There is, however, one region in which configurational interaction may be expected to play an unimportant part and in which the neutron–proton interaction can be properly taken into account, at least to the extent that nuclear forces are charge independent. This region is the $1f_{7/2}$ shell with *both* N and Z between 20 and 28. The stable odd mass nuclei in this region are ^{43}Ca, ^{45}Sc, ^{47}Ti, ^{49}Ti and ^{51}V. Discarding both the Kurath and Bohr suggestions would lead us at first sight to suppose that none of these nuclei could be anomalous. However, the classification of states in *jj*-coupling (Flowers 1952) shows that for the unique case of 7 particles in the 7/2-shell, with isotopic spin 3/2, the states of symplectic type (1110), including the anomalous 5/2 state, not only occur as the first group of excited states, but *occur twice*. Now states having the same isotopic spin and the same symplectic symmetry will interact very strongly, the non-diagonal term containing in general the 'large' integrals $E^{(0)}$ and $E^{(1)}$ (in the notation of Edmonds and Flowers 1952 a). On the other hand, the normal state of seniority 1 is as always unique, so that the non-diagonal terms in this case can involve only the 'small' integrals $E^{(2)}$ and $E^{(3)}$ (inasmuch as we neglect departures from charge independence). This means that one of the two states of seniority 3 and $J=5/2$ will be depressed very considerably below what is normally expected for states of that symplectic type, and may be lower than the normal state even for very short range forces.

Therefore, only for 7 particles and isotopic spin 3/2 would we expect an anomaly in the ground state spin. The corresponding nucleus is ^{47}Ti which is indeed the only one of these nuclei to be anomalous. There is, however, a counterpart to ^{47}Ti among the unstable nuclei : the 600-day ^{49}V, having 7 holes in the $1f_{7/2}$ shell and isotopic spin 3/2, may also be anomalous if the above explanation of ^{47}Ti is correct ; and this should be the only anomaly among the unstable odd-mass nuclei in this region. In this particular case, at least, we see that the two problems posed by the occurrence of anomalous spins are interdependent, and that their solution lies within the framework of the independent particle model provided that proper account is taken of the neutron–proton interactions. It may well be that the neutron–proton interaction plays an equally decisive role in the other cases too.

REFERENCES

AJZENBERG, F., and LAURITSEN, T., 1952, *Rev. Mod. Phys.*, **24,** 321.
BOHR, A., 1952, *Det. Kgl. Danske Vidensk. Selskab*, **26,** 14.
BOHR, A., and MOTTELSON, B. R., 1953, *Det. Kgl. Danske Vidensk. Selskab*, **27,** 16.
EDMONDS, A. R., and FLOWERS, B. H., 1952 a, *Proc. Roy. Soc.* A, **214,** 515; 1952 b, *Ibid.*, **215,** 120.
FLOWERS, B. H., 1952, *Proc. Roy. Soc.* A, **212,** 248.
JEFFRIES, C. D., 1953, *Phys. Rev.*, **90,** 1130.
KOCH, J., and RASMUSSEN, E., 1949, *Phys. Rev.*, **76,** 1417.
KURATH, D., 1950, *Phys. Rev.*, **80,** 98.
MAYER, M. G., MOSZKOWSKI, S. A., and NORDHEIM, L. W., 1951, *Rev. Mod. Phys.*, **23,** 315.
MIDDLETON, R., and TAI, C. T., 1952, *Proc. Phys. Soc.* A, **65,** 752.
SCHAWLOW, A. L., and TOWNES, C. H., 1951, *Phys. Rev.*, **82,** 268.
TALMI, I., 1952, *Helv. Phys. Acta*, **25,** 185.
WALCHI, H. E., 1953, *Oak Ridge National Laboratory Report* No. 1469.

XXXIX. *Experiments on Supersonic Flow over Flat-Nosed Circular Cylinders at Yaw*

By I. M. HALL
Fluid Motion Laboratory, University of Manchester*

[Received December 9, 1953 ; revised MS. received January 13, 1954]

SUMMARY

The flow pattern around flat-nosed circular cylinders at yaw was investigated by rotating the body about a line in the free-stream direction and taking schlieren photographs at different positions of the body.

It was found that the shape of the bow shock wave was practically unaltered by yaw, except for the nose regions, but the separation bubble at the shoulder was considerably distorted. Even for small angles of yaw there was a region on the suction side of the body where there was no reattachment.

On the lee side of the body there was a wake which was compared with the vortex wake in the two-dimensional flow past a circular cylinder started impulsively from rest. Good qualitative agreement was obtained. For high angles of yaw shock waves were found springing from the wake.

§1. INTRODUCTION

IN the inviscid flow past a slightly yawed, slender body of revolution the transverse, or cross-flow component is independent of the axial component. When viewed in a plane which is perpendicular to the axis and travels with the axial flow, the cross flow develops like the flow past a two-dimensional circular cylinder started from rest. The cylinder may expand or contract with time to conform to the changing cross section of the body as the distance from the nose increases. In incompressible flow a similar argument may be applied to the flow in the boundary layer of a yawed body, but in compressible flow the axial and cross-flow components are no longer independent. However, the flow may be expected to be qualitatively similar to the incompressible flow, and experiments described in this paper show that this is the case.

Allen and Perkins (1951) used these ideas to explain certain peculiarities in the flow about inclined bodies of revolution. In particular, they demonstrated that the pressure distribution over a yawed airship-shaped body was consistent with a separation of the cross flow which is known to occur on the leeward side of a circular cylinder. Further, it was shown experimentally that vortices were present in the flow and that these could be identified with the vortex wake which forms behind a circular cylinder started from rest.

---

* Communicated by P. R. Owen.

The present paper describes the flow about a flat-nosed cylinder set at angles of yaw of from 5° to 30°, in a stream of Mach number 1·96. Such a body is far removed from the slender pointed bodies at slight yaw used in the previous arguments concerning the nature of the cross flow. However, the constant cross section enables easy comparison to be made between the cross flow and the flow past a two-dimensional circular cylinder. It is also of interest to discover whether the development of the cross flow at high angles of yaw is qualitatively similar to the two-dimensional flow.

A new technique was used, which made it possible to study the three-dimensional flow pattern using a conventional schlieren system.

§ 2. NOTATION

a	radius of best circles as approximations to contours for bow shock wave.
b	displacement of the centres of these circles from z-axis along $\phi=0°$.
d	diameter of cylinder.
r	distance of a phenomenon from the z-axis, measured on a photograph.
x	distance from centre of nose measured along the axis of the body.
z	distance from centre of nose measured in the free-stream direction.
R	polar coordinate in planes $z=$constant.
V	free-stream velocity.
α	angle of inclination of axis of body to free-stream direction.
θ	angle between the vertical plane and the plane of symmetry of the model.
ϕ	polar coordinate in planes $z=$constant.
ψ	polar coordinate in planes $x=$constant.

N.B.—It is convenient to define θ, ϕ and ψ in the range (0°, 180°) only.

§ 3. EXPERIMENTS

The experiments were made in an intermittent vacuum-operated tunnel with a free-stream Mach number of 1·96 and Reynolds number of $3{\cdot}4\times10^5$ per inch. The working section was 5 inches by 4 inches and the stagnation pressure was approximately atmospheric. The tunnel was described by Bardsley and Mair (1951).

The flow was observed with a conventional two-mirror schlieren system. Each mirror had a diameter of 5 inches and a focal length of 60 inches. For photography, a spark discharge with a duration of about one microsecond was used.

The models were made from $\frac{1}{4}$-inch diameter silver steel rods bent in one plane as shown in fig. 1. AB and CD were straight and BC was a smooth bend so that the angle α between AB and CD was the required angle of yaw. The models were supported at points between C and D so that CD was in the free-stream direction. As α was increased AB was made shorter to ensure that the reflection of the bow wave from the tunnel walls did not interfere with the flow pattern upstream of B.

To obtain a complete picture of the flow the model was rotated about CD and schlieren photographs were taken at various values of the angle θ between the plane of the body and the downward vertical (fig. 2). The apparent angle of yaw in the photographs is $\tan^{-1} (\tan \alpha \cos \theta)$.

Photographs taken at θ and at $-\theta$ will obviously be identical. Furthermore, the picture at 180° $-\theta$ is simply the inversion of that at θ. Hence, the complete flow pattern can be studied by observations at values of θ between 0° and 90°. Photographs were taken of the flow past models with angles of yaw, α, equal to 5°, 10°, 20°, and 30°.

Fig. 1

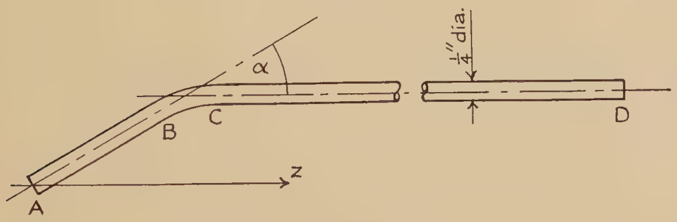

The model.

Fig. 2

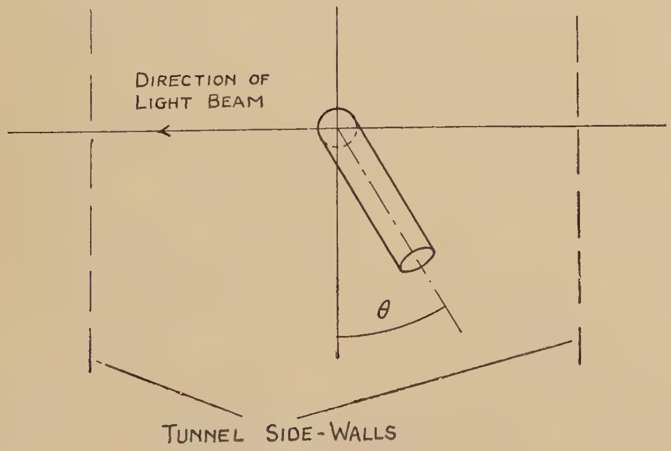

Setting of the model in the wind tunnel.

The intervals of θ between the values at which photographs were taken were chosen small enough to give a complete picture of the flow pattern. Figures 3–14 (Pl. 4, figs. 3–8; Pl. 5, figs. 9–14) show typical photographs. The values of α and θ for all the photographs are given in table 1.

Table 1

$\alpha=5°$

θ (deg.)	0	30	60	90
Fig. No.	3	—	—	—

$\alpha=10°$

θ (deg.)	0	6	12	24	30	36	42	54	60	72	90
Fig. No.	4	—	—	5	—	—	6	—	—	—	7

$\alpha=20°$

θ (deg.)	0	6	12	18	24	36	54	60	72	90
Fig. No.	8	—	9	—	—	—	—	10	—	11

$\alpha=30°$

θ (deg.)	0	18	30	36	54	60	72	90
Fig. No.	12	—	—	13	—	—	—	14

§ 4. Interpretation of the Photographs

Care must be taken in interpreting the photographs because the phenomena revealed by the schlieren system are not necessarily coplanar. Each photograph records the trace in a vertical plane of the cylindrical surfaces which have generators in the direction of the light beam and touch regions with large density gradients perpendicular to the schlieren knife edge. If the light beam were rotated about the tunnel centre line a series of such traces would be recorded, and the envelope of the surfaces would determine the shape and position of the light-refracting surface : a shock wave, for example. In practice, this information was obtained by keeping the schlieren system fixed and rotating the body.

It is convenient to analyse the flow pattern in a series of planes z=constant. In order to obtain the traces of the flow phenomena in one of the planes, the apparent distance, r, of each phenomenon (such as a point on a shock wave surface) from the z-axis is measured for several values of θ at the given value of z. These measurements then prescribe the position of a family of tangents to the trace of the light-refracting surface in the plane under consideration. The envelope of these tangents can be determined graphically. An example of the method of construction is given in fig. 15, and actual contours constructed by this method are shown in fig. 16.

If we define a cylindrical coordinate system (R, ϕ, z) fixed relative to the body such that $R=r$ and $\phi=\theta$ for $\theta=0°$ and $\theta=180°$, we have R as a function of ϕ for each contour. It can be shown that on a contour ϕ and θ are related by

$$\tan(\phi-\theta)=\frac{1}{r}\frac{dr}{d\theta}\,.$$

The radial distance R is given by

$$R = r \sec(\phi - \theta).$$

It is clear that in general the actual values of ϕ for two phenomena visible on the same photograph will not be the same. For example, in fig. 16

Fig. 15

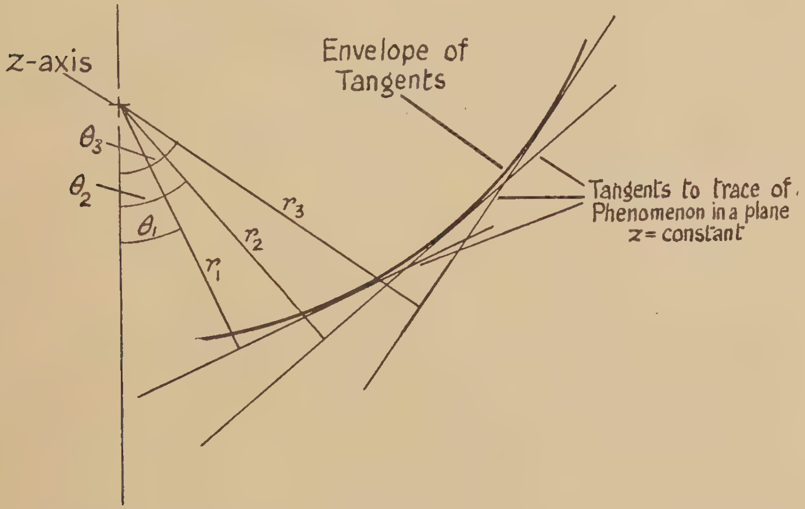

Construction of the trace of a phenomenon in a plane z=constant.

Fig. 16

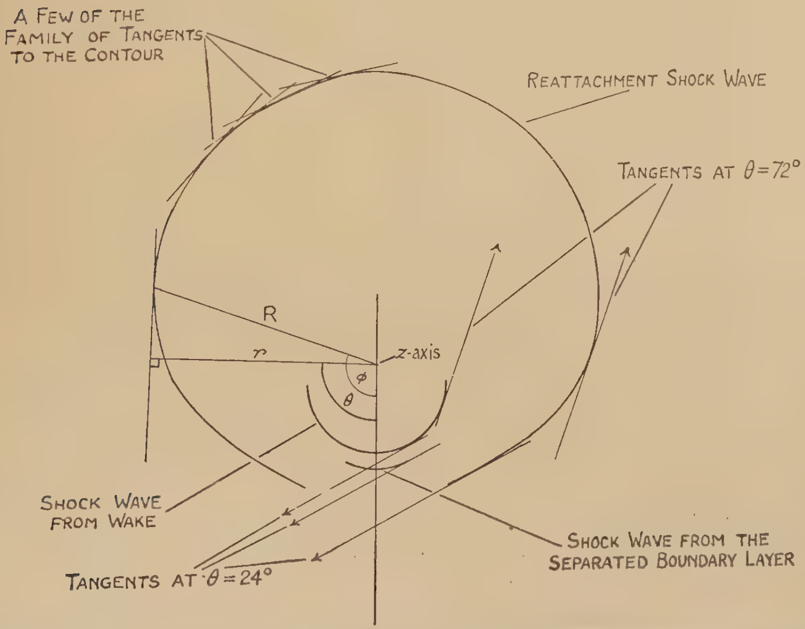

Traces of shock waves in the plane $z=2d$ when the cylinder is at 20° yaw.

the values of ϕ for the three shock waves at $\theta=24°$ are 30°, 24°, and 12° approximately, and the values of ϕ for the two shock waves visible at $\theta=72°$ are 95° and 60°.

The faint mark from top left to bottom right on the photographs and the horizontal mark at the bottom on some of them are due to scratches on the tunnel windows. The indistinct approximately hyperbolic lines appearing at various distances downstream of the bow shock wave are due to the interaction of this wave with the boundary layer on the tunnel windows. The reflection of this shock wave from the bottom liner is also visible in some photographs. Furthermore there are three Mach waves visible from each of the liners.

§ 5. DISCUSSION OF RESULTS

Bow Shock Wave

It was found that the inclination of the body had very little effect on the shape of the bow shock wave, except in the neighbourhood of the nose; here the wave was distorted for the larger angles of yaw in such a way that the normal part occurred towards the pressure side of the body, i.e. in the direction $\phi=180°$. Even for $\alpha=30°$ the shape downstream of the nose was very nearly a surface of revolution.

The contours for constant z were therefore approximated by circles. The centres of these circles were found to be displaced a distance b from the axis in the plane $\phi=0°$, and b was found to be a smooth function of z increasing to an approximately constant value for $z>3d$. The values of R and z at the vertex of the shock wave are given below for each angle of yaw: $R=-b$ at the vertex.

Table 2

α	5°	10°	20°	30°
R/d	0·02	0·06	0·14	0·21
z/d	—0·44	—0·44	—0·44	—0·42

There was a decrease in the values of the radius, a, with increasing α at constant z. This decrease was nearly independent of z for positive z.

Curves showing the variation of a and b with z are given in figs. 17 and 18. Too much significance should not be attached to the values of b for positive z since they could not be determined very accurately. Probably the main significance of these results lies in the smallness of the ratio b/a, showing that the bow shock wave is very nearly a surface of revolution about the z-axis.

Only for 30° yaw were the actual contours significantly different from circles. At $z=3d$ the radius of the best circle was 3% less than R at $\phi=0°$ and $\phi=180°$, with the same deviation in the opposite sense at $\phi=90°$. A similar deviation occurred for smaller yaw but was not significant compared with the estimated errors in measurements. The

Fig. 17

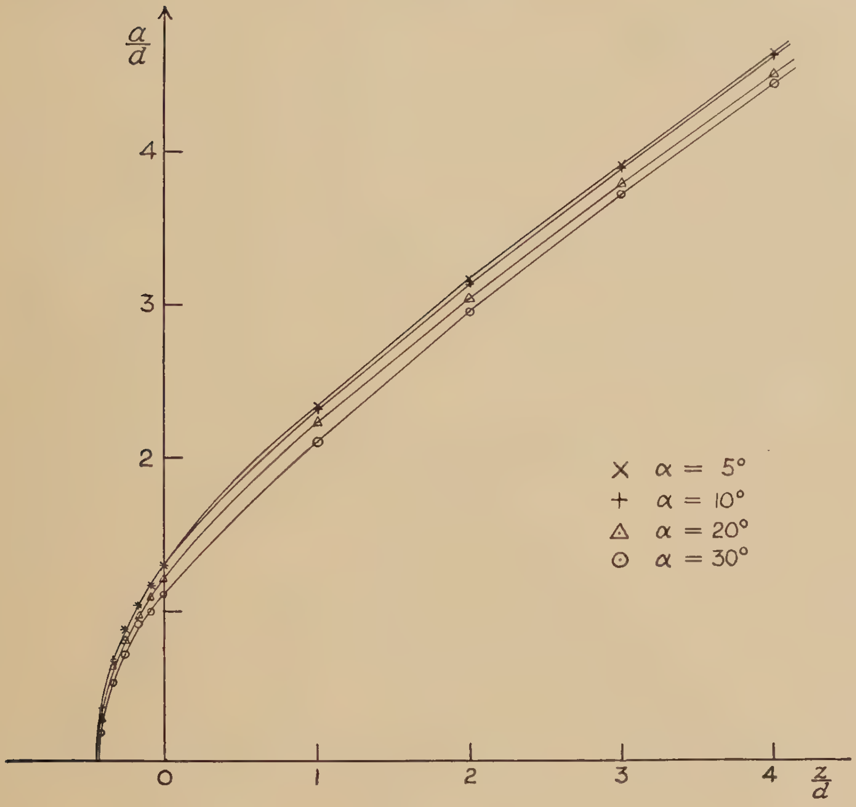

Radii of approximate contours of the bow shock wave.

Fig. 18

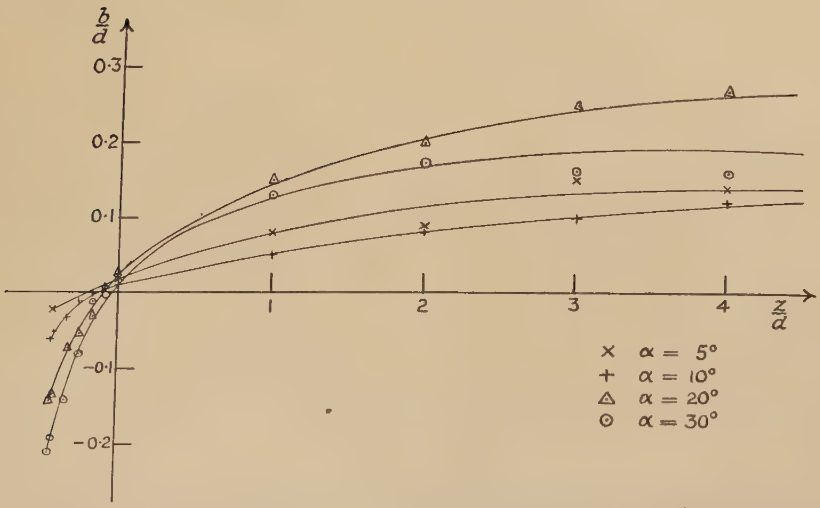

Displacement of centres of approximate contours from the z-axis.

deviation decreased with z and eventually became of the opposite sense, i.e. the best circle was outside the actual contour near $\phi=0°$ and $\phi=180°$ and inside it near $\phi=90°$.

Viscosity Effects on the Nose

It is convenient to define an angle ψ as the variation around the axis of the body. ψ is zero in the direction of the cross-flow component of the free stream velocity.

In the flow past a flat-nosed body at zero yaw the boundary layer separates at the shoulder and reattaches a short distance downstream (Holder and Chinneck 1951). The shape of this separation ' bubble ' is considerably distorted when the body is yawed. The length of the bubble is decreased at $\psi=180°$ and increased at $\psi=0°$ as would be expected but the latter effect is such that even at 5° yaw there is no reattachment near $\psi=0°$ (fig. 3).

The length of the ' bubble ' increases with decreasing ψ ,at first slowly and then more rapidly until below $\psi=40°$ approximately reattachment does not seem to occur. Below this value of ψ the separated boundary layer is carried downstream approximately in the free-stream direction and forms a detectable ' wake '. For larger yaw the bubble is shorter near $\psi=180°$ but its length increases more rapidly when ψ decreases and there is a larger region without reattachment.

The flow in the separation bubble is more complex than in the case of zero yaw. In addition to the circulatory (back) flow which occurs for zero yaw, there is also a flow around the cylinder in the direction of decreasing ψ. This draws fluid from inside the separation bubble near $\psi=180°$ to the region between the separated boundary layer and the body near $\psi=0°$.

The concavity of the stream lines near reattachment produces a weak shock wave, conical for zero yaw. Just downstream of this shock wave there is another quasi-conical shock wave visible for $\alpha \geqslant 10°$ (e.g. figs. 7, 11, 14) and in some photographs a third shock wave can be distinguished between these two (figs. 5, 9).

It was found, when the actual contours were constructed, that there was no evidence that the central one of these three shock waves overlaps the shock wave associated with the reattachment. It is only visible for small values of θ and in fact is found to occur for an even smaller range of ϕ (fig. 16). It seems to be produced by a concavity of the stream lines in the separated boundary layer and converges rapidly with the shock wave downstream of it.

The downstream shock wave is visible on photographs up to about $\theta=120°$ for $\alpha=10°$ and to a slightly higher value for larger α (fig. 10). These values of θ correspond to much lower values of ϕ since r decreases rapidly with increasing θ for constant z ; since ψ is always less than ϕ if $\tan \phi$ is positive, the range of ψ is found to be even less. The shock wave seems to decrease in strength with increasing θ (increasing ϕ, increasing ψ) and from its position it is suggested that this shock wave is caused by the deflection at the beginning of the cross-flow wake (see below).

Wake and Cross-flow Effects

In the undisturbed free-stream the flow can clearly be resolved into a flow parallel to the body axis and a cross flow. Let us consider a particular plane in the cross flow being swept downstream by the axial flow. If we neglect variations in the axial flow due to the body and due to viscosity, the flow in this plane would be impulsively disturbed on reaching the nose of the body, and, at a distance x along the axis of the body, the flow pattern would be expected to be the same as the flow pattern at time $x/(V \cos \alpha)$ in the corresponding two-dimensional flow around a circular cylinder started impulsively from rest with a velocity $V \sin \alpha$.

The two-dimensional flow is illustrated by Goldstein (1938). At first the flow is irrotational and then the boundary layer builds up and separates at the rear stagnation point when the cylinder has moved a distance approximately equal to one third of its radius. The separation point moves forward and two symmetrical vortices form behind the cylinder. These increase in size and are cast off asymmetrically.

Fig. 19

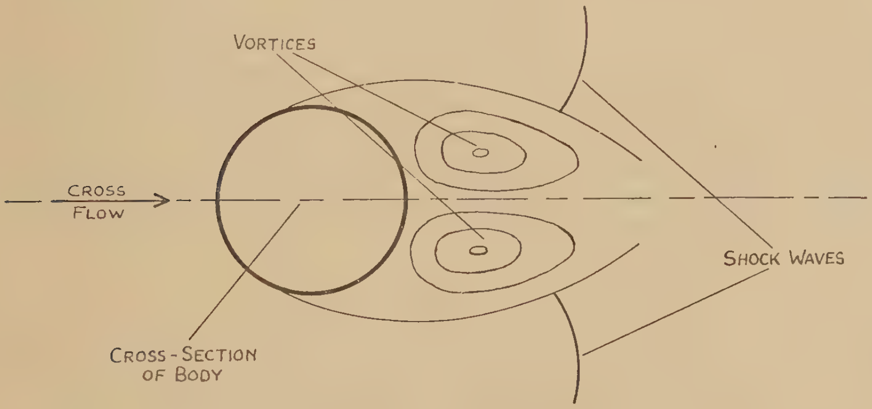

Sketch of cross-flow pattern for large yaw.

It is observed in the schlieren photographs (figs. 4, 8, 12) that there is a wake on the suction side of the body which seems to start further downstream than the theoretical value of $(d \cot \alpha)/6$ (Goldstein 1938). This was to be expected since this value refers to the initial separation, whereas nothing would be visible until the separation point had moved forward a short distance. The wake spreads with increasing x corresponding to the growth of the vortices as they are swept downstream.

For 5° yaw the wake is hardly detectable (fig. 3) but for 10° and 20° yaw (figs. 4, 8) it is clearly defined at $\theta=0$ as adjacent light and dark regions on the schlieren photographs. The knife edge was horizontal recording positive density gradients upwards as dark regions. For this particular value of θ the light deflections due to the two vortices add up and we need only consider one of them. Since the density gradient in a vortex is radial and positive outwards the two-dimensional picture should show density gradients outwards from the centre of the vortices. This enables an estimate of the shape of the vortices to be made (fig. 19). For $\alpha=30°$ the wake can be clearly distinguished from the outer flow but does not indicate a well-defined vortex formation; this is probably due to the vortices being cast off.

The critical Mach number of a circular cylinder is roughly 0·4, and from table 3 it can be seen that for $\alpha=20°$ and 30° sonic velocity should be reached in the cross flow. In the photographs a shock wave can be observed springing from the wake (figs. 8, 9, 12, 13) and when this shock wave is fitted to the cross-flow picture (fig. 19) it is found to be of approximately the same shape and in approximately the same position as the transonic shock wave observed, for example, by Wood and Gooderum (1952) for circular arc sections.

This shock wave recedes from the body as the cross flow develops and therefore it would be expected to be inclined at a small angle to the body. This is observed in the photographs.

Figure 13 gives a striking example of how the features of the flow can be described by considering the cross flow in a plane swept downstream by the axial flow to be similar to the flow about a circular cylinder started impulsively from rest. In this photograph, it can be seen that the shock wave springing from the wake crosses the body in the neighbourhood of the bend. This behaviour of the shock wave is easily explained by considering the cross flow in a plane travelling with the axial flow; when this plane reaches the bend in the body the cylinder is brought to rest relative to the cross flow but the shock wave on its leeward side continues its motion and eventually travels ahead of the cylinder.

Table 3

	α	0°	5°	10°	20°	30°
Mach No.	axial flow	1·96	1·95	1·93	1·84	1·70
	cross flow	0·00	0·17	0·34	0·67	0·98

§ 6. CONCLUSIONS

By rotating a yawed body of revolution about an axis in the free-stream direction the complete flow picture can be observed. This technique could also be used for investigating the flow around a body with axis in the free-stream direction where the cross section is not a circle.

The bow shock wave for a flat-nosed cylinder at yaw was found to be practically unaltered in shape and inclination within the range of angle of yaw considered, but the boundary layer separation at the nose was considerably distorted, even for 5° yaw, and there was a region on the suction side of the body where there was no reattachment. Downstream of the shock wave from the reattachment there was another shock wave thought to originate from the beginning of the wake.

The development of the cross flow with increasing distance from the nose of the body was found to be similar to the two-dimensional flow about a circular cylinder started impulsively from rest. In support of this idea, the presence of vortices on the leeward side of the body was inferred from the schlieren photographs. At large angles of yaw, corresponding to a high cross flow Mach number, shock waves appeared. These could be associated with the shock waves which would be expected to spring from the wake of a circular cylinder at a Mach number in excess of the critical one, and their development as the cross flow was swept downstream could be described qualitatively in terms of the two-dimensional flow about a circular cylinder.

ACKNOWLEDGEMENTS

The author's thanks are due to Dr. N. H. Johannesen for suggesting the problem and for his continued interest in the work, also to Professor M. J. Lighthill and Mr. P. R. Owen for helpful discussions.

During the course of the work the author was assisted by a grant from the Department of Scientific and Industrial Research of the Ministry of Supply.

REFERENCES

ALLEN, H. J., and PERKINS, E. W., 1951, *N.A.C.A. Report* 1048.

BARDSLEY, O., and MAIR, W. A., 1951, *Phil. Mag.*, **42,** 29.

GOLDSTEIN, S. (Editor), 1938, *Modern Developments in Fluid Dynamics*, pp. 63 and 181–186.

HOLDER, D. W., and CHINNECK, A., 1951, *A.R.C.* 14216 (unpublished).

WOOD, G. P., and GOODERUM, P. B., 1952, *N.A.C.A.*, TN 2801.

XL. CORRESPONDENCE

Etch Pit Attack on Plastically Deformed Aluminium

By P. J. E. Forsyth
Metallurgy Department, R.A.E., Farnborough

[Received January 20, 1954]

The experiments described by S. Amelinckx (1953), in which the alignment of etch pits along slip bands occurred, are of great interest. We have found similar effects on surfaces where slip bands have been produced by cyclic stresses, the metal being pure aluminium electrolytically polished, fatigued, and subsequently etched by anodic attack in an aqueous solution of 5% $HCl+2\%$ HNO_3 (Jacquesson and Manec 1950). This affinity for slip bands suggested that the reagent might be useful for revealing regions where glide had occurred. It was found, however, that the repolished surface was randomly attacked. No tendency for the etch pits to align themselves was noted even when repolishing was so light that undulations revealing the positions of the slip bands could still be seen. It was concluded that alignment of etch pits along slip bands was purely a surface effect where the ledge formed by the glide became a preferential position for attack. A number of tests have now been repeated with the etching reagent (50% HCl 47% HNO_3 3% HF) quoted by Amelinckx. The pronounced slip band attack produced by etching strained specimens with no subsequent repolish (figs. 1 and 2 (figs. 1–4, Plate 6)) is similar to that illustrated by Amelinckx. However, it has again been found that removal of the surface containing the slip steps eliminates the tendency for etch pit alignment. This is true of the bands produced by light static deformation and also the more heavily delineated bands produced by a few stress reversals. Figures 3 and 4 show specimens which have been electrolytically polished, deformed, then lightly electrolytically repolished and finally etched. They are therefore directly comparable with figs. 1 and 2 except that they have received an intermediate repolish. It can be seen that the etch pit attack is variable, depending mainly on grain orientation to the surface even to the extent of attacking the wide undulations where the electrolytic polish has not yet completely smoothed out the slip bands. It can also be seen that the attack along the undulations often ends abruptly at the grain boundaries, although the undulations themselves pass into a neighbouring grain (arrow A, fig. 3).

It might be expected that if rows of screw dislocations emerge at the crystal surface then any section made by repolishing should cut some of them. Therefore, it seems that if etch pits are sensitive to screw dislocation sites, this sensitivity somehow depends on the presence of a ledge or cliff on the crystal surface.

An alternative and simpler explanation would seem to be that glide produces a ledge and bares a fresh crystal surface which may be more susceptible to attack, the attack being independent of any screw dislocations in the glide plane. This explanation is substantiated by the observation that the degree of etch pit attack is greatly dependent on the grain orientation with respect to the polished surface.

ACKNOWLEDGMENT

This letter is published by the permission of the Chief Scientist, Ministry of Supply. Crown copyright reserved. Reproduced by permission of the Controller, H.M. Stationery Office.

REFERENCES

AMELINCKX, 1953, *Phil. Mag.*, **44**, 1048.
JACQUESSON and MANEC, 1950, *Compt. Rendus*, 959.

ERRATUM

The Brownian Movement of Linear and Non-Linear Systems, by D. K. C. MACDONALD, 1954, *Phil. Mag.*, **45**, 63.

The last line of eqn. (14 *a*) should read:

$$= 2\left\{kTC - \left[\exp(-\alpha t/C) \times \int_{-\infty}^{\infty} \frac{\exp(-q^2/2kTC)q^2\,dq}{(1+Bq^2)^{1/2}} \Big/ \int_{-\infty}^{\infty} \exp(-q^2/2kTC)\,dq\right]\right\} \qquad \ldots\ldots (14\,a)$$

XLI. *Notices of New Books and Periodicals received*

Numerical Solution of Differential Equations. By William Edmund Milne. (London: Chapman & Hall, Ltd.; New York: John Wiley & Sons, Inc., 1953.)

It is a welcome sign of an increasing interest in numerical analysis that a number of new books dealing with various aspects of the subject are appearing. The present book is concerned primarily with the numerical solution of ordinary and partial differential equations with the aid of desk computing machines. There is a three page appendix dealing with automatic digital computers but, on the whole, the author has not, in writing the book, been very much influenced by the advent of these machines.

The book would appear to be based largely on a course of lectures and the mathematical knowledge required to read it is not great. The reader is asked to follow numerical examples in some detail. Some of the methods described are of importance only in leading up to methods which the author specially advocates. He has, very wisely, not attempted to produce a compendium of all the methods which may be used. There is a carefully selected bibliography containing some 260 items.

M. V. W.

Ionic Processes in Solution. By Ronald W. Gurney. (International Chemical Series.) (New York: McGraw-Hill Company Inc., 1953.) [Pp. 275.] Price 46*s*. 6*d*.

A previous book by the author, published by the Cambridge University Press in 1936, dealt largely with the quantum mechanical interpretation of those properties of ions in solution which are independent of concentration. The present book, as the author points out in his Preface, is not meant to be a revision or an extension of his former book. In fact, it can best be described as an introduction to the principles of the electrochemistry of solutions from the point of view of thermodynamics and elementary statistical mechanics. Irreversible processes such as diffusion phenomena, ionic conductance and the viscosity of electrolytes are only briefly discussed.

The first six chapters are mainly concerned with the fundamental principles relevant to the study of ionic solutions and their interpretation on the basis of molecular physics and of quantum theory. The remaining chapters (7 to 16) deal mainly with the application of these principles to certain selected experimental data, including the discussion of ionic equilibria, free energy and entropy of ionic solutions and the theory of galvanic cells, in both aqueous and non-aqueous systems.

The book is conceived in a very original way and is written in the graphic style characteristic of this author, who has succeeded here in giving a clear description of the molecular physical basis of theoretical electrochemistry. As this is neither a textbook nor a monograph, in the usual sense, the omission of important references may have some justification.

According to the author, the book is intended primarily for graduate students and research workers. In the opinion of the reviewer, it should be of considerable value to physicists who wish to familiarize themselves with physico-chemical problems of ionic solutions and it should also be very stimulating to chemists, as it deals with the often neglected physical aspects of this subject.

It is a matter for deep regret that the untimely death of Dr. Gurney has deprived us of the opportunity to follow his further developments of these topics.

J. Weiss.

[The Editors do not hold themselves responsible for the views expressed by their correspondents.]

Fig. 1

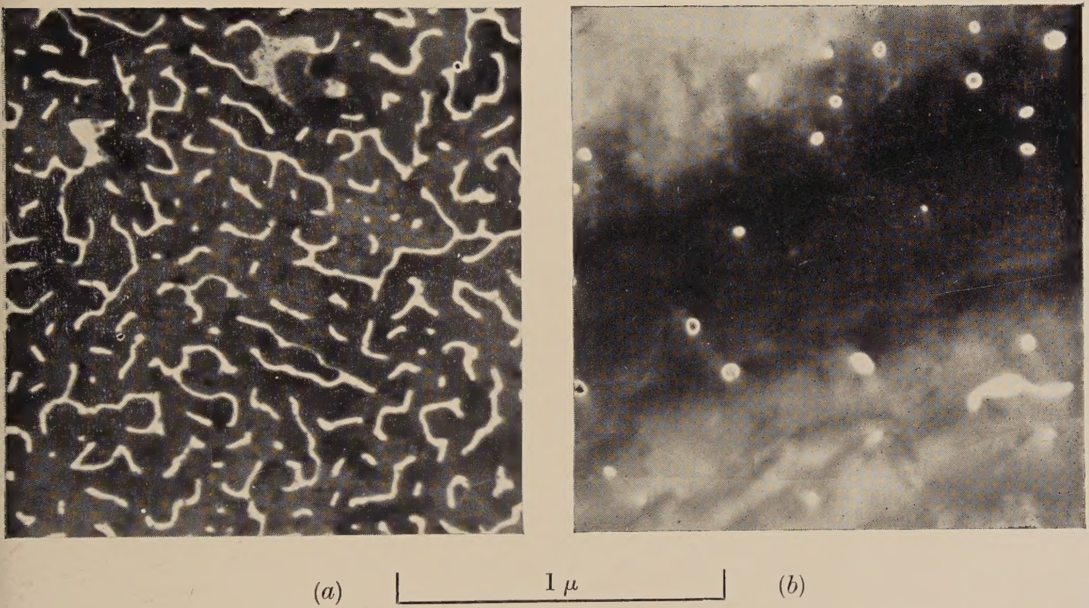

(*a*) Structure of polycrystalline film of nickel condensed on rocksalt at room temperature.

(*b*) Structure of monocrystalline film of nickel condensed on rocksalt at 450°c.

Fig. 3

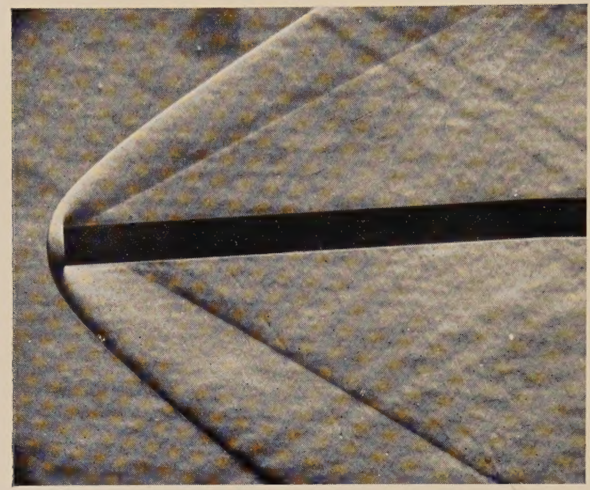

α=5°, θ=0°.

Fig. 4

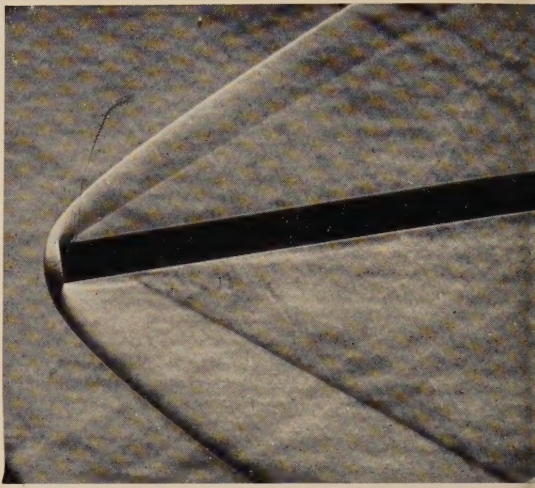

α=10°, θ=0°.

Fig. 5

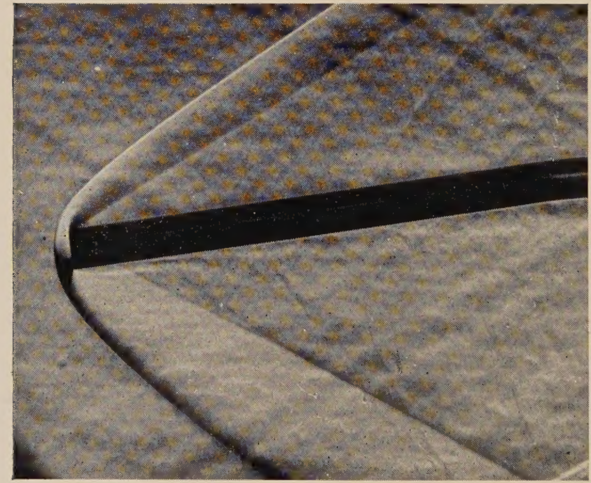

α=10°, θ=24°.

Fig. 6

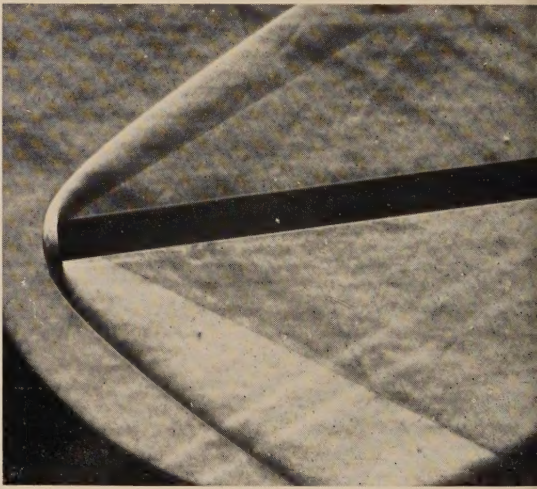

α=10°, θ=42°.

Fig. 7

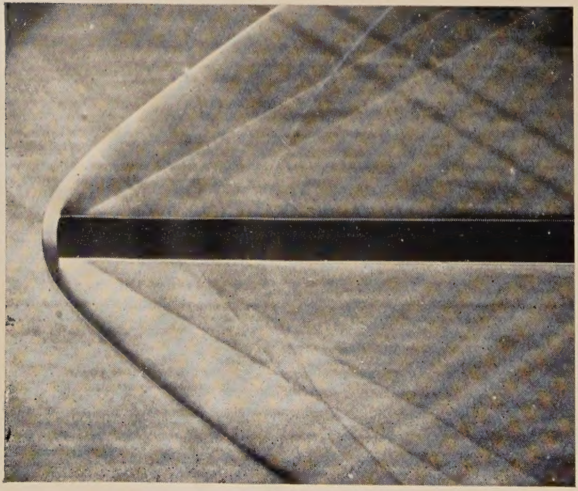

α=10°, θ=90°.

Fig. 8

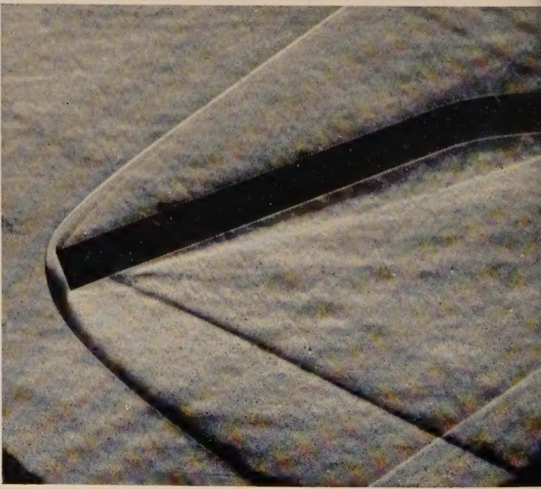

α=20°, θ=0°.

Fig. 9

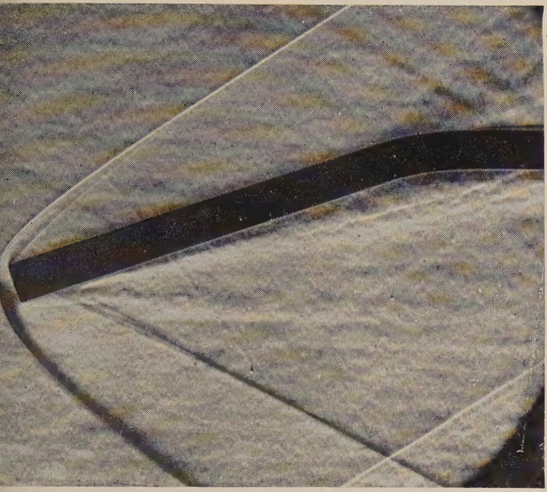

α=20°, θ=12°.

Fig. 10

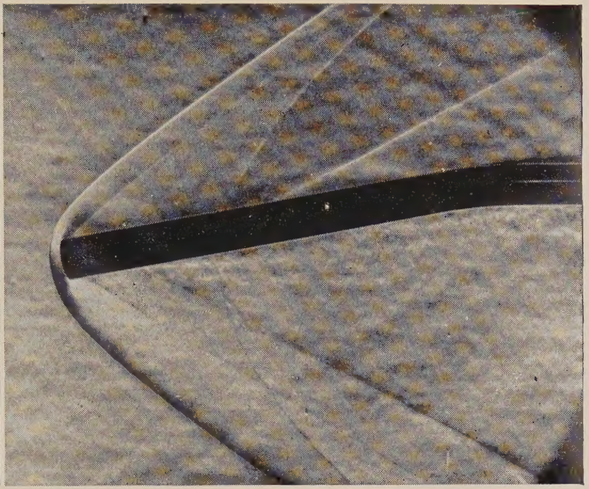

α=20°, θ=60°.

Fig. 11

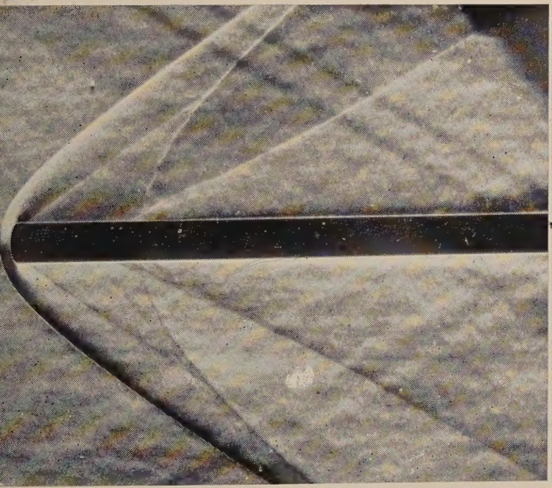

α=20°, θ=90°.

Fig. 12

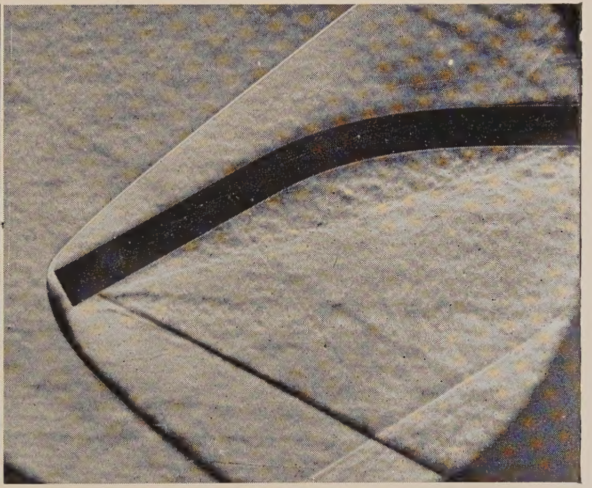

α=30°, θ=0°.

Fig. 13

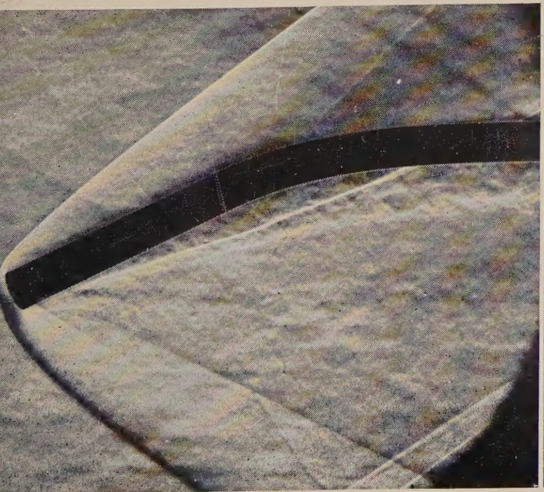

α=30°, θ=36°.

Fig. 14

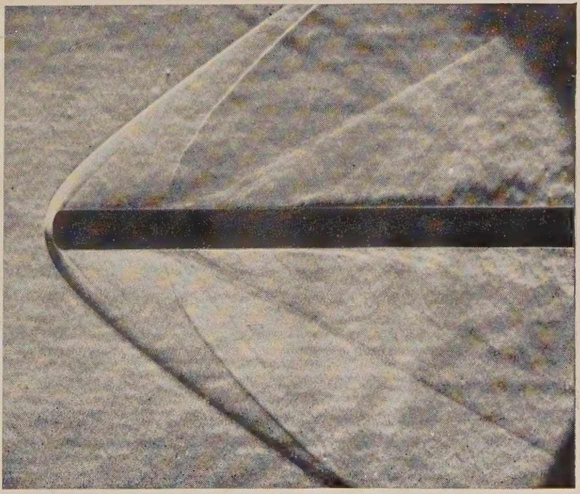

α=30°, θ=90°.

Fig. 1

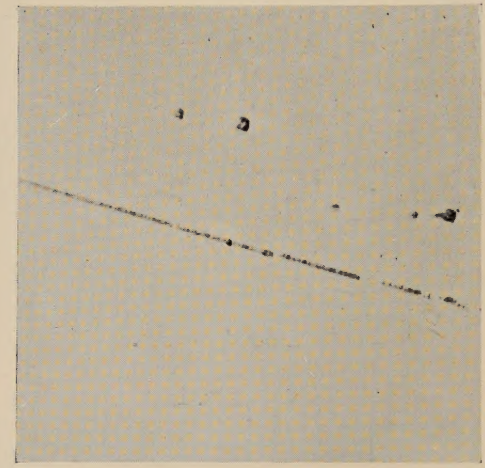

×500

Fig. 2

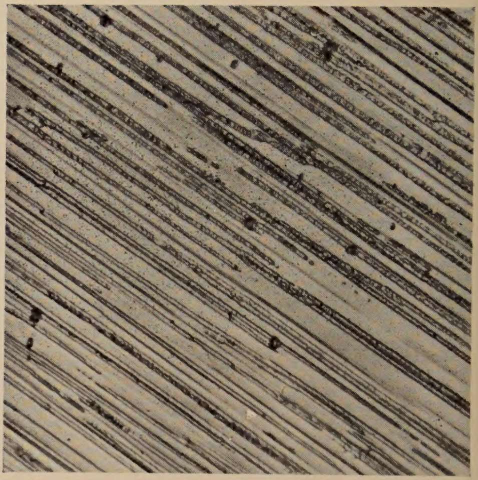

×500

Fig. 3

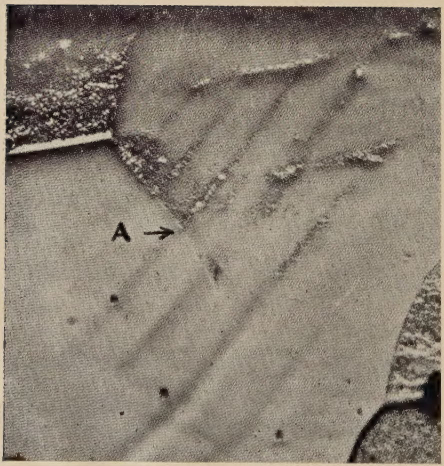

×500

Fig. 4

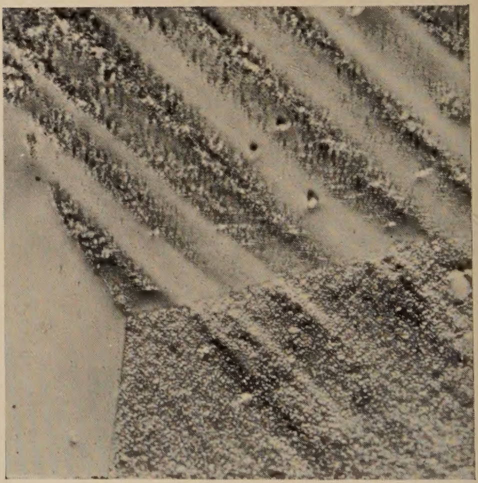

×500